# Micromechanical Sensing for Real Time Monitoring of Filamentous Fungi Growth


Thesis submitted to the

**University of Dublin**

for the degree of

**Doctor in Philosophy**

**Niall Maloney**

Supervisor:

Prof. Martin Hegner

School of Physics,

Trinity College Dublin

and

Centre for Research on Adaptive

Nanostructures and Nanodevices

August 2013

# Declaration

I declare that this thesis has not been submitted as an exercise for a degree at this or any other university and it is entirely my own work.

I agree to deposit this thesis in the University's open access institutional repository or allow the Library to do so on my behalf, subject to Irish Copyright Legislation and Trinity College Library conditions of use and acknowledgement.

Niall Maloney

August 10, 2013

# Summary

Since the early 1990s the use of cantilevers as biosensors has risen dramatically. Advances in semiconductor fabrication technologies has resulted in the reproducible production of high quality cantilever arrays. When operated in dynamic mode the cantilever is oscillated at its resonance frequency. Mass loading on the sensor produces a shift in resonance frequency, thus rendering the cantilever an ultra-sensitive 'mass balance'. Despite this high sensitivity there has only been a limited number of incidences where cantilevers have been employed for the real time monitoring of microorganism growth. In this thesis the development of several devices designed for the measurement of cantilever resonance frequencies is outlined. As it is desired to use cantilevers for fast microorganism growth detection these devices have been designed accordingly.

**Fibre Optic Based Measurement of Resonance Frequencies**: The development of a fibre optic based readout device for the measurement of flexural resonance frequencies of cantilevers in an array is described. Measurement of frequencies is via the laser beam deflection method. Movement in the position of the deflected laser spot results in modulation of light intensity entering an optic fibre. The rate of modulation allows the frequency of oscillation to be determined. Using this device a mass responsivity of ~ 51 ± 1 pg/Hz is achieved for an agarose functionalised cantilever. The detection of *Aspergillus niger* (*A. niger*) growth is possible within 15 hours.

**Device for Measurement of Higher Order Resonance Modes:** The development of a device capable of the measurement of higher order flexural resonance modes is described. Measurement of resonance frequencies is based on the laser beam deflection method where the movement of a deflected laser spot on a PSD is used to determine frequencies. This device is capable of measuring up to four resonance modes for eight cantilevers with a thickness of 2 μm in an array. Frequency measurements for multiple cantilevers are facilitated by a 2D automated translation stage system which moves a laser spot to predetermined positions on the cantilever array. The use of higher resonance modes results in a mass responsivity that is 13 times higher than that which is possible when using the fundamental resonance mode. This increased sensitivity will allow for growth detection measurements to be performed on microbes such as bacteria and yeasts which are outside the scope of the work.

**Single Fungal Spore Detection:** Detection of the growth of single *A. niger* spores is shown using multiple resonance modes. Detection times as low as 15 hours have been achieved which is an order of magnitude faster than conventional growth detection techniques. The ability to detect the growth of single spores within a short time is advantageous in a clinical setting as it allows for a reduction in the number of isolates required for detection of infection. A high-magnification camera implemented into the device facilitates imaging of cantilevers during growth measurements. Through use of the camera and higher order resonance modes a quantitative measurement of the progression of hyphal growth along a cantilever's longitudinal axis is possible. Events occurring on the cellular level, such as the secretion of hydrophobins, are also detected. This work will enable automatic measurements to be performed without visual analysis of cantilevers as changes in mechanics are able to be described in detail.

**Antibiotic Susceptibility Testing:** Antibiotic susceptibility tests are performed for the first time using cantilevers. The susceptibility of *Aspergilli* to antifungal drugs is demonstrated. In the case of *A. niger* it is shown that at a concentration of 0.03 μg/mL fluconazole delays germination times, while at 128 μg/mL it is seen to fully inhibit growth. In the case of the clinically relevant species *Aspergillus fumigatus* (*A. fumigatus*), the effect of amphotericin B is investigated at a concentration of 0.03 μg/mL. At this concentration *A. fumigatus* is found to be susceptible to amphotericin B.

**Piezoresistive Microcantilevers for Fungal Growth Detection:** The use of the piezoresistive readout technique for the measurement of cantilever resonance frequencies, at elevated environmental conditions (>94% RH, 30 °C), is successfully demonstrated. A comparison to the laser beam deflection method is made and it is observed that there is no loss in sensitivity, with both methods revealing a mass responsivity of ~ 32 pg/Hz for an agarose functionalised cantilever. Peaks have been found to have a slightly higher signal to noise ratio (157:1) when compared to the optical beam deflection method (140:1). The use of these sensors for the measurement of *A. niger* growth was attempted but Joule heating of the Au piezoresistor during their operation results in unsuitable growth conditions and therefore spore death.

# Acknowledgements

I would like to thank my supervisor Prof. Martin Hegner for giving me the opportunity to be part of his team for his help guidance and support over the past four years; for providing great working conditions and an even better atmosphere. Thank you

Special thanks and gratitude to Dr. Gyöngyi Lukács, for her professionalism, unlimited biological knowledge, support and most especially her friendship. Your presence in the lab over the past four years has made working in CRANN a pleasure. Thank you for the seemingly endless supply of coffee, pastries, and scratch cards. Your quick wit, humour, and loyalty will be sorely missed.

Thanks to the other members of the Nanobio team in CRANN for their support; Dr. Jason Jensen, Dr. Rohit Mishra, Dr. Vivek Jadhav, Dr. Paul Fleming, Michael Walther, Florian Wruck, Sinead Cullen, and Sarah-Louise Ball.

A big thanks to Jason for his practical and theoretical help, humour, friendship, and proof reading. Thanks to Michael for his instrumental help and for dragging me up the mountains on my bike….I guess.

I would also to extend my thanks to past group members who have help me throughout the years, namely Dr. Helene Gaussier and Dr. Dunja Skoko. Thanks to Prof. Michael Roukes and Dr. Warren Fon for hosting me in Caltech and allowing me to gain experience in the field of integrated sensors.

Thanks to the guys in the mechanical workshop (Dave, Gordon, Paddy and Dave) for always accommodating my last minute adjustments and requests.

Thanks to Dr. Ronan Daly and Daniel Fox for assistance with the ever impossible agarose layer.

Last but not least a big thank you to my parents, Jimmy and Noreen, my brother, Darryl and my sister Bronagh for their constant love, support, and encouragement.

# Contents

# Acronyms

**AFM** *Atomic force microscope*

**AMB** *Amphotericin B*

**AST** *Antibiotic susceptibility test*

**bp** *Base pair*

**cfu** *Colony forming unit*

**DAQ** *Data Acquisition*

**DI** *Deionised*

**DNA** *Deoxyribonucleic acid*

**DOD** *Drop on demand*

**DOF** *Depth of focus*

**EtOH** *Ethanol*

**FIB** *Focused ion beam*

**LabVIEW** *Laboratory Virtual Instrumentation Engineering Workbench*

**LB** *Luria Broth*

**ME** *Malt Extract*

**MIC** *Minimum inhibitory concentration*

**PBS** *phosphate buffered saline*

**PCR** *Polymerase chain reaction*

**PDA** *Potato dextrose agar*

**PDMS** *Polydimethylsiloxane*

**PEEK** *Polyether ether ketone*

**PMMA** *Poly(methyl methacrylate)*

**PSD** *Position sensitive detector*

**QCM** *Quartz crystal microbalance*

**qPCR** *Quantitative polymerase chain reaction*

**R.H.** *Relative humidity*

**RTPCR** *Real time polymerase chain reaction*

**RPMI** *Roswell Park Memorial Institute medium*

**SEM** *Scanning electron microscope*

**SOI** *Silicon on insulator*

**SPR** *Surface plasmon resonance*

**SPW** *Surface plasmon wave*

**VI** *Virtual instrument*

# Chapter 1
# Introduction

## 1.1 Microorganisms

Microorganisms are microscopic organisms which have been widely studied since they were first observed by Antonie van Leeuwenhoek in 1675. Microorganisms can be classed as Prokaryotes (Bacteria and Archaea) or Eukaryotes (Fungi, Protists, Animals, and Plants) based on their internal cell structure.

Prokaryotic cells range in size from 0.1-10 μm while eukaryotic cells are larger and range in size from 2-100 μm. The main difference between the two cell types is that eukaryotes have their DNA (deoxyribonucleic acid) in a membrane-enclosed nucleus, while prokaryotes have a simpler internal cell structure where DNA is present in a large double stranded molecule called the chromosome which aggregates within the cell in the nucleoid region [1]. As well as a nucleus, eukaryotes also have mitochondria and chloroplasts which play specific roles in energy generation by carrying out respiration and photosynthesis respectively [1]. In eukaryotic cells the key processes of transcription and translation are partitioned; transcription occurs in the nucleus and translation in the cytoplasm while prokaryotes couple transcription to translation directly within the cytoplasm [1]. A simple internal structure and smaller cell size allow Prokaryotes a higher growth rate compared to Eukaryotes. Illustrations of cell types and filamentous fungi are shown in Figure 1.1.

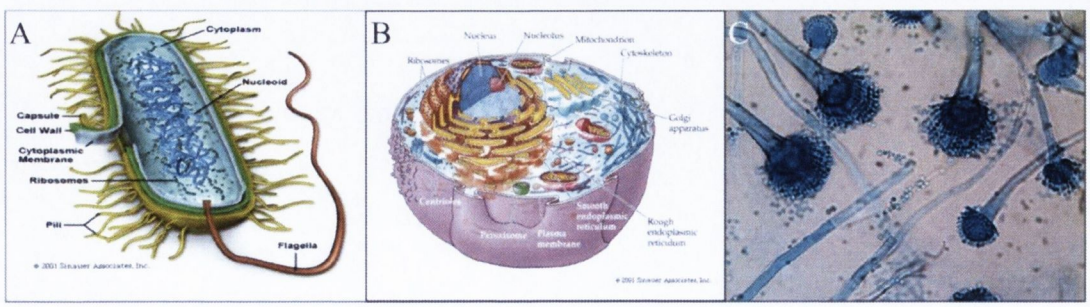


Figure 1.1: Different cell types. (A) Prokaryotic cell. (B) Eukaryotic Cell. (C) Filamentous fungi (*A. fumigatus* taken from http://www.eapcri.eu/)

*Aspergilli* are Ascomycota filamentous fungi which are commonly found in soil, on decaying plant material, in air, and in water supplies. Opportunistic pathogenic *Aspergilli* grow easily and rapidly at a broad range of culture temperatures and on a wide variety of media. Growth of species at 37 °C is a feature that usually differentiates the pathogenic from non-pathogenic isolates [2]. *Aspergillus fumigatus* (*A. fumigatus*) is the most common *Aspergilli* isolated from human infections (50-60 %) followed by *Aspergillus flavus* (*A. flavus*), *Aspergillus terrus* (*A. terrus*), and *Aspergillus niger* (*A. niger*) (10-15% each) [2]. Infection typically presents in persons with immunosuppression related to conditions such as cancer, AIDS, old age, chronic diabetes, cystic fibrosis, and organ transplants [3]. Spores are typically inhaled into the lungs and invasive tissue infection can occur after hyphal germination [4]. Fungal colonies consist of mycelium which is a network of hyphae. It is the efficient growth of hyphae that plays a crucial role in fungal colonisation of a substrate.

Two *Aspergillus* species utilised in this work are *A. niger* and *A. fumigatus*. *A. niger* spores are brown/black with a rough surface. Diameters of spores range from 4–5 μm. Spores are able to grow in the temperature range of 6–47 °C with an optimum at 35–37 °C [5]. Colonies are initially white but become black upon the production of fruiting bodies [2]. *A. fumigatus* conidia have smooth surfaces and are 2–3 μm in diameter. Growth of this species can occur at temperatures up to 50 °C. Colonies are grey/green in colour with a cottony texture. The hyphae of both species are septate (divided into cells) and hyaline (glass like appearance) [2].

### 1.1.1 Microorganism Growth

Growth is an increase in the number of cells/biomass in a population. In the case of bacteria, growth proceeds by binary fission where a growing cell elongates until the cell divides into two new cells [1]. Fungi reproduce asexually by the growth and spread of hyphal filaments, by asexual production of spores or by cell division [1].

Figure 1.2 shows a typical growth curve for a batch culture (culture growing in an enclosed vessel) which is common to both bacteria and fungi. The plot shows the variation in biomass over time. The curve consists of the following phases; lag (A), exponential (B), stationary (C), and death (D). The lag phase is the adaptation time required for growth to

occur. Lag time can vary depending on several factors, for example when a microbial population is transferred from a rich culture medium to a poorer one there is a long lag time, whereas if an exponentially growing culture is transferred into the exact same conditions no lag time is observed. Growth begins in the exponential phase. In the exponential phase growth is balanced and the rate of change of any extensive property ($X$) (*e.g.* biomass, DNA) can be described by

$$X = X_o e^{\mu T} \qquad 1.1$$

where $X_o$ is the initial extensive property, $\mu$ is the growth rate constant and $T$ is time. In the case of filamentous fungi growth does not reach this state fully or maintain it for very long [6]. After a certain amount of time growth enters a stationary phase where the growth rate is zero, this is usually due to lack of nutrition or an accumulation of waste products which inhibit growth. Microorganisms are still viable in the stationary phase but they eventually die and the cycle enters the death phase (D).

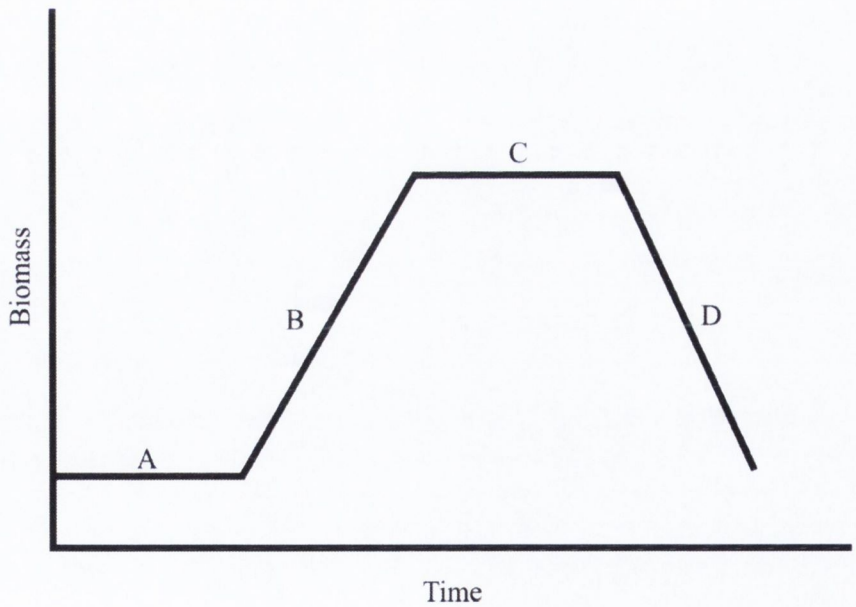


Figure 1.2: Typical microorganism growth cycle showing biomass with respect to time. Microbial growth can be divided into four stages. (A) Lag phase: Time required for growth to occur. (B) Exponential phase: The rate of change of any extensive property ($X$) (e.g. biomass, DNA) occurs at an exponential rate. (C) Stationary phase: Growth rate is zero. (D) Death phase: The number of live cells begins to decline.

Microorganism growth is greatly affected by the chemical and physical state of their environment. Water availability, pH, and oxygen availability are factors which play a role in cell processes however temperature is deemed to be the most important factor affecting the survival of microorganisms (for experiments described in this thesis). For each microbial species there are three cardinal temperatures; minimal, optimal, and maximal. Below the minimum temperature the organism's cytoplasmic membrane stiffens to the point where it no longer functions properly for nutrient transport or can no longer develop a proton motive force resulting in the cessation of growth. At the optimal temperature the organism's cellular components are functioning at their maximum rate and this is reflected in a maximum growth rate. Above the maximum temperature denaturing of one or more essential cell components (e.g. a key enzyme) occurs resulting in cell death. Cardinal temperatures are characteristic for any given microorganism but can differ widely from species to species [1].

### 1.1.2 Microorganism Detection

In clinical settings there has been an increase in the number of patients presenting with infections which show antibiotic resistance. Antibiotic Susceptibility Testing (AST) is performed to determine Minimum Inhibitory Concentrations (MIC) of antibiotics. Discussion of this topic is dealt with in detail in Chapter 6 where AST is performed using cantilever arrays.

In areas such as the pharmaceutical, cosmetic, and food industries microbial infections through contamination still pose a threat. Antimicrobial preservatives are added to sterile liquid drugs such as multi-dose parenteral products for the purpose of inhibiting and/or killing the growth of microorganisms that may have contaminated the product through opening of its container [7]. Antimicrobial Effectiveness Tests (AET) are routinely performed to ensure that microbial contamination does not occur and that preservatives are functional. Conventional methods to date rely on contaminating a sample containing preservatives with prescribed inoculums of a microorganism. Samples are removed from the contaminated product at defined time intervals and colony counting is performed using the pour plate method. Three major pharmacopeia, the *United States Pharmacopeia* (*USP*), the *European Pharmacopeia* (*EP*), and the *Japanese Pharmacopeia* (*JP*) outline

procedures for performing AETs [8-10]. Table 1.1 shows the testing intervals and acceptance criteria for a parenteral product according to the major pharmacopeia.

The conventional methods used involve incubation of microbes on a nutrient rich medium. This step is typically followed by incubation on selective media which show preferable support of target microbes. These inexpensive methods provide the desired sensitivity and growth information but are time consuming as detections are based on the growth of a single microbe into a colony. For example in the case of *A. niger* this process requires 5-14 days for a positive result [11].

Polymerase chain reaction (PCR) is also conventionally used for pathogen detection. PCR is based on the detection of short DNA sequences containing the target microbe's genetic material. Here isolation and amplification of the target sequence requires pre-existing knowledge of the characteristic nucleotide sequence of microbial agents. Using traditional PCR techniques 5-24 hours are required to produce a detection result [12].

Table 1.1: Combined table of acceptance criteria for antimicrobial effectiveness tests for a parenteral product according to *EP*, *JP*, and *USP*. The numbers represent a log reduction in number of Colony Forming Units (cfu). R-Recommended, M-Mandatory, NI-No increase, NR no recovery. Data taken from [7]

| | | | Log Reduction | | | | |
|---|---|---|---|---|---|---|---|
| Pharmacopeia | Microorganism | | 6 Hours | 24 Hours | 7 Days | 14 Days | 28 Days |
| EP | Bacteria | R | 2 | 3 | - | - | NR |
| | | M | - | 1 | 3 | - | NI |
| | Fungi | R | - | - | 2 | - | NI |
| | | M | - | - | - | 1 | NI |
| JP | Bacteria | | - | - | - | 1 | NI |
| | Fungi | | - | - | - | NI | NI |
| USP | Bacteria | | - | - | 1 | 3 | NI |
| | Fungi | | - | - | NI | NI | NI |

Real time PCR (RT-PCR) or quantitative PCR (qPCR) allows for real time detection. Here detection is based on attachment of a fluorescent probe to the target sequence which provides a quantitative result. The advantage of these techniques is their sensitivity in non-culturable samples and an ability to identify antibiotic resistant strains [13, 14]. The main drawbacks when using PCR are cost, lack of portability, non-label free detection, and an inability to discriminate between live and dead cells [12, 15].

In the case of the discussed *Aspergillus* species identification is difficult due to the fact that isolation of fungi is challenging [16]. New techniques have been developed based on the detection of fungal polysaccharides in different clinical samples [17]. During growth of most *Aspergillus* species thermostable polysaccharides, known as galactomannans, are released from the fungal cell wall. These can be detected and quantified in various body fluids by enzyme immunoassay tests [18]. There is a direct relationship between serum levels of galactomannans and the evolution of the disease, however antifungal treatment of a patient decreases the sensitivity of this test [19]. There are other commercial tests which detect the 1,3-BD-glucan polysaccharide present in the cell wall of many fungi. This test however is nonspecific. Similar to PCR the above polysaccharide detection based tests are unable to discriminate between live and dead cells. Their use is advantageous however in the case of non-culturable samples [18].

### 1.1.3 Biosensors

Biosensors have begun to be developed for rapid and label free detection of pathogens. Biosensors are defined as analytical devices that integrate a biologically derived molecular recognition molecule with a suitable physicochemical mechanism. Typically the recognition molecules used are antibodies, phages, aptamers, or single stranded DNA [15]. Transduction of the biological signal for pathogen detection is typically via optical, electrical, or mechanical means.

#### Optical biosensors

**Surface Plasmon Resonance** (SPR) is based on the excitation of electrons by an incident light beam resulting in the generation of a Surface Plasmon Wave (SPW). Biosensors based on this phenomenon typically consist of a thin metal film liquid interface. The metal

film is functionalised with a receptor layer (*e.g.* antibodies) and hence changes in the resonance condition occur upon binding of the target molecule (*e.g.* antigen) flown through a microfluidic channel [20]. Shifts in resonance can be determined through changes in reflected angle, wavelength, or intensity of the reflected light beam. A multi-channel SPR device has been described by Taylor et al [21], which allows for the detection of mixed bacterial suspensions at a concentration of $3.4 \times 10^3$-$1.2 \times 10^5$ colony forming units (cfu)/ml dependant on the species detected. The detection of fungal spores has also been reported using this method at a concentration of $3.1 \times 10^5$ spore/mL. SPR allows for rapid real time label-free detection of microbes, however the use of antibody-antigen biology does not allow for live/dead cell discrimination. Recent development of this technique has seen the use of bacteriophages as the molecular recognition layer allowing for the detection of *Escherichia coli* (*E. coli*) and methicillin resistant *Staphylococcus aureus* (MRSA) within 20 minutes at a concentration of $10^3$ (cfu)/mL. The use of bacteriophages does not facilitate live/dead cell discrimination either but these phages are capable of detecting very specific membrane proteins embedded in the targeted microorganism. These proteins are equally abundant in live or dead cells [22].

**Evanescent field fibre optic sensors** detect pathogens through changes in the evanescent field arising from alterations in refractive index due to analyte binding. Two types of fibre optic sensors exist; one is a tapered tip fibre which gradually decreases in diameter to form a tip. The second is a continuous taper fibre which decreases to a constant diameter and then increases again forming a waist sensing region. The tapered tip or waist act to increase the evanescent field around the fibre and thus these are the sensing regions. Typically the sensing region of the fibre is functionalised with antibodies. In a continuous taper fibre sensor, the evanescent field is altered through absorption of light by pathogens resulting in reduced output intensity at the fibres end. Using a continuous taper fibre optic biosensor, functionalised with *E. coli* specific antibodies, cells could be detected at concentrations as low as 70 cfu/mL [23]. The majority of work published with these sensors use additional optical fluorescent probes also rendering them non label-free [24]. Drawbacks of this technique are the poor stability of the bio recognition elements and a sensitivity to ambient light conditions [25].

**Mechanical Biosensors**

The **Quartz Crystal Microbalance** (QCM) consists of a thin quartz plate with electrodes evaporated on both sides. Detection is based on a mass increase on the surface resulting in a decrease in resonance frequency. Most crystals typically have a diameter between 6 – 25 mm and resonate between 5 and 30 MHz [26]. Several reports have been published on the detection of bacteria using this technique. A list of species detected accompanied with detection times (ranging from 10-60 minutes) can be found in [27]. The sensitivity of this technique was found to range from 170-$1.3x10^7$ cfu/ml depending on the species in question and the culture matrix used. These techniques usually detect microbes via antibody immobilisation on the sensor surface and thus a decrease in resonance frequency due to binding of mass is observed. The preparation of the sensor surface requires careful selection of antibodies specific to the microorganism being studied. The detection of *Staphylococcus aureus* (*S. aureus*) growth is reported in [28]. By this technique the piezoelectric plate is placed in the culture medium with *S. aureus* (initial concentration $1.57x10^6$ cfu/mL). As the growth of *S. aureus* starts the viscosity of the culture medium increases causing an increase in the motional resistance and a decrease in resonance frequency due to the loss in mechanical energy dissipated to the surrounding medium. The growth of *S. aureus* was seen after a lag time of approximately 2 hours and an exponential growth rate was observed. After 12 hours the signal was seen to stabilise. The preparation of the sensor surface is minimal, requiring only a 5 min cleaning step ($H_2SO_4 + H_2O_2$) and 30 min autoclaving. The use of a reference sensor was not possible as it would also respond to changes in viscosity.

**Electrochemical Biosensors**

**Ampometric Biosensors** measure changes in the ionic concentration of analytes. This technique is the most commonly used electrochemical biosensor for pathogen detection however it does not facilitate label free detection and so is not discussed further.

**Impedimetric Biosensors** measure changes in impedance over a range of frequencies that change as a result of biomolecular interaction. Whilst label free detection of pathogens is possible using this technique it is hindered by a low detection limit when compared to other biosensors [29]. There is a wide range of electrode functionalisation methods available which are discussed in detail in [30]. Typically electrodes are functionalised with

antibodies for recognition of pathogens. Functionalisation with bacteriophages has been developed of late allowing for detection of *S. aureus* with a detection limit of $10^4$ cfu/mL [31].

## 1.2 Nanomechanical Sensing

The advent of the atomic force microscope (AFM) in the 1980s [32] created the availability of micron sized cantilevers. Vast improvements in silicon processing technologies in the intervening decades have resulted in the reproducible production of relatively inexpensive high quality cantilevers. While traditionally used as surface probes, pioneering work in the 1990s saw the first use of cantilevers for sensing applications [33-36]. Since then published works detailing the use of cantilevers for sensing have increased greatly. These sensors allow for unprecedented sensitivities to be achieved, indicating their potential for use as mechanical transducers in the field of biosensing. Recently several reviews have been published outlining the current state of the art for cantilever sensing applications including detection mechanisms used and remaining challenges [37-40].

### 1.2.1 Cantilever Sensors

Cantilevers have been employed as mechanical transducers in the areas of mass, gas, chemical, and environmental sensing [41, 42]. The most widely used sensors are made from silicon due to well established fabrication techniques developed in the semiconductor industry. In recent years the reported use of polymer cantilever sensors has increased [43], however silicon sensors are still seen as the gold standard by researchers. Sensor dimensions can range from sub-micron to 100s of microns. A common feature is that the cantilever's thickness ($t$) is significantly less than its length ($L$) (*i.e.* $t<<L$)

Figure 1.3 shows an array of eight cantilevers which are typically used during this PhD thesis. The sensors are micro fabricated using a dry-etching silicon-on-insulator technique. Each array consists of eight cantilevers that are separated by a pitch of 250 μm. Each cantilever has a length, width, and thickness of 500, 100, and 0.5 – 7 μm respectively. The high precision and reproducibility of the cantilever array fabrication is illustrated by a

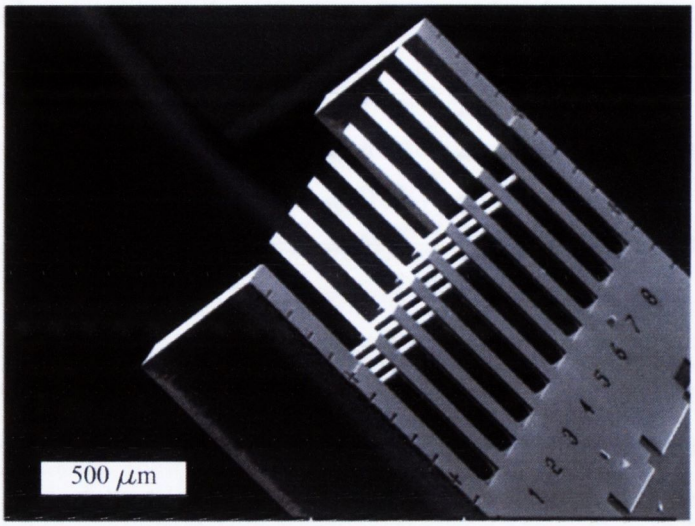


Figure 1.3: Typical cantilever array used throughout this work, fabricated by the IBM Zurich research laboratory. The array consists of eight cantilevers separated by a pitch of 250 μm. The high number of cantilevers allows for the use of *in situ* reference cantilevers during experiments. The cantilevers shown have a length, width, and thickness of 500 μm, 100 μm and 0.5 - 7 μm respectively.

0.5% variation in resonance frequencies across an array [41]. Cantilever arrays are now produced in batch on four inch wafers which has significantly reduced their cost.

Cantilevers are sensitive to virtually any stimulus; therefore the use of carefully prepared reference sensors is essential in order to correctly interpret measured signals. The use of cantilever arrays allows for multiple tests to be performed while also providing *in situ* reference sensors for the elimination of unwanted responses. The use of reference sensors was first reported by Lang *et al.*, where uncoated sensors were used as *in situ* references for Poly(methyl methacrylate) (PMMA) coated cantilevers used for gas detection [44].

Measurements are typically performed by tracking the static deflection (static mode) or resonance frequency (dynamic mode) of the sensors with respect to time. Measurement of cantilever motion can be performed using a variety of techniques. The mostly widely used technique is the laser beam deflection method which was developed for AFM [45]. By this method the motion of a laser beam, deflected by the cantilever, onto a photo detector is used to amplify cantilever motion. Whilst most optical based devices are based on only one of these modes, the development of devices capable of measurement of both in parallel has been reported [46, 47]. Using this technique a displacement resolution of 1nm and

hundreds of picograms mass resolution in liquid has been achieved. Whilst this technique is highly accurate it requires the use of larger external optical components making devices bulky.

The other two widely used techniques are piezoresistive [48] and piezoelectric [49] readout. Piezoresistive readout is based on deformation induced resistance changes in integrated resistors located in or on the cantilevers clamped end. This technique is suitable for the measurement of both static and dynamic signals. A detailed description of this technique is given in Chapter 7. Piezoelectric readout is based on electric potentials generated, between the surfaces of a solid dielectric, by the mechanical stress of cantilever motion. Conversely an applied voltage can be used to generate motion in these cantilevers and they can thus be used as self-actuating sensors [50]. Other techniques used are capacitive [51] and interferometric [52].

## 1.3 Modes of Operation

### 1.3.1 Static Mode

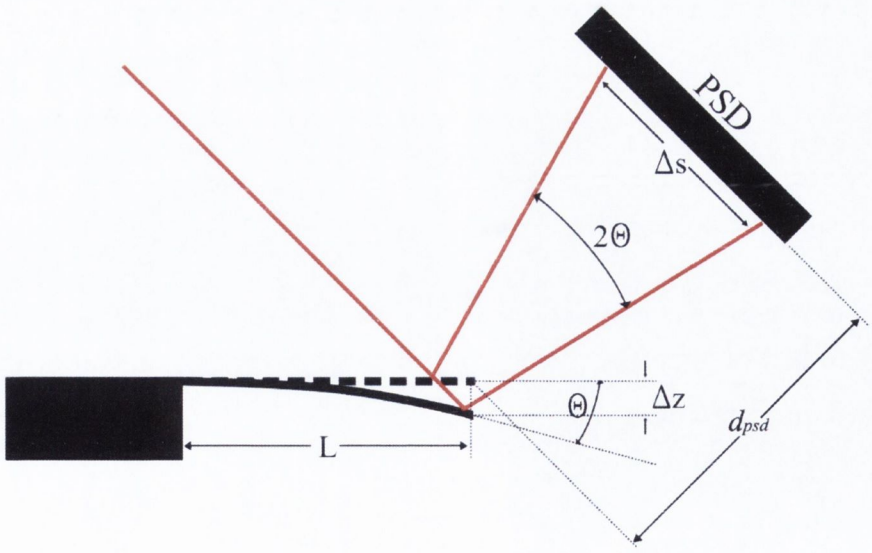


Figure 1.4: Schematic of the static deflection of a cantilever. The use of the laser beam deflection method for the measurement of deflection is shown. Bending of the cantilever ($\Delta z$) results in movement of a laser spot on a PSD.

In static mode the deflection of a cantilever is monitored with respect to time. Typically in static mode one side of the cantilever is activated with a functional layer and bending is induced by the adsorption of a specific target molecule. The adsorption of molecules onto the functional layer produces either compressive or tensile stress at the interface between the two layers. This stress is released via a bending of the cantilever. Typically cantilevers with small spring constants are used to increase observed deflections. Polymer cantilevers have also been utilised for static deflection measurements due to their low spring constants [43].

Measurement of the cantilever deflection is typically via the laser beam deflection method as illustrated in Figure 1.4. The deflection of the cantilever ($\Delta z$), can be related to the movement of the deflected laser spot on the position sensitive detector (PSD) ($\Delta s$) by the following equation [53]

$$\Delta z = \frac{L}{4d_{psd}}\Delta s = G\Delta s \qquad 1.2$$

assuming the bending angle of the cantilever ($\Theta$) is small, where $d_{psd}$ is the distance from the PSD to the cantilever tip, and $L$ is the length of the cantilever. Thus $G$, known as the calibration factor, is a purely geometrical factor. A more accurate determination of $G$ can be made using the equipartition theorem as described in [53].

The deflection of the cantilever can in turn be related to the radius of curvature ($R$) of the cantilever by Equation 1.3 [41].

$$R = \frac{2\Delta z}{L^2} \qquad 1.3$$

The change in surface stress ($\Delta\sigma$), due to adsorption of molecules can thus be determined using Stoney's formula [54],

$$\Delta\sigma = \frac{Et^2}{6R(1-\upsilon)} \qquad 1.4$$

where $E$, $t$ and $\upsilon$ are the Young's modulus, thickness, and Poisson ratio of the cantilever respectively.

### 1.3.2 Dynamic Mode

When operated in dynamic mode the resonance frequency of the cantilever is tracked with respect to time. Uniform adsorption of mass results in a negative resonance frequency shift. Thus, when operated in dynamic mode a cantilever can be thought of as a sensitive 'mass balance'. Measurement of resonance frequencies is typically via the laser beam deflection method as illustrated in Figure 1.5. This is the method used for the majority of the work presented in this thesis. Positioning of the laser spot at nodes of vibration, where the slope of the cantilevers mode shape is largest, maximises the deflection of the laser spot on the PSD allowing for accurate measurement of frequencies.

The $n^{th}$ mode resonance frequency ($f_n$) of a cantilever is given by [55]

$$f_n = \frac{\beta_n^2}{2\pi}\sqrt{\frac{EI}{m_b L^3}} \qquad 1.5$$

where $I$ is the moment of inertia and $m_b$ is the mass of the cantilever. Here the eigenvalues $\beta_n$ satisfy [56]

$$1 + cos\beta_n cosh\beta_n = 0. \qquad 1.6$$

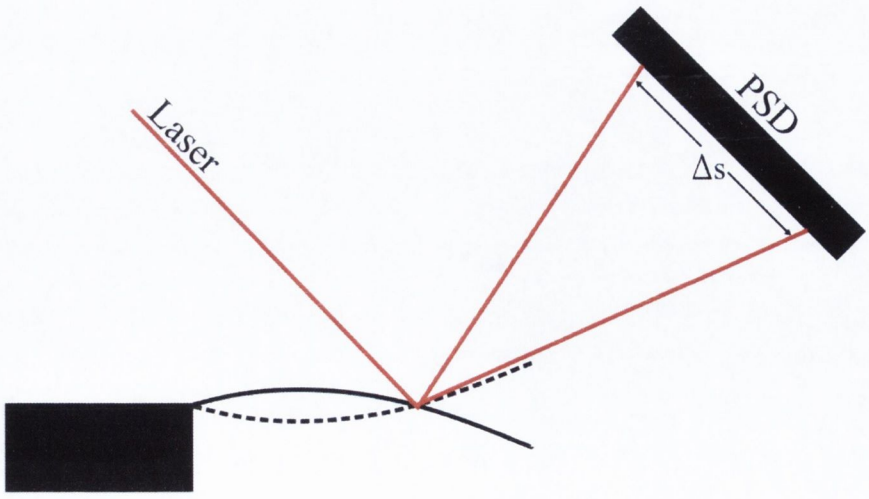


Figure 1.5: Illustration of Dynamic mode Operation. A laser spot is focused onto a node of vibration. Oscillation of the cantilever at its resoance frequency results in the movement of the deflected laser spot on the surface of a PSD.

It is found that $\beta_1$ =1.875, $\beta_2$ = 4.694.... $\beta_n$ = $\pi(n-0.5)$ (where $n$=1,2,3....). A mass ($\Delta m$) uniformly adsorbed on the cantilever's surface can be related to a change in resonance frequency ($\Delta f$) by [55]

$$\Delta m = \frac{\beta_n^4}{4\pi^2 L^3} EI \left(\frac{1}{f_n'^2} - \frac{1}{f_n^2}\right) \qquad 1.7$$

where $f_n'$ and $f_n$ correspond to the cantilever resonance frequencies after mass addition and of the unloaded beam respectively. The effect of adsorbed point masses is seen to have a different effect on the resonance frequencies of cantilevers. This is discussed in detail in Chapter 5.

The mass sensitivity ($S$) of a cantilever is given by [55]

$$S = \frac{\Delta f}{\Delta m} = \frac{f_n}{2m_b}. \qquad 1.8$$

Combining Equations 1.5 and 1.8 gives

$$S = \beta_n^2 C \qquad 1.9$$

where $C$ is given by

$$C = \frac{1}{4\pi m_b^{3/2}} \sqrt{\frac{EI}{L^3}}. \qquad 1.10$$

Thus, the mass sensitivity of a measurement increases when higher modes of vibration are used. The quality factor ($Q$) of a cantilever is defined by

$$Q = \frac{2\pi W_s}{W_d} \qquad 1.11$$

where $W_s$ is the stored vibrational energy and $W_d$ is the energy lost per cycle of vibration that can include thermoelastic loses, viscous damping due to the surrounding medium, and acoustic loses to the support. The $Q$ factor determines the slope of the amplitude and phase curves near resonance and hence significantly determines the accuracy of resonance frequency measurement [39]. Each of the loss mechanisms mentioned has an associated quality factor ($Q_i$) and thus the overall quality factor can be given by

$$\frac{1}{Q} = \sum_i \frac{1}{Q_i}. \qquad 1.12$$

If only viscous, acoustic, support, and thermoelastic losses are considered the quality factor is seen to increase with mass loading on the cantilever [57]. Cantilevers operated in dynamic mode have been employed for mass detection since the mid-1990s by Thundat *et al.* [33]. Development of sensor fabrication techniques has resulted in nanoscale cantilever sensors which have achieved a mass resolution of 1 ag ($a=10^{-18}$) in ambient conditions as described by the group of Rouke's [58].

Throughout this thesis acquired resonance peaks are fit using a simple harmonic oscillator model [58]

$$A(f) = A_{bl} + \frac{A_0 f_n^2}{\sqrt{(f^2 - f_n^2)^2 + \frac{f^2 f_n^2}{Q^2}}} \qquad 1.13$$

where $A_{bl}$ is the amplitude of the baseline, $A_0$ is the zero frequency amplitude, $f$ is the frequency, and $Q$ the quality factor. The $f_n$ and $Q$ values are extracted from acquired peaks via a best fit of Equation 1.13 using a Levenberg-Marquardt algorithm [60].

## 1.4 Cantilevers as Biosensors

The unprecedented sensitivity offered by cantilevers has resulted in their emergence as biosensors in the last 20 years. The biggest advantage of using these sensors is that they allow for label free detection to be performed. In the first reported use of cantilevers as biosensors Fritz *et al.* demonstrated that it was possible to detect single base pair (bp) mismatches between two 12-mer oligonucleotides in a liquid environment [61]. Since this time the use of cantilevers has been reported in the fields of proteomics [62, 63] and genomics [64-66]. The detection of single virus particles [67, 68] and binding of bacteriophage particles to *E. coli* FhuA protein receptors reconstituted in *lipid bilayers* has also been shown [69]. The majority of these works have been performed using static mode measurements with some, namely virus detection, being performed using dynamic mode.

Another area where cantilevers have been applied is in the detection of microbial cells. Several works have been published where cantilevers operated in dynamic mode have been utilised as mass sensors for pathogen detection. The detection of *E. coli* using antibody sensitised cantilevers was first reported at the beginning of the millennium [70, 71]. Here the dip-dry method was used where functionalised sensors are incubated in cell suspensions and then removed and dried. Using this method the detection of a single bacterial cell was possible. Other work was published shortly after this employing the dip-dry method with antibody sensitised cantilevers for the detection of *Listeria innocua* (*L. innocua*) [72]. Here it was estimated that 62 bacterial cells were captured by the antibodies on the cantilever after incubation in a phosphate buffered saline (PBS) cell suspension at a concentration of $5 \times 10^6$-$5 \times 10^8$ cfu/mL. The group of Mutharasan has published extensive work detailing the detection of *E. coli* using antibody sensitised sensors [73-77] in various liquid environments. Here, rather large Piezoelectric Excited Millimetre sized Cantilevers (PEMC) operated in dynamic mode are utilised. Specific antibody sensitised versions of these sensors have also allowed for the detection of *Bacillus anthracis* (*B. anthracis*) [78, 79] from suspension and also from a mixed suspension containing different *Bacillus* species [80]. Similar methods have allowed for the detection of *Acholeplasma laidlawii* (*A. laidlawii*) [81] in liquid broth and *Listeria monocytogenes* (*L. monocytogenes*) in milk [82].

Techniques moving away from antibody-antigen immobilisation have also been reported. The detection of yeast cells (*Saccharomyces cerevisiae* (*S. cerevisiae*)) using poly-L-lysine functionalised PEMCs has been demonstrated [83]. Recently the detection of *E. coli* has been reported using α-D-mannose functionalised sensors. Detection is based on binding of fimbriae (lectins used by the cell for adhesion) on the bacterial cell wall with the α-D-mannose receptors. Using this technique it was possible to differentiate between cells expressing normal fimbriae and those expressing abnormal fimbriae [84].

Only two works have been published which employ the static deflection mode for pathogen detection. The first reported work uses an antibody sensitised V-shaped cantilever in a fluid cell for the detection of *Salmonella enterica* (*S. enterica*) without the use of an *in situ* reference sensor [85]. Here the limit of detection is reported to be 25 cells. Static detection of *Bacillus subtilis* (*B. subtilis*) was also reported using a peptide functionalisation to anchor cells to the cantilever [86]. Detection limits using cantilever

sensors range from 1-$10^8$ cfu/mL. Detection is greatly influenced by the size of the sensor used. The main issue with the work discussed here is not its sensitivity but its inability to perform live/dead cell discrimination which is also one of the main drawbacks of currently used PCR techniques.

### 1.4.1 Microorganism Growth Detection

In order to overcome the difficultly of live/dead cell discrimination the use of cantilever sensors for the real time monitoring of microbe growth has been developed. A limited number of works have been published outlining the use of cantilever sensors in this fashion with all but one employing the dynamic mode of operation for detection.

The group of Mutharasan has again been active in this area. Using a PEMC the detection of *E. coli* was possible within 1 hour. A liquid drop of agar medium was deposited on the sensor and allowed to dry after spreading. A 50 µL droplet of *E. coli* suspension was then deposited on the sensor. The sensor was incubated at 29 °C. The relative humidity levels used are not discussed but just indicated as being stable. These measurements were not performed using an *in situ* reference sensor and as all nutrition is located on the sensor's surface the cause of the negative resonance frequency shift is unclear and is not disclosed [87]. The detection of *E. coli* has also been reported in a liquid environment using a poly-L-lysine sensitised PEMC. Here detection is based on the accumulation of 2',7'-bis-(2-carboxyethyl)-5-(and-6)-carboxyfluorescein acetoxymethyl ester (BCECF-AM) in live cells. Upon the introduction of BCECF-AM into the fluid chamber it is possible to detect growth of ~2000 cells in < 1 hour [88]. As indicated by Equation 1.8 the sensitivity of a measurement is inversely proportional to the mass of the cantilever used. The mass responsivities reported in [87, 88] are in the order of pg/Hz. These values are of the same magnitude as those which are reported in subsequent sections of this thesis and other publications where micron sized sensors are employed. The measurements reported in [87, 88] are single cantilever measurements without the use of *in situ* reference sensors which, as is shown here, is a requirement for successful monitoring of microorganism growth. For these reasons it is believed that these measurements deserve a second look in regards to specificity and whether the presented data is free from convolution by environmental influences.

The group of Hegner has utilised silicon cantilever arrays for the detection of bacteria and fungi. Here all growth measurements are conducted in a humid environment (> 95 %) and it is postulated that an increase in mass is observed on the sensors surface due to assimilation of water from the air by growing microbes. All measurements were performed with *in situ* reference sensors allowing for elimination of unwanted signals. The detection of *A. niger* growth within 4 hours is reported in [11, 89]. Nutrition is supplied by immersion of the sensor in malt extract medium after immobilisation of spores on the sensors using the antibody immunoglobulin G. A second technique used for detection of growth is the functionalisation of sensors with an agarose matrix [90, 91]. The nutrition for growth is retained in the agarose layer, thus the sensor resembles a miniaturised petri dish. Using this method growth of *E. coli* was reported within 1 hour. These measurements were performed using a commercial AFM. Detection of *A. niger* has also been reported using agarose functionalised sensors [92] and is described in Chapter 3 of this thesis.

Using static deflection of cantilevers detection of the growth of *S. cerevisiae* cells has been reported [93]. Polymer (polyimide) microcantilevers in a liquid flow cell were used. Cell deposition was performed by immersion of the cantilever in a cell suspension and allowing cells to sediment on the gold coated side of the sensors. By this method monitoring of yeast growth was possible in real time. A point to note is that cells are not bound to the sensors surface. This may lead to cross contamination between sensors as different solutions are flown through the liquid cell. The authors mention that the cantilever deflection observed is likely related to the surface stress changes due to cell-cell and cell-substrate interactions but note that further investigation is required to determine the origin of the bending signal.

## 1.5 Mechanism of Growth Detection

In this thesis cantilever sensors are utilised for the detection of *Aspergillus* growth. To detect growth, cantilevers are operated in dynamic mode. Measured frequency shifts are caused by additional mass loading onto the cantilevers. The cantilever surface is

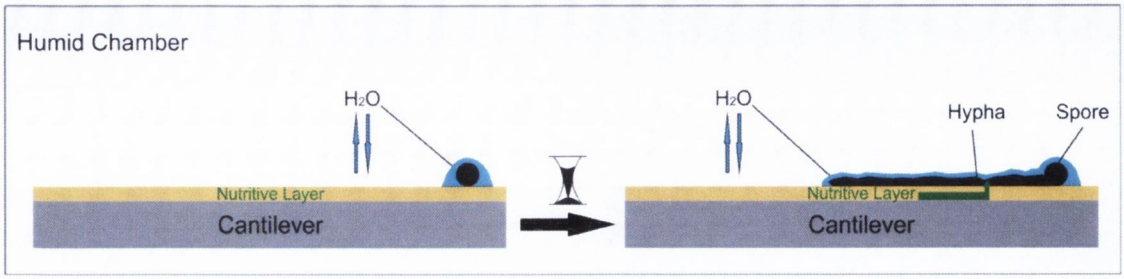


Figure 1.6: Fungal spore growing on cantilever. An agrose matrix on the sensor holds nutriltion for sustained growth. A water layer forms around the hydrophilic spore. Growth of hypha results in additional water adsorption on the sensor. This increase in mass on the sensor is measureable as a frequency shift.

functionalised with an agarose matrix which is loaded with nutrients to form a nutritive layer similar to that reported in [92]. The nutrition, which fungal spores assimilate out of the nutritive layer to generate biomass, stays inside the cells and as a fact of this the mass change on the cantilever is zero. Therefore no frequency shift due to microbial growth should be observed. Any detected frequency shifts can be interpreted as follows. The water contained in the nutritive layer is in equilibrium with the humid environment in which the cantilever is housed. When spores start to germinate they assimilate water from the humid environment. The resulting hyphal filaments are hydrophilic and thus adsorb water onto their surfaces. Observed frequency shifts are therefore due to additional water loading on the sensor. This is illustrated in Figure 1.6. The stiffness of the hyphal filaments is also seen to have an effect on the resonance frequency however this is dealt with in the subsequent chapters.

The growth of hyphal filaments may result in a change in surface stress as a result of hypha-surface interactions. This change in surface stress in theory could induce a static bending of the cantilever through the minimisation of this surface energy variation. Thus, any measurable bending of the cantilever would give a qualitative indication of viable spore growth. The change in surface stress is dependent on the magnitude of interaction between the hypha and the surface of the cantilever. The force at which hypha adhere to the cantilever can vary greatly. Surface stress changes are also greatly reduced through the presence of a relatively soft nutritive agarose layer. No static deflection of the cantilever is observed through-out this work and thus any surface stress variations induced through

hypha-cantilever interactions are deemed to be insufficient to produce any measureable effect.

## 1.6 Scope

To date microorganism determination and growth detection using microcantilevers has been mostly performed using single cantilevers without the use of suitable reference sensors [73-84]. Where microcantilever arrays have been utilised, measurements have been performed using a commercial AFM head requiring manual manipulation of input optics for measurement of several cantilevers [89-91]. In order to perform rapid and reliable growth measurements there is a need for a device capable of the automated readout of cantilevers in an array. In this thesis the development of three devices capable of the readout of the dynamic response of cantilevers in an array is outlined. These devices are geared towards the measurement of microbe growth and are hence designed to operate at elevated humidity conditions. This thesis outlines the development of these devices in a chronological order with growth measurements performed using each also described.

**Chapter 2** outlines the cantilever preparation techniques used for the described experiments. Particular attention is paid to methods of microbe deposition on sensors.

**Chapter 3** describes the further development of an existing fibre optic based device for the measurement of cantilever resonance frequencies. *A. niger* growth measurements performed using this device are described. Issues with this instrument and justification for development of addition cantilever devices are given.

**Chapter 4** presents the development of a device capable of the readout of higher resonance modes of cantilevers in an array. Measurements outlining the performance of this device are described. The majority of biological measurements presented in the remainder of this thesis are carried out using this instrument.

**Chapter 5** describes the detection of single *A. niger* spore growth. Real time imaging of the sensors during frequency measurements facilitates detailed interpretation of the multimodal response of cantilevers.

**Chapter 6** presents the use of cantilevers for the performance of antibiotic susceptibility testing. Tests are performed using two *Aspergillus* species, one of which has significant clinical relevance.

**Chapter 7** outlines the use of piezoresistive cantilevers for the measurement of fungi growth.

## 1.7 References


1. Madigan, M., Martinko, J., Dunlap, P., Clark, D., *Brock Biology of Microorganisms 12th edn.* 2009, Pearson Benjamin Cummings, ISBN0-321-53615-0.
2. Patterson, T., *Aspergillosis*, in *Essentials of Clinical Mycology*, C.A. Kauffman, et al., Editors. 2011, Springer New York. p. 243-263.
3. Vandeputte, P., S. Ferrari, and A.T. Coste, *Antifungal resistance and new strategies to control fungal infections.* International journal of microbiology, 2012. **2012**: p. 713687.
4. Maschmeyer, G., A. Haas, and O.A. Cornely, *Invasive Aspergillosis - Epidemiology, diagnosis and management in immunocompromised patients.* Drugs, 2007. **67**(11): p. 1567-1601.
5. Schuster, E., et al., *On the safety of Aspergillus niger - a review.* Applied Microbiology and Biotechnology, 2002. **59**(4-5): p. 426-435.
6. Koch, A.L., *Kinetics of Mycelial Growth.* Journal of General Microbiology, 1975. **89**(Aug): p. 209-216.
7. Moser, C.L. and B.K. Meyer, *Comparison of Compendial Antimicrobial Effectiveness Tests: A Review.* Aaps Pharmscitech, 2011. **12**(1): p. 222-226.
8. *United States Pharmacopeia. USP <51>. Antimicrobial effectiveness testing. Rockville, MD.*
9. *European Pharmacopeia. EP <5.1.3> Efficacy of antimicrobial preservatives.*
10. *Japanese Pharmacopeia. JP <19> Preservative effectiveness tests.*
11. Nugaeva, N., et al., *Micromechanical cantilever array sensors for selective fungal immobilization and fast growth detection.* Biosensors and Bioelectronics, 2005. **21**(6): p. 849-856.
12. Lazcka, O., F.J.D. Campo, and F.X. Muñoz, *Pathogen detection: A perspective of traditional methods and biosensors.* Biosensors and Bioelectronics, 2007. **22**(7): p. 1205-1217.
13. Sibley, C.D., G. Peirano, and D.L. Church, *Molecular methods for pathogen and microbial community detection and characterization: Current and potential application in diagnostic microbiology.* Infection, Genetics and Evolution, 2012. **12**(3): p. 505-521.
14. Kourkoumpetis, T.K., et al., *Polymerase Chain Reaction-Based Assays for the Diagnosis of Invasive Fungal Infections.* Clinical Infectious Diseases, 2012. **54**(9): p. 1322-1331.
15. Sharma, H. and R. Mutharasan, *Review of Biosensors for Foodborne Pathogens and Toxins.* Sensors and Actuators B: Chemical, 2013. In Press.
16. Del Bono, V., M. Mikulska, and C. Viscoli, *Invasive aspergillosis: diagnosis, prophylaxis and treatment.* Curr Opin Hematol, 2008. **15**(6): p. 586-93.
17. Maschmeyer, G., A. Haas, and O.A. Cornely, *Invasive aspergillosis: epidemiology, diagnosis and management in immunocompromised patients.* Drugs, 2007. **67**(11): p. 1567-601.
18. Galimberti, R., et al., *Emerging systemic fungal infections.* Clin Dermatol, 2012. **30**(6): p. 633-50.
19. Müller, F.-M.C., M. Seidler, and A. Beauvais, *Aspergillus fumigatus biofilms in the clinical setting.* Medical Mycology, 2011. **49**(S1): p. S96-S100.

20. Narsaiah, K., et al., *Optical biosensors for food quality and safety assurance—a review.* Journal of Food Science and Technology, 2012. **49**(4): p. 383-406.
21. Taylor, A.D., et al., *Quantitative and simultaneous detection of four foodborne bacterial pathogens with a multi-channel SPR sensor.* Biosensors and Bioelectronics, 2006. **22**(5): p. 752-758.
22. Tawil, N., et al., *Surface plasmon resonance detection of E. coli and methicillin-resistant S. aureus using bacteriophages.* Biosensors and Bioelectronics, 2012. **37**(1): p. 24-29.
23. Rijal, K., et al., *Detection of pathogen Escherichia coli O157:H7 AT 70 cells/mL using antibody-immobilized biconical tapered fiber sensors.* Biosensors and Bioelectronics, 2005. **21**(6): p. 871-880.
24. Ohk, S.H., et al., *Antibody–aptamer functionalized fibre-optic biosensor for specific detection of Listeria monocytogenes from food.* Journal of Applied Microbiology, 2010. **109**(3): p. 808-817.
25. Perumal, V. and U. Hashim, *Advances in biosensors: principle, architecture and applications.* J Appl Biomed, 2013. **11**.
26. Handley, J., *Product Review: Quartz Crystal Microbalances.* Analytical Chemistry, 2001. **73**(7): p. 225 A-229 A.
27. Cooper, M.A. and V.T. Singleton, *A survey of the 2001 to 2005 quartz crystal microbalance biosensor literature: applications of acoustic physics to the analysis of biomolecular interactions.* Journal of Molecular Recognition, 2007. **20**(3): p. 154-184.
28. Zhang, S., et al., *Monitoring Environmental WasteWater Using A Piezoelectric Impedance Microbial Sensing Technique.* International Journal of Environmental Analytical Chemistry, 2002. **82**(3): p. 113 - 122.
29. Singh, A., S. Poshtiban, and S. Evoy, *Recent Advances in Bacteriophage Based Biosensors for Food-Borne Pathogen Detection.* Sensors, 2013. **13**(2): p. 1763-1786.
30. Wang, Y., Z. Ye, and Y. Ying, *New Trends in Impedimetric Biosensors for the Detection of Foodborne Pathogenic Bacteria.* Sensors, 2012. **12**(3): p. 3449-3471.
31. Balasubramanian, S., et al., *Lytic phage as a specific and selective probe for detection of Staphylococcus aureus--A surface plasmon resonance spectroscopic study.* Biosens Bioelectron, 2007. **22**(6): p. 948-55.
32. Binnig, G., C.F. Quate, and C. Gerber, *Atomic Force Microscope.* Physical Review Letters, 1986. **56**(9): p. 930-933.
33. Thundat, T., et al., *Thermal and Ambient-Induced Deflections of Scanning Force Microscope Cantilevers.* Applied Physics Letters, 1994. **64**(21): p. 2894-2896.
34. Thundat, T., et al., *Detection of mercury vapor using resonating microcantilevers.* Applied Physics Letters, 1995. **66**(13): p. 1695-1697.
35. Barnes, J.R., et al., *A femtojoule calorimeter using micromechanical sensors.* Review of Scientific Instruments, 1994. **65**(12): p. 3793-3798.
36. Barnes, J.R., et al., Photothermal spectroscopy with femtojoule sensitivity using a micromechanical device. Nature, 1994. **372**(6501): p. 79-81.
37. Anja, B., et al., *Cantilever-like micromechanical sensors.* Reports on Progress in Physics, 2011. **74**(3): p. 036101.
38. Calleja, M., et al., *Challenges for nanomechanical sensors in biological detection.* Nanoscale, 2012. **4**(16): p. 4925-4938.
39. Tamayo, J., et al., *Biosensors based on nanomechanical systems.* Chemical Society Reviews, 2013. **42**(3): p. 1287-1311.

40. Arlett, J.L., E.B. Myers, and M.L. Roukes, *Comparative advantages of mechanical biosensors.* Nature Nanotechnology, 2011. **6**(4): p. 203-215.
41. Lang, H.P., M. Hegner, and C. Gerber, *Nanomechanical Cantilever Array Sensors*, in *Springer Handbook of Nanotechnology*, B. Bhushan, Editor. 2010, Springer Berlin Heidelberg. p. 427-452.
42. Waggoner, P. and H. Craighead, *Micro- and nanomechanical sensors for environmental, chemical, and biological detection.* Lab on a Chip, 2007. **7**(10): p. 1238-1255.
43. Johansson, A., et al., *SU-8 cantilever sensor system with integrated readout.* Sensors and Actuators A: Physical, 2005. **123–124**(0): p. 111-115.
44. Lang, H.P., et al., *A chemical sensor based on a micromechanical cantilever array for the identification of gases and vapors.* Applied Physics a-Materials Science & Processing, 1998. **66**: p. S61-S64.
45. Meyer, G. and N.M. Amer, *Novel optical approach to atomic force microscopy.* Applied Physics Letters, 1988. **53**(12): p. 1045-1047.
46. Jensen, J., N. Maloney, and M. Hegner, *A Multi-Mode Platform for Cantilever Arrays Operated in Liquid* Sensors and Actuators B: Chemical (In Press), 2013(0).
47. Battiston, F.M., et al., *A chemical sensor based on a microfabricated cantilever array with simultaneous resonance-frequency and bending readout.* Sensors and Actuators B-Chemical, 2001. **77**(1-2): p. 122-131.
48. Boisen, A., et al., *Environmental sensors based on micromachined cantilevers with integrated read-out.* Ultramicroscopy, 2000. **82**(1–4): p. 11-16.
49. Itoh, T. and T. Suga, *Development of a force sensor for atomic force microscopy using piezoelectric thin films.* Nanotechnology, 1993. **4**(4): p. 218.
50. Rogers, B., et al., *Mercury vapor detection with a self-sensing, resonating piezoelectric cantilever.* Review of Scientific Instruments, 2003. **74**(11): p. 4899-4901.
51. Blanc, N., et al., *Scanning force microscopy in the dynamic mode using microfabricated capacitive sensors.* Journal of Vacuum Science & Technology B, 1996. **14**(2): p. 901-905.
52. Korsunsky, A.M., et al., *On the micromechanics of micro-cantilever sensors: Property analysis and eigenstrain modeling.* Sensors and Actuators a-Physical, 2007. **139**(1-2): p. 70-77.
53. R.Mishra, et. al., *Rapid and Reliable Calibration of Laser Beam Deflection System for Microcantilever-Based Sensor Setups.* Journal of Sensors, 2012. 6 pages. doi:10.1155/2012/617386
54. Stoney, G.G., *The Tension of Metallic Films Deposited by Electrolysis.* Proceedings of the Royal Society of London. Series A, Containing Papers of a Mathematical and Physical Character, 1909. **82**(553): p. 172-175.
55. Murali Krishna, G. and et al., *Higher modes of vibration increase mass sensitivity in nanomechanical microcantilevers.* Nanotechnology, 2007. **18**(44): p. 445502.
56. Tamayo, J., et al., *Effect of the adsorbate stiffness on the resonance response of microcantilever sensors.* Applied Physics Letters, 2006. **89**(22): p. -.
57. Dufour, I., et al., *Effect of Coating Viscoelasticity on Quality Factor and Limit of Detection of Microcantilever Chemical Sensors*. Sensors Journal, IEEE 7, no. 2 (2007): 230-236.
58. Li, M., H.X. Tang, and M.L. Roukes, *Ultra-sensitive NEMS-based cantilevers for sensing, scanned probe and very high-frequency applications.* Nature Nanotechnology, 2007. **2**(2): p. 114-120.

59. Jensen, J. and M. Hegner, *Predictions of the Compressible Fluid Model and its Comparison to Experimental Measurements of* Journal of Sensors, 2011. **2012**.
60. Levenberg, K., *A method for the solution of certain problems in least squares.* Quart. Applied Math., 1944. **2**: p. 164-168.
61. Fritz, J., et al., *Translating biomolecular recognition into nanomechanics.* Science, 2000. **288**(5464): p. 316-318.
62. Arntz, Y. and et al., *Label-free protein assay based on a nanomechanical cantilever array.* Nanotechnology, 2003. **14**(1): p. 86.
63. Backmann, N., et al., *A label-free immunosensor array using single-chain antibody fragments.* Proceedings of the National Academy of Sciences of the United States of America, 2005. **102**(41): p. 14587-14592.
64. Zhang, J., et al., *Rapid and label-free nanomechanical detection of biomarker transcripts in human RNA.* Nature Nanotechnology, 2006. **1**(3): p. 214-220.
65. Mertens, J., et al., *Label-free detection of DNA hybridization based on hydration-induced tension in nucleic acid films.* Nature Nanotechnology, 2008. **3**(5): p. 301-307.
66. Huber, F., et al., *Direct detection of a BRAF mutation in total RNA from melanoma cells using cantilever arrays.* Nature Nanotechnology, 2013. **8**(2): p. 125-129.
67. Gupta, A., D. Akin, and R. Bashir, *Single virus particle mass detection using microresonators with nanoscale thickness.* Applied Physics Letters, 2004. **84**(11): p. 1976-1978.
68. Ilic, B., Y. Yang, and H.G. Craighead, *Virus detection using nanoelectromechanical devices.* Applied Physics Letters, 2004. **85**(13): p. 2604-2606.
69. Braun, T., et al., *Quantitative time-resolved measurement of membrane protein-ligand interactions using microcantilever array sensors.* Nature Nanotechnology, 2009. **4**(3): p. 179-185.
70. Ilic, B., et al., *Single cell detection with micromechanical oscillators.* Journal of Vacuum Science & Technology B, 2001. **19**(6): p. 2825-2828.
71. Ilic, B., et al., *Mechanical resonant immunospecific biological detector.* Applied Physics Letters, 2000. **77**(3): p. 450-452.
72. Gupta, A., D. Akin, and R. Bashir, *Detection of bacterial cells and antibodies using surface micromachined thin silicon cantilever resonators.* Journal of Vacuum Science & Technology B: Microelectronics and Nanometer Structures, 2004. **22**(6): p. 2785-2791.
73. Maraldo, D., et al., *Method for label-free detection of femtogram quantities of biologics in flowing liquid samples.* Analytical Chemistry, 2007. **79**(7): p. 2762-2770.
74. Campbell, G.A. and R. Mutharasan, *A method of measuring Escherichia coli O157 : H7 at 1 cell/mL in 1 liter sample using antibody functionalized piezoelectric-excited millimeter-sized cantilever sensor.* Environmental Science & Technology, 2007. **41**(5): p. 1668-1674.
75. Campbell, G.A., et al., *Detect of Escherichia coli O157 : H7 in ground beef samples using piezoelectric excited millimeter-sized cantilever (PEMC) sensors.* Biosensors & Bioelectronics, 2007. **22**(7): p. 1296-1302.
76. Campbell, G.A. and R. Mutharasan, *Detection of pathogen Escherichia coli O157 : H7 using self-excited PZT-glass microcantilevers.* Biosensors & Bioelectronics, 2005. **21**(3): p. 462-473.

77. Campbell, G.A. and R. Mutharasan, *Escherichia coli O157 : H7 detection limit of millimeter-sized PZT cantilever sensors is 700 Cells/mL.* Analytical Sciences, 2005. **21**(4): p. 355-357.
78. Campbell, G.A., D. deLesdernier, and R. Mutharasan, *Detection of airborne Bacillus anthracis spores by an integrated system of an air sampler and a cantilever immunosensor.* Sensors and Actuators B-Chemical, 2007. **127**(2): p. 376-382.
79. Campbell, G.A. and R. Mutharasan, *Detection of Bacillus anthracis spores and a model protein using PEMC sensors in a flow cell at 1 mL/min.* Biosensors & Bioelectronics, 2006. **22**(1): p. 78-85.
80. Campbell, G.A. and R. Mutharasan, *Piezoelectric-excited millimeter-sized cantilever (PEMC) sensors detect Bacillus anthracis at 300 spores/mL.* Biosensors & Bioelectronics, 2006. **21**(9): p. 1684-1692.
81. Xu, S., H. Sharma, and R. Mutharasan, *Sensitive and Selective Detection of Mycoplasma in Cell Culture Samples Using Cantilever Sensors.* Biotechnology and Bioengineering, 2010. **105**(6): p. 1069-1077.
82. Sharma, H. and R. Mutharasan, *Rapid and sensitive immunodetection of Listeria monocytogenes in milk using a novel piezoelectric cantilever sensor.* Biosensors & bioelectronics, 2013. **45**: p. 158-62.
83. Yi, J.W., et al., *In situ cell detection using piezoelectric lead zirconate titanate-stainless steel cantilevers.* Journal of Applied Physics, 2003. **93**(1): p. 619-625.
84. Tzen, T.-R.J., et al., *Adhesin-Specific Nanomechanical Cantilever Biosensors for Detection of Microorganisms.* Journal of Heat Transfer-Transactions of the Asme, 2011. **133**(1).
85. Weeks, B.L., et al., *A microcantilever-based pathogen detector.* Scanning, 2003. **25**(6): p. 297-9.
86. Dhayal, B., et al., *Detection of Bacillus subtilis Spores Using Peptide-Functionalized Cantilever Arrays.* Journal of the American Chemical Society, 2006. **128**(11): p. 3716-3721.
87. Detzel, A.J., G.A. Campbell, and R. Mutharasan, *Rapid assessment of Escherichia coli by growth rate on piezoelectric-excited millimeter-sized cantilever (PEMC) sensors.* Sensors and Actuators B: Chemical, 2006. **117**(1): p. 58-64.
88. Xu, S. and R. Mutharasan, *Cell Viability Measurement Using 2 ',7 '-Bis-(2-carboxyethyl)-5-(and-6)-carboxyfluorescein Acetoxymethyl Ester and a Cantilever Sensor.* Analytical Chemistry, 2011. **83**(4): p. 1480-1483.
89. Natalia Nugaeva, K.Y.G., Natalia Backmann, Marcel Düggelin, Hans Peter Lang, Hans-Joachim Güntherodt and Martin Hegner *An Antibody-Sensitized Microfabricated Cantilever for the Growth Detection of Aspergillus niger Spores.* Microscopy and Microanalysis, 2007. **13**: p. 13-17.
90. Gfeller, K.Y., N. Nugaeva, and M. Hegner, *Micromechanical oscillators as rapid biosensor for the detection of active growth of Escherichia coli.* Biosensors and Bioelectronics, 2005. **21**(3): p. 528-533.
91. Gfeller, K.Y., N. Nugaeva, and M. Hegner, *Rapid biosensor for detection of antibiotic-selective growth of Escherichia coli.* Applied and Environmental Microbiology, 2005. **71**(5): p. 2626-2631.
92. Maloney, N., et al., *Fibre Optic Readout of Microcantilever Arrays for Fast Microorganism Growth Detection.* Journal of Sensors, 2012. 6 pages. doi:10.1155/2012/405281.

93. Liu, Y., et al., *Label-free and real-time monitoring of yeast cell growth by the bending of polymer microcantilever biosensors.* Sensors and Actuators B: Chemical, 2013. **178**(0): p. 621-626.

# Chapter 2
# Cantilever Preparation

Growth of microbial cells is dependent on the provision of sufficient nutrition. In a clinical and industrial setting nutrition is typically provided by a solid agar medium contained in a petri dish. Here we treat a cantilever as a miniaturised petri dish and construct the nutritional layer around it. The cantilever is thus acting as the support for microbial growth and also the mechanical transducer capable of growth detection.

Cantilevers are extremely sensitive to virtually any stimulus and careful preparation is required to yield sensitive biosensors. In order to ensure the detection of the intended microbial target preparation protocols must take steps to ensure a sterile sensor is produced. In the subsequent sections the steps taken to prepare a cantilever biosensor capable of microorganism growth detection are outlined. First the cantilever array is cleaned before functionalisation with an epoxy-silane monolayer which allows for the covalent linkage of an agarose hydrogel to the sensors surface. For all biological measurements described throughout this thesis the preparation of the sensor follows these steps. Multiple techniques can be used for the provision of nutrition and the deposition of microbial cells, all of which are discussed in detail.

All chemicals and reagents are of analytical grade and were purchased from Sigma-Aldrich (Arklow, Ireland), unless otherwise stated.

## 2.1 Cleaning

Common contaminants on silicon wafers are organic vapours originating from lubricants, greases and photo resists used during processing, and organic compounds from plastic storage containers and human contact [1]. To ensure efficient functionalisation is carried out it is necessary to introduce cleaning steps to remove contaminants which may prevent the formation of a uniform agarose layer.

### 2.1.1 Piranha Cleaning

A hydrogen peroxide ($H_2O_2$) sulphuric acid ($H_2SO_4$) solution, named "piranha" solution, is widely used in the semiconductor industry to remove gross organic materials from Si wafers [1]. The cantilever array is immersed in several piranha baths ($H_2O_2$:$H_2SO_4$ = 1:1) for varying lengths of time (see Appendix 1). This "wet chemical" cleaning process eliminates organics via oxidation and renders the silicon surface hydrophilic through hydroxylation. This process may result in sulphur contamination due to the use of $H_2SO_4$, which is removed by rinsing several times with nanopure water and EtOH. The chemicals used in this protocol are extremely dangerous and highly reactive. This cleaning protocol was subsequently replaced by plasma etching which is much safer and more time efficient to perform.

### 2.1.2 Plasma Etching

Oxygen plasma can be used to eradicate organic contaminants from silicon surfaces. The organics are dissociated or excited by the adsorption of UV radiation generated by the plasma. Atomic O and ozone ($O_3$) are also generated by the dissociation of $O_2$ caused by UV radiation [1]. The generated oxygen species react with the excited molecules or free radical products of dissociated organics to produce fragmented volatile compounds which are evacuated from a chamber under partial vacuum. Treatment with $O_2$ plasma results in oxidation of the Si surface. Cantilever arrays are exposed to $O_2$ plasma for 3 minutes at a pressure of 3 mbar. A protocol used for plasma cleaning of the silicon cantilever arrays is shown in Appendix 2.

## 2.2 Silanisation

The use of self-assembled functional silane monolayers allows for the subsequent covalent linkage of polysaccharides to silicon wafers [2]. The cantilever array is incubated in an epoxy silane solution (3-glycidyloxypropyl-trimethoxysilane: N-ethyldiisopropylamine: water free toluene; 1: 1: 100) for 45 min and then washed twice in water-free toluene for 15 minutes. The cantilever array is then dried under nitrogen gas. See Appendix 3 for a detailed protocol.

## 2.3 Agarose Hydrogel Functionalisation

Agarose is a highly purified polysaccharide which is obtained from seaweed agar and is widely used in the field of DNA gel electrophoresis [3, 4]. Gels are formed due to entangling of individual polymer molecules upon cooling and the formation of hydrogen bonds between the individual polymer chains (Figure 2.1). The formed gels are capable of holding large amounts of water within their interior network [5]. A unique property of agarose hydrogels is that they are reversible with a hysteresis cycle over a temperature range. Numerous types of agarose are commercially available which differ in gelling temperature, melting temperature, gel strength, and pore size which is dependent on the length of the individual polymer chains.

Several types of agarose, including low gelling point agarose, were tested for suitability at the start of this project. SeaKem Agarose Gold® was found to be the most suitable for the formation of a uniform agarose layer. Modification of the cantilevers with agarose is carried out to provide a sponge like structure capable of retaining nutritional medium for the support of viable microorganism growth. Functionalisation is performed in dimension-matched glass capillary tubes (see Section 2.4.1). Agarose Gold has a gelling and melting temperature of ~ 36 °C and ≥ 90 °C respectively. To prevent gelation the capillary tubes are preheated for 35 minutes using a radiation lamp (Osram; Switzerland). Different methods of heating and preheating times were tested empirically. It was found that excessive heating results in rapid expulsion of the agarose solution from the front of the capillary tubes which renders the cantilever array to be functionalised unusable. Insufficient heating results in the gelation of the agarose gel in the capillary tubes which can prevent the solution reaching the front of the capillary tubes or can cause lumps of agarose to form on the cantilevers when immersed in the solution. The concentration of agarose solution used effects the gel strength and pore size. Different concentrations of gel solution were tested, ranging from 0.5-4 %. The optimal concentration was found to be 1 % (wt/vol). Concentrations below this were found to form a layer which appeared to have viscosity which was too low for retention of nutritional medium. Higher concentrations resulted in gelation when flown through the capillary tubes. The agarose gel strength at a concentration of 1% is ≥ 1800 g/cm$^2$. When used for DNA gel electrophoresis a 1% gel is used for the separation of DNA molecules with a length of 400-8000 base pairs (bp), where the length of a bp is 3.4 Å. This is indicative of the hydrogels pore size.

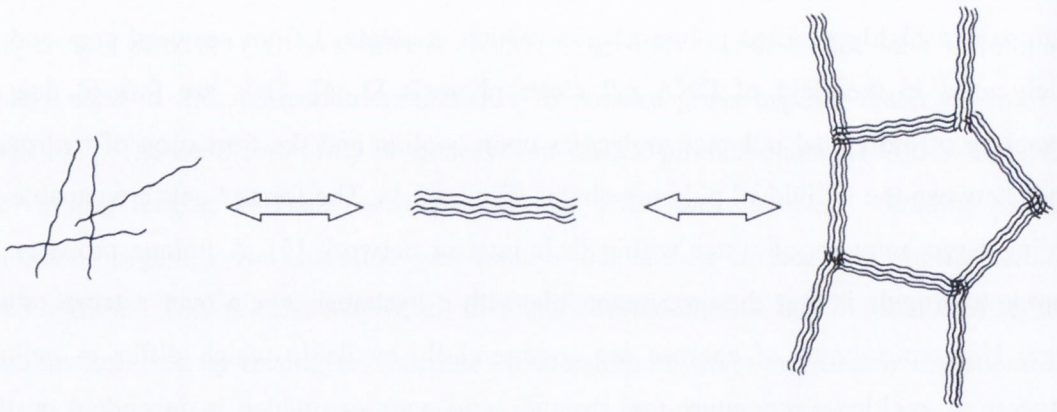

Figure 2.1: Agarose gel formation. Gels are formed as a result of the formation of hydrogen bonds between the individual polymer chains. The formed gels are capable of holding large amounts of water within their interior network.

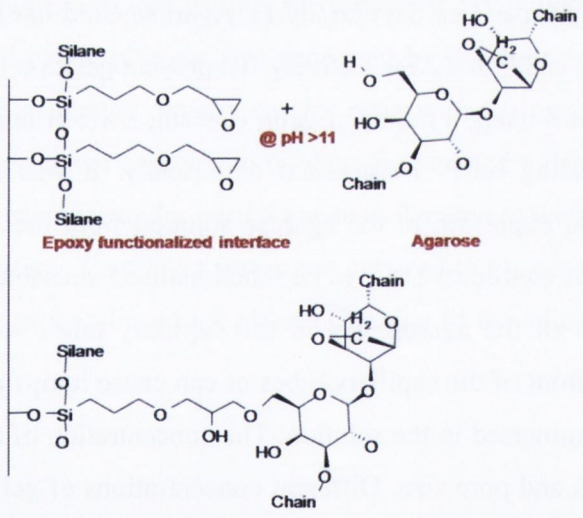


Figure 2.2: An epoxy silane is bound to the cantilever surface in order to bind an agarose layer to the cantilever surface. At a pH higher than 11 the hydroxyl groups of the sugar groups are deprotonated. The deprotonated $O^-$ allows a nucleophilic covalent linkage to the activated epoxy group on the interface. This enables the anchoring of individual agarose polymer chains on the sensor interface.

Covalent anchorage of the exposed hydroxyl groups on agarose to cantilevers functionalised with epoxy terminated groups is possible in alkali conditions (Figure 2.2). The pH of the 0.5 mL agarose solution (which is normally used in our functionalisation procedure) is adjusted to 11.9 by addition of 2 μL of 2 M NaOH solution prior to the filling of the capillary tubes. The adjusted pH results in the deprotonation of the agarose's hydroxyl groups. This facilitates a nucleophilic covalent linkage to the activated epoxy group on the cantilever. Best results have been observed when agarose functionalisation is performed immediately after silanisation. Elongated incubation at elevated pH levels and at high temperature results in hydrolysis of the agarose sugar chains. In this case gelation is not possible due to presence of shortened chains in the mixture. A colour change from clear to yellow is indicative of this occurring.

The protocol for preparation of the 1% (wt/vol) agarose solution and the functionalisation protocol can be found in Appendix 4. Figure 2.3 shows images of a blank silicon (which has been silanised) and two agarose functionalised sensors. The agarose layers shown display the typical variances which are observed in layer quality (Image B having a smoother more uniform layer). The visual differences in the layers as shown have been found to have no effect on resonance frequency measurements or microbial growth. The crescent shaped feature at the free end of the cantilevers is a common feature for all agarose functionalised sensors. It is a result of the removal of the cantilever through the agarose air interface. Non uniformities or accumulations of agarose are typically observed at the cantilever's clamped end. Figure 2.4 shows a scanning electron microscopy (SEM) image of a cantilever array where agarose accumulation has resulted in the formation of lumps at the cantilever's clamped end. This is due to the cooling of the agarose solution at the end of the capillary tube.

Several attempts have been made to measure the thickness of the agarose layer on the cantilever. Stylus profilometry is not possible due to the structure of the cantilever array. Methods such as AFM are hampered by the strong adhesion of the cantilever tip to the agarose structure in ambient conditions. The help of the Ultramicroscopy group (advanced microscopy laboratory, TCD) was enlisted to help with this problem. After gold coating of an agarose functionalised sensor (to prevent charge accumulation) a focused ion beam (FIB) was used to mill a trench in the structure. In Figure 2.5 a side view by SEM is

presented. A line intensity profile of the gold/agarose/silicon cross section returns a value of ~30 nm for the thickness of the dry agarose layer.

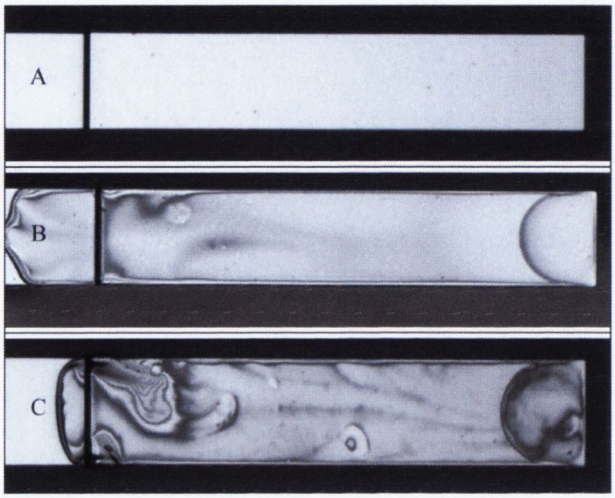


Figure 2.3: Images of agarose functionalised cantilevers, the width of a bar is 100 μm and the dark line on the left represents the clamped end of the cantilever. The crescent shaped feature at the free end of the cantilevers is a common feature for all agarose functionalised cantilevers and is a result of the removal of the cantilever through the agarose air interface. (A) Blank silicon cantilever after silanisation. (B) Agarose functionalised cantilever. (C) Agarose functionalised cantilever with surface irregularities.

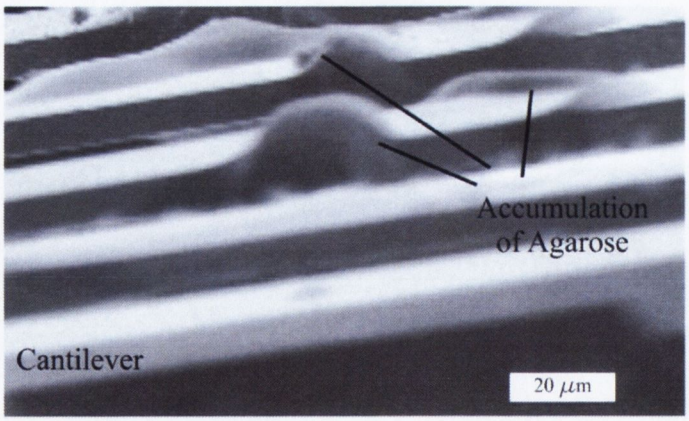


Figure 2.4: SEM side view image of agarose accumulations at the cantilevers clamped end. This is due to the cooling of the agarose solution at the end of the capillary tube.

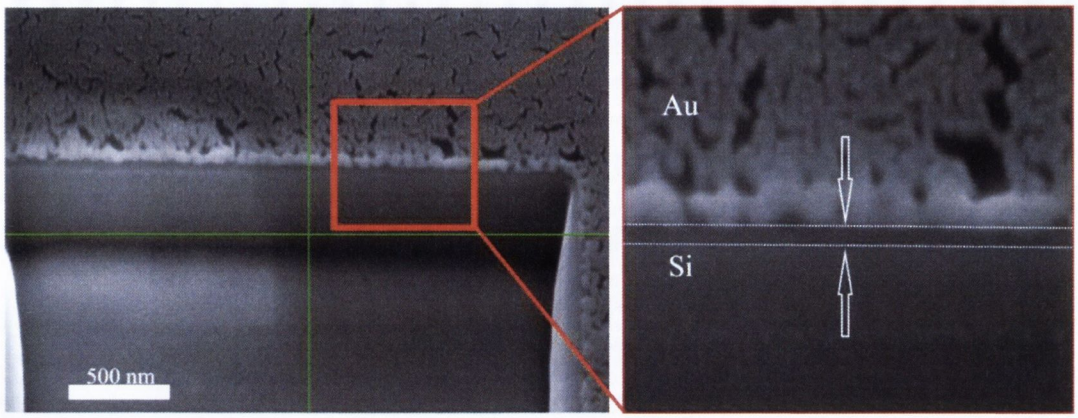


Figure 2.5: SEM image of Au/agarose/Si cross section after focused ion beam milling. An intensity profile returns an agarose thickness of ~ 30 nm. Image courtesy of Daniel Fox (TCD).

## 2.4 Microorganism and Nutritional Medium Deposition Techniques

Due to the physical size of the cantilevers and the small volume of cells to be deposited new techniques have been developed to enable the functionalisation of individual sensors in an array. In the subsequent sections three techniques for the deposition of cells and nutritional medium are discussed and compared.

Deposition of microbes can be carried out using capillary functionalisation, ink-jet printing, or glass needle manipulation. When capillary or ink-jet printing is used the cells are suspended in growth medium before deposition is carried out. Hence deposition of microbes and nutrition is carried out in parallel. In the case of glass needle manipulation the cantilever array is immersed in the desired nutritional medium before deposition of cells.

### 2.4.1 Capillary Functionalisation

Immersion of cantilevers into liquid filled capillary tubes is one of the most widely used functionalisation techniques at present [6]. This technique has been used for the deposition of bacterial cells [7, 8] and fungal spores [9, 10] in suspension. Capillary functionalisation is carried out using a custom device which allows for insertion of cantilevers into the

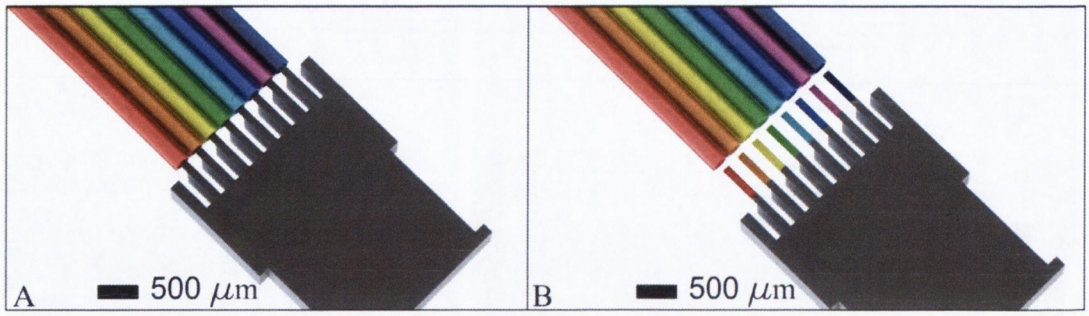


Figure 2.6: Capillary functionalisation of cantilever array (A) When the tubes are aligned as shown the pitch from the centre of each tube matches that of the cantilevers in the array (250 μm). (B) Using this technique cantilevers can receive individual functionalisations, allowing for multiple test and reference cantilevers to be included in one array.

suspension filled capillary tubes (OD 250±10 μm, ID 180±10 μm, length 50 mm, King Precision Glass Inc., CA, USA). When the tubes are aligned as shown in Figure 2.6, the pitch from the centre of each tube matches that of the cantilevers in the array (250 μm). Using this technique cantilevers can receive individual functionalisations (indicated in Figure 2.6 B by the use of different colours). When this is the case, the end of each capillary tube is placed into a larger capillary tube which acts as a liquid reservoir. When each cantilever is to receive the same functionalisation (*e.g.* during agarose functionalisation) the ends of the capillary tubes are inserted into the cut tip of an eppendorf tube which acts as a reservoir. Immersion times in the capillaries vary dependent on the functionalisation being carried out. For agarose coating immersion is for only 2-5 seconds. For deposition of spores and nutrition immersion times are typically in the order of 10 minutes. This provides sufficient time for sedimentation of microbes on the sensor.

Prior to use the capillary tubes are cleaned using oxygen plasma (3 min). The tubes are then rinsed with EtOH and dried prior to use. These cleaning steps ensure any lubrication or debris remaining from capillary manufacturing is removed. This is especially important when performing agarose functionalisation as debris in the tubes provides a nucleation point for the agarose. This can resulting in the formation of lumps on the cantilever as shown in Figure 2.4. These steps also ensure that any microbial contamination is also removed.

Capillary functionalisation allows for the uniform coverage of the sensor's surface with nutritional medium. This renders the entire cantilever structure suitable for the support of

viable microorganisms. The location of cell deposition however is not controllable as cells can sediment anywhere on the sensor's surface. This poses great difficulties when trying to interpret resonance frequency responses during growth measurements. Cell suspension coverage on the sensor can be controlled by the extent to which the cantilevers are inserted into the capillary tubes as shown in Figure 2.7 (A). Here agarose coated cantilevers were immersed to full, half and 1/5 of their lengths for 6, 4, and, 2 minutes respectively. The capillary tubes were loaded with *E. coli* suspension (10% Luria Broth (LB), $2.5\times10^8$ cfu/mL). The extent of nutritional coverage on the cantilevers is indicated by the green lines. It is observed that cells (~ 2 μm diameter) accumulate in the liquid front at the open end of the capillary tubes resulting in an increased cell deposition on the cantilevers at this position (Figure 2.7 (B)). The images shown in Figure 2.7 are SEM images, the protocol for sample preparation and cell dehydration for SEM imaging can be found in Appendix 5.

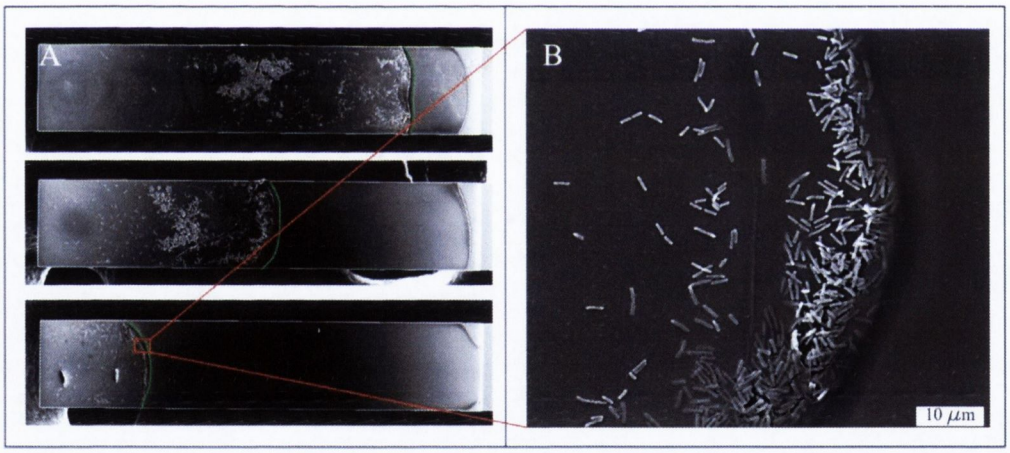


Figure 2.7: Scanning electron microscope images of cantilever arrays after capillary functionalisation. (A) Agarose-coated cantilevers were immersed to full, half and 1/5 of their lengths for 6, 4, and 2 minutes, respectively. The capillary tubes were loaded with *E. coli* suspension (10% LB, $2.5\times10^8$ cells/mL). The extent to which the cantilevers are inserted into the capillary tubes provides some control on the area functionalised. (B) Magnification of the point where the liquid/air interface during capillary functionalisation is located. Microbes accumulate at the liquid front at the open end of the capillary tubes resulting in increased numbers of deposited cells.

### 2.4.2 Ink-Jet Printing

Drop on Demand (DOD) Ink-jet printing is a deposition technique for liquid phase materials where a solute is dissolved or dispersed in a solvent. Ink-jet printing is widely used in several biological fields such as tissue engineering [11], drug deposition [12], and the deposition of proteins for the creation of diagnostic microarrays [13]. In the field of cantilever array research ink-jet printing has been used for the functionalisation of cantilever arrays with different biomolecules [14, 15] and live microbial cells [16]. Typically droplet formation is via a piezoelectric print head (piezoelectric actuator on a micro pipette) where the voltage supplied to a piezoelectric actuator generates short pressure waves in the liquid contained in a capillary tube. When the kinetic energy of the generated pressure waves is sufficient to overcome the surface tension at the capillaries open end a small volume of liquid breaks off the liquid column to form a droplet. A more detailed description of droplet formation can be found in [17].

The DOD dispensing system (MD-P-801, Microdrop, Norderstedt, Germany) used is comprised of a piezo-driven pipette (AD-K-501) mounted on a three axis micro positioning system which has a positional accuracy of 1 μm in all directions (Figure 2.8). Pipettes with three different nozzle diameters (30, 50, 70 μm) are available. The volume of the formed droplet is dependent on the pipette used, the viscosity of the solvent used, and the voltage and pulse length applied to the piezo actuator. In order to deposit one droplet per pulse these parameter settings have to be adjusted for each individual suspension prior to deposition. The final spot diameter depends on the surface tension of the printed material and on the surface on which it is deposited. Instrument control is via a computer program that also allows for automated patterns of droplets to be generated. A camera with accompanying custom made optics is mounted on the system. This allows for accurate positioning of the pipette over the desired deposition position via its 180 ° viewing range.

Prior to functionalisation the pipette is aligned to the desired deposition position. The prepared cell suspensions are loaded into 96-well microtiter plates (Sterilin Ltd., Norwick, UK). The position of each well is pre-programmed in the control software allowing for rapid filling of the pipette. Prior to filling the pipette is cleaned with EtOH to remove any microbial contamination. The pipette is left to dry and then washed once with the solution to be deposited to ensure any remaining ethanol is removed. Using a stroboscopic camera

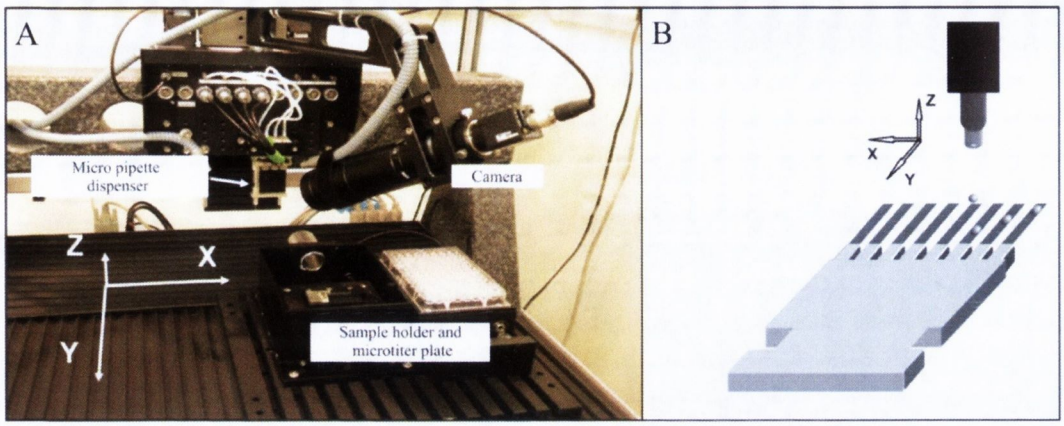


Figure 2.8: (A) Ink-jet printing instrument. The DOD dispensing system (MD-P-801, Microdrop, Norderstedt, Germany) used is comprised of a piezo-driven pipette (AD-K-501) mounted on a three-axis micro positioning system with a positional accuracy of 1 μm in all directions. Solutions to be deposited are loaded into a microtiter plate. A camera with accompanying optics, which has a viewing range of 180 °, aids alignment to spotting positions. (B) Schematic of ink-jet printing of droplets on a cantilever array. Droplet formation is via a piezoelectric print head.

incorporated into the instrument the parameters (i.e. applied voltage, pulse length) for droplet formation are optimised. Subsequently the deposition on the cantilever sensors is performed. The above must be repeated for each solution to be deposited.

Figure 2.9 shows SEM images of three agarose functionalised cantilevers where 10 drops of *E. coli* cell suspension (10% LB, $2.5\times10^8$ cfu/mL) were deposited at each position. The internal diameter of the pipette nozzle used was 50 μm. The position of the deposited spots is marked in green. The use of the ink-jet printing technique allows for the accurate deposition of cells within the confines of the deposited droplet and is therefore accurate to with 1/3 of the cantilevers length due to spreading of the droplets upon impact on the sensor surface as shown in Figure 2.9. This renders interpretation of the frequency response of cantilevers due to microbial growth easier when compared to capillary functionalisation. The use of this technique also keeps the location of the deposited cells to one side of the cantilever sensor which helps the optical readout. The ability to deposit on the backside of the cantilever protects the cells from subsequent laser exposure. Although a laser wavelength of 830 nm is chosen to have the smallest impact on biological material, it still is adsorbed by the underlying silicon cantilever which could cause local heating.

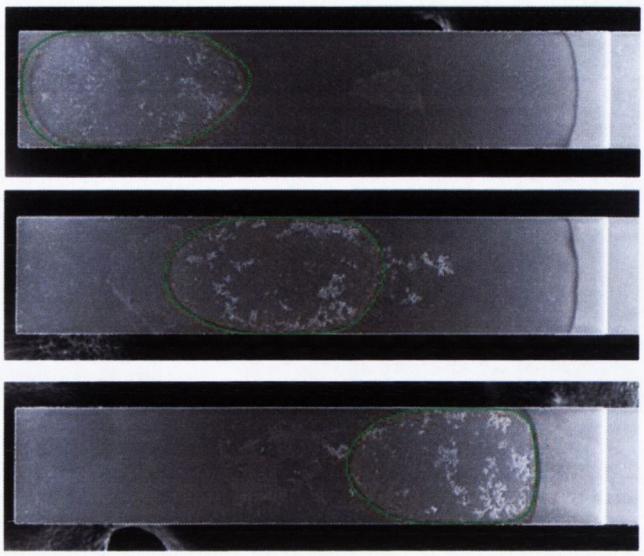

Figure 2.9: SEM image of three agarose functionalised cantilevers where 10 drops of *E. coli* cell suspension (10% LB, $2.5\times10^8$ cells/mL) were deposited at each position. The internal diameter of the pipette used was 50 µm. The position of the deposited spots is marked in green. It can be seen that the majority of cells remain in the deposited droplet. Droplets spread upon impact on the sensors surface.

It has been observed that the use of a solvent with a low viscosity results in a spreading of the droplet along the cantilevers longitudinal axis upon impact. Similarly, the use of a highly concentrated growth medium results in a large droplet remaining at the impact site. This can have an adverse effect on growth measurements as droplet evaporation occurs slowly due to the hydrophilic constituents of nutritional mediums. This results in a rise in resonance frequency during growth measurements.

### 2.4.3 Glass Needle Deposition

The deposition of single microbial cells is a difficult task. Several novel techniques have been developed to date which enable the deposition of single viable microbial cells. Direct write dip pen nanolithography [18] allows for the pick-up and deposition of cells on a substrate. The manipulation of the cells is via adhesion to a hydrogel modified cantilever tip. The FluidFM technology [19] uses a cantilever with a hollow channel running along its length to provide suction. This enables the pick-up and deposition of individual bacterial cells. Micro-contact printing, using Polydimethylsiloxane (PDMS) stamps with a high

aspect ratio, has also been utilised for the deposition of individual bacterial cells in arrays [20]. These techniques are not suited to cell deposition on cantilever arrays due to the fragility of the sensors and size constraints. For the deposition of single fungal spores we use the handmade glass needle technique [21]. Here a glass pipette is heated and pulled to form a glass needle. This needle is then used to pick up individual spores and to deposit them on agarose functionalised cantilevers. The pulled needle is mounted in a custom designed mount which is in turn mounted on a XYZ positioning system constructed using three manual translation stages (4046M; Parker, CA, USA). Figure 2.10 shows an image of the assembled glass needle device.

To produce glass needles a glass capillary tube (Model G-1, OD 1mm, ID 0.6mm, length 90 mm, Narishige Inc., London UK) is heated at its mid-point and then pulled apart to produce two glass needles using a vertical pipette puller (PC-10 Puller; Narishige Inc., London, UK). A weight attached to the instrument is used to pull the pipette. After sufficient heating of the tube (centred in a heating coil) it weakens structurally allowing the gravitation force of the weight to take over. Ideally the needle produced should have sufficient flexibility to allow for manipulation of spores.

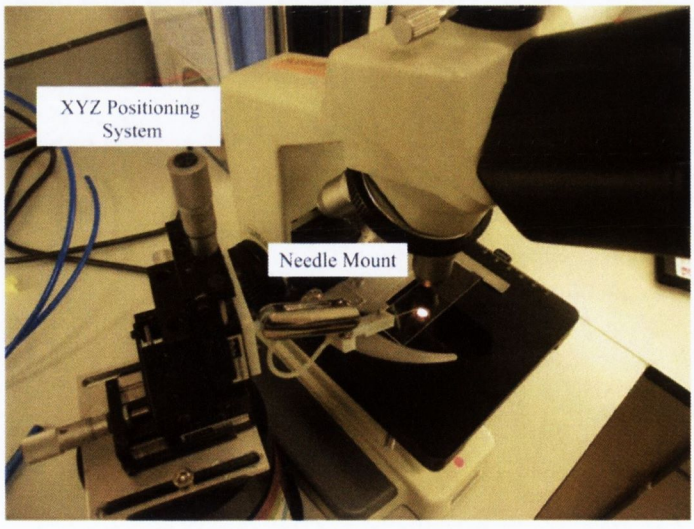


Figure 2.10: Instrument for needle deposition. The pulled needle is mounted in a custom holder which is in turn mounted on an XYZ positioning system.

Fungal spores are washed from an agar slant using 0.01% tween solution. 100 µL of this spore suspension is pipetted onto a glass slide which was previously washed with EtOH and allowed to dry. The pipetted drop is spread along the glass slide and allowed to dry. The pulled glass needle is washed by immersion in EtOH and then placed into the focal plane of an optical transmission microscope (B3 series; Motic), using the XYZ positioning system. The glass slide, with the dried spore suspension, is then also brought into the focal plane of the microscope objective. At this point both the tip of the glass needle and the glass slide are touching.

Spores are brought into contact with the needle via movement of the glass slide using the microscope stage positioning system (Figure 2.11 (A)). Upon contact, spores adhere to the micro needle. Prior to deposition of the spore nutritional soaking of an agarose functionalised cantilever is performed. This can be performed via immersion of the

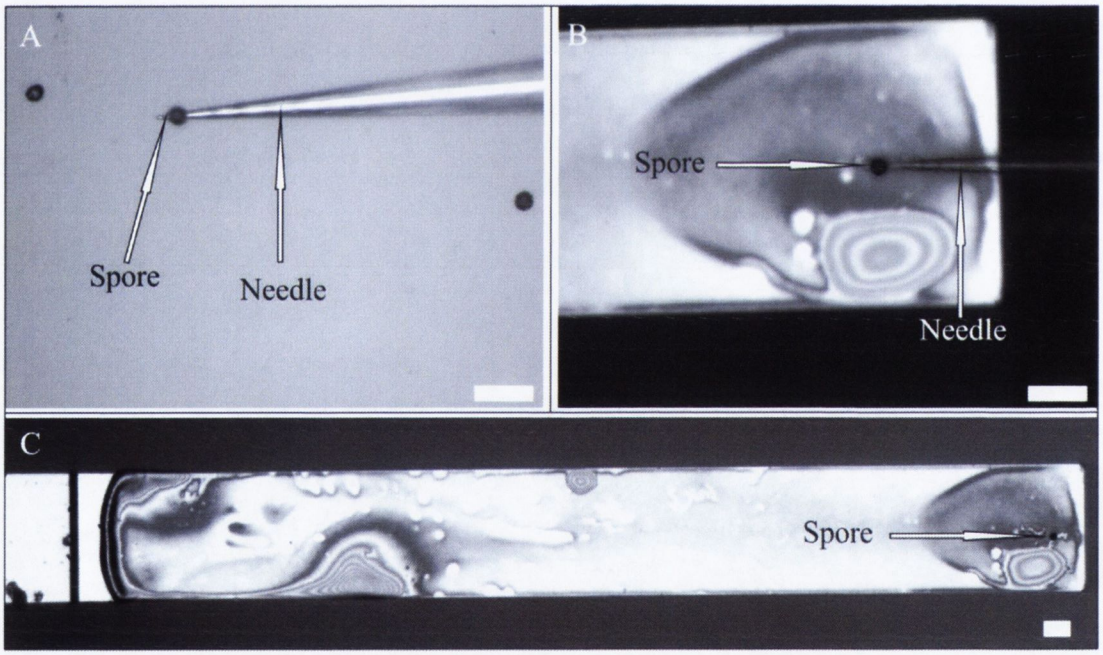


Figure 2.11: Optical microscope images of glass needle deposition of an individual *A. niger* spore on an agarose functionalised cantilever. (A) A spore is harvested from a dried spore suspension on a glass slide. The spore adheres to the glass needle upon contact. (B) Spore is deposited onto an agarose functionalised cantilever which has been pre-soaked in nutritional medium (*e.g.* 1X RPMI). Wetting of the agarose layer is required for the cell to be deposited onto the cantilever. (C) The use of this technique allows full control of the amount and the position of spores deposited on the front end of the cantilever sensor. Scale bars are 20 µm in all images

cantilever array in growth medium for 10 minutes. Droplets of medium can also be deposited using the ink-jet printing technique. The nutrition soaked cantilever array is placed into the focal plane of the microscope objective and the spore is deposited (Figure 2.11 (B)). Placement of a spore is aided by wetting of the agarose layer with nutrition medium. Deposition of a spore on a dry agarose layer is difficult.

Figure 2.11 (C) shows an image of a single *A. niger* spore which has been deposited using the glass needle technique. This technique provides full control on the amount of microbes deposited and also the positions where they are deposited. Positional control provides a nanomechanical insight into the dynamics of spore growth. It also allows for easy interpretation of the resonance frequency response of cantilevers due to the dynamic spread of growing hyphal filaments.

## 2.5 References


1. Kern, K.A.R.a.W., *Handbook of Silicon Wafer Cleaning Technology.* William Andrew Publishing, NY USA, 2008(2nd Edition).
2. Elam, J.H., H. Nygren, and M. Stenberg, *Covalent coupling of polysaccharides to silicon and silicon rubber surfaces.* Journal of Biomedical Materials Research, 1984. **18**(8): p. 953-959.
3. Johansson, B.G., *Agarose Gel Electrophoresis.* Scandinavian Journal of Clinical & Laboratory Investigation, 1972. **29**(s124): p. 7-19.
4. Sambrook, J. and D.W. Russell, *Agarose Gel Electrophoresis.* Cold Spring Harbor Protocols, 2006. **2006**(1): p. pdb.prot4020.
5. Phillips, G.O. and P.A. Williams, *Handbook of Hydrocolloids (2nd Edition)*, Woodhead Publishing.
6. McKendry, R., et al., *Multiple label-free biodetection and quantitative DNA-binding assays on a nanomechanical cantilever array.* Proceedings of the National Academy of Sciences of the United States of America, 2002. **99**(15): p. 9783-9788.
7. Gfeller, K.Y., N. Nugaeva, and M. Hegner, *Micromechanical oscillators as rapid biosensor for the detection of active growth of Escherichia coli.* Biosensors and Bioelectronics, 2005. **21**(3): p. 528-533.
8. Gfeller, K.Y., N. Nugaeva, and M. Hegner, *Rapid biosensor for detection of antibiotic-selective growth of Escherichia coli.* Applied and Environmental Microbiology, 2005. **71**(5): p. 2626-2631.
9. Maloney, N., et al., *Fibre Optic Readout of Microcantilever Arrays for Fast Microorganism Growth Detection.* Journal of Sensors, 2012. p. 6. doi:10.1155/2012/405281
10. Natalia Nugaeva, K.Y.G., Natalia Backmann, Marcel Düggelin, Hans Peter Lang, Hans-Joachim Güntherodt and Martin Hegner *An Antibody-Sensitized Microfabricated Cantilever for the Growth Detection of Aspergillus niger Spores.* Microscopy and Microanalysis, 2007. **13**: p. 13-17.
11. Tao, X., et al., *Hybrid printing of mechanically and biologically improved constructs for cartilage tissue engineering applications.* Biofabrication, 2013. **5**(1): p. 015001.
12. Sandler, N., et al., *Inkjet printing of drug substances and use of porous substrates-towards individualized dosing.* J Pharm Sci, 2011. **100**(8): p. 3386-95.
13. McWilliam, I., M. Kwan, and D. Hall, *Inkjet Printing for the Production of Protein Microarrays*, in *Protein Microarrays*, U. Korf, Editor. 2011, Humana Press. p. 345-361.
14. Bietsch, A., et al., *Rapid functionalization of cantilever array sensors by inkjet printing.* Nanotechnology, 2004. **15**(8): p. 873-880.
15. Braun, T., et al., *Quantitative time-resolved measurement of membrane protein-ligand interactions using microcantilever array sensors.* Nature Nanotechnology, 2009. **4**(3): p. 179-185.
16. Lukacs, G., N. Maloney, and M. Hegner, *Ink-Jet Printing: Perfect Tool for Cantilever Array Sensor Preparation for Microbial Growth Detection.* Journal of Sensors, 2012. p. 7. doi:10.1155/2012/561256
17. Tekin, E., P.J. Smith, and U.S. Schubert, *Inkjet printing as a deposition and patterning tool for polymers and inorganic particles.* Soft Matter, 2008. **4**(4): p. 703-713.

18. Kim, J., et al., *Direct-Write Patterning of Bacterial Cells by Dip-Pen Nanolithography.* Journal of the American Chemical Society, 2012. **134**(40): p. 16500-16503.
19. Dorig, P., et al., *Force-controlled spatial manipulation of viable mammalian cells and micro-organisms by means of FluidFM technology.* Applied Physics Letters, 2010. **97**(2): p. 023701-3.
20. Xu, L., et al., *Microcontact Printing of Living Bacteria Arrays with Cellular Resolution.* Nano Letters, 2007. **7**(7): p. 2068-2072.
21. Goh, T.-K., *Single-spore isolation using a hand-made glass needle.* Fungal Diversity, 1999. **2**: p. 47-63.

# Chapter 3

# Fibre Optic Based Cantilever Device

This chapter deals with the development of a device for the dynamic readout of microcantilever arrays. Typically the measurement of cantilever resonance frequencies using optical beam deflection [1] is via a position sensitive detector (PSD). The growth of microorganisms is dependent on the provision of sufficient nutrition and water. Here water is provided via a humid environment (~94 %). No electronic device is capable of operation in these elevated conditions for any period of time, let alone the time required for detection of microorganism growth. To avoid complications due to condensing water on electronic components (such as the PSD and amplifier electronics) optical fibres are employed to measure resonance frequencies. The measurement of frequencies with fibre optics is dependent on the modulation of light (light/no light/light etc.), by deflection off an oscillating cantilever, entering an optic fibre. The device existing at the start of my studies along with its issues will be described followed by a detailed description of the newly developed device and its performance.

## 3.1 Existing Device and Issues

To enable a homogeneous illumination of all eight cantilevers the setup was run with two parallel laser diodes (L808P200, Thorlabs) mounted in individual collimation tubes (LT230P-B, Thorlabs, NA: 0.55). The outputs from the collimation tubes were coupled into two optic fibres (AFS105/125Y Thorlabs) using five axis fibre aligners (Model 9091, New Focus). To eliminate interference between the two laser beams a shutter system was used to alternate illumination by the beams. The laser beams were focused onto the cantilever array using a convex cylindrical lens (Edmund Optics). The deflected signal was picked up using eight optic fibres (Conrad Electronics GmbH) with a diameter of 0.5 mm.

The device was housed in a refrigeration unit (Intertronic, Switzerland). A HygroClip-SC05 (Rotronic, Switzerland) sensor connected to a HygroPalm (Rotronic, Switzerland), was used to measure the temperature and humidity. LabVIEW software was used to regulate temperature and humidity. Fuzzy logic software was used to supply a voltage to a

peltier element in the box to control temperature. Two mass flow controllers (EL-Flow, Bronkhorst HI-TEC, Switzerland) were used to bubble compressed air through a temperature controlled water reservoir to provide humidity control. The humidity could also be increased using a nebuliser inside the box. This was used to enable quick up-regulation of humidity at the start of an experiment. The pick-up fibres were held in a cylindrical tube that could be manipulated vertically (z direction) using two spring-loaded screws. It was not possible to manipulate the tube in the x (left and right) and y (back and forth) directions.

This resulted in two issues; firstly in order to achieve a situation of no cross talk, as shown in Figure 3.1, the reflection from the cantilever array needs to match the pitch of the eight optical fibres. Without fine movement in the y-direction this could not be achieved. Secondly, the measurement of resonance frequencies was dependent on the modulation of the reflected light entering the fibres. Sufficient modulation only occurs when the fibre is positioned away from the centre of the reflection where the intensity of light is less. Since it was not possible to manipulate the fibres in the x direction this position was not achievable. It was also very difficult to ensure that the pick-up fibres were in line with the cantilever array because they were held in a cylindrical holder which could rotate. The core diameter of the fibres used was 480 µm. This diameter proved to be too large and as a

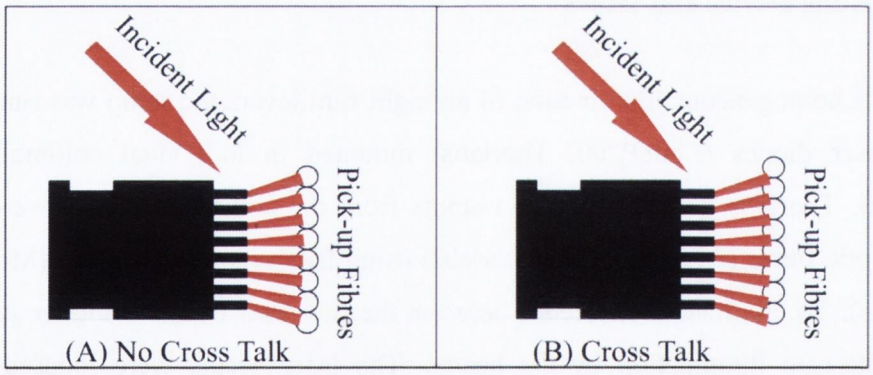


Figure 3.1: Cantilever array alignment to enable fibre optical readout. An oscillating cantilever will result in movement of a laser spot across the end of an optic fibre. The resulting modulation in light intensity admitted by the fibre is used to determine resonance frequency. (A) Illustration of situation of no cross talk between pick-up fibres. Light deflected from each sensor enters the assigned optic fibre ensuring measurement of the correct resonance frequency. (B) Situation of cross talk occurring. Light deflected from each sensor enters the assigned pick-up fibre but also the adjacent fibre resulting in convolution of the acquired signal.

result the fibres were susceptible to cross talk from adjacent fibres. Illuminating the front portion of each cantilever precisely would ensure maximum deflection of the light at resonance. A convex cylindrical lens was initially used to focus light from a bare optic fibre onto the cantilever array, these components were mounted at a fixed distance from each other, and fine adjustment was not possible resulting in a poor focus on the cantilever array. This difficulty in focusing resulted in an increased optical noise in the device.

The initial humidity control had several problems; the capacity of the Bronkhorst mass flow controllers was not sufficient to be regulated precisely at a specific set point. The small peltier heating element inside the box was limited in its capacity to allow fast ramping to the temperatures required for microorganism growth experiments. Taking these factors into account it was decided to redesign the environmental controls, the device housing, and the optical system.

## 3.2 New Fibre Optic Device

This device is based on the device discussed in the previous section. The detection of resonance frequencies is dependent on the modulation of light intensity entering optic fibres. Several changes were made to the device to ensure accurate measurement of resonance frequencies and overcome the issues described in previous section. The changes made include a new optical system, a new actuation mount for cantilever arrays, and a new environmental chamber with accompanying control software, all of which are discussed in the subsequent sections. Next, tests were performed which demonstrated the ability of this device to track changes in resonance frequencies and were followed by experiments which show the detection of *A. niger* growth.

### 3.2.1 Optics

An image of the new optical setup is shown in Figure 3.2. All components were purchased from Thorlabs (Cambridgeshire, UK), unless otherwise stated. A collimated laser beam (beam diameter = 3.4 mm) is provided to the system using a pig tailed laser diode (LPS-830-FC, $\lambda$= 830 nm, maximum power 12 mW) which is accompanied by a collimator (F280FC-B).

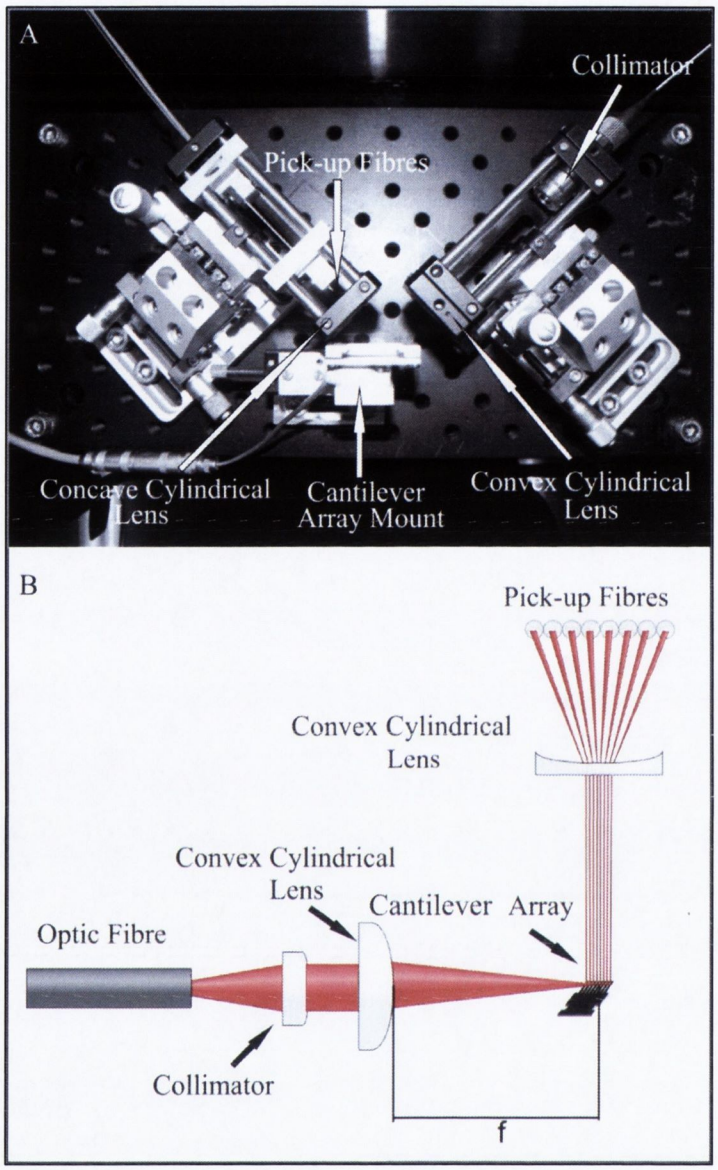


Figure 3.2: (A) Viewgraph of fibre optic microcantilever device. A collimated laser beam is focused into a line along a cantilever array using a convex cylindrical lens. The deflected signal from each cantilever is directed into one of eight optic fibres (one for each cantilever) using a concave cylindrical lens. The optical axis is maintained using two cage systems which are mounted on two Gothic arch XYZ translation stages. Horizontal distance from hole to hole is 25 mm on breadboard. (B) Illustration of the optical setup for the fibre optic device. A collimated beam is focused into a line across the cantilever array using a convex cylindrical lens. The reflection from each cantilever is directed into eight pick-up fibres, one corresponding to each cantilever in the array, via a concave cylindrical lens.

The laser diode is driven with an external module (ITC502 - Benchtop Laser Diode and Temperature Controller ±200 mA / 16 W) and is temperature controlled (TCLDM9 - TE-Cooled Mount). A wavelength of 830 nm was chosen to minimise damage to biological samples [2]. The collimated beam is focused into a line across the cantilever array using a convex cylindrical lens (47764, f = 20 mm; Edmund Optics, UK). A 16 mm cage system consisting of 16 mm cage plates (SP03) and cage rods (SR3) is utilised to maintain the optical axis of the device. Custom mounts were fabricated to enable the mounting of the cylindrical lens in the cage plate. The input optics of the device is shown in Figure 3.3 (A). The optical cage system is mounted onto an XYZ micro translation stage (Gothic arch 9061-XYZ; Newport, CA, USA) which allows for fine positioning of the focused laser line on the cantilever array. Using Equations 3.1 and 3.2 [3],

$$W_{CL} = \left(\frac{4\lambda}{\pi}\right)\left(\frac{f}{D_{COLL}}\right) \qquad 3.1$$

$$DOF = \left(\frac{8\lambda}{\pi}\right)\left(\frac{f}{D_{COLL}}\right)^2 \qquad 3.2$$

the focused beam width on the cantilever ($W_{CL}$) and the depth of focus ($DOF$) are found to be ~6 μm and ~70 μm respectively where, $\lambda$ is wavelength of the laser diode, $f$ is focal length of convex cylindrical lens, and $D_{COLL}$ is the collimated beam diameter.

The reflection from each cantilever is directed into eight pick-up fibres (BFL48-200, outer diameter = 0.5 mm, core diameter = 0.2 mm) via a concave cylindrical lens (LK1363L1-B, f = -7.7 mm). Fibres with this core diameter and cladding size (0.3 mm) were chosen to increase the distance between the cores of adjacent pick-up fibres and reduce the risk of cross talk and convolution of resonance frequency spectra. A distance of ~8 mm between the pick-up fibres and the concave cylindrical lens is required for the measurement of resonance frequencies of all cantilevers in an array. The optic fibres are held in a line along the optical axis using a custom designed holder. The output optic axis is maintained using identical cage rods and plates as the input optical axis. The output cage system is mounted on an XYZ micro translation stage to facilitate fine positioning during device alignment. An image of the device output optics is shown in Figure 3.3 (B). The optical components are arranged on an optical breadboard. The pick-up fibres are coupled to a custom built

photo-detector device housing eight photo diodes (one for each cantilever) which is housed outside the environmental chamber.

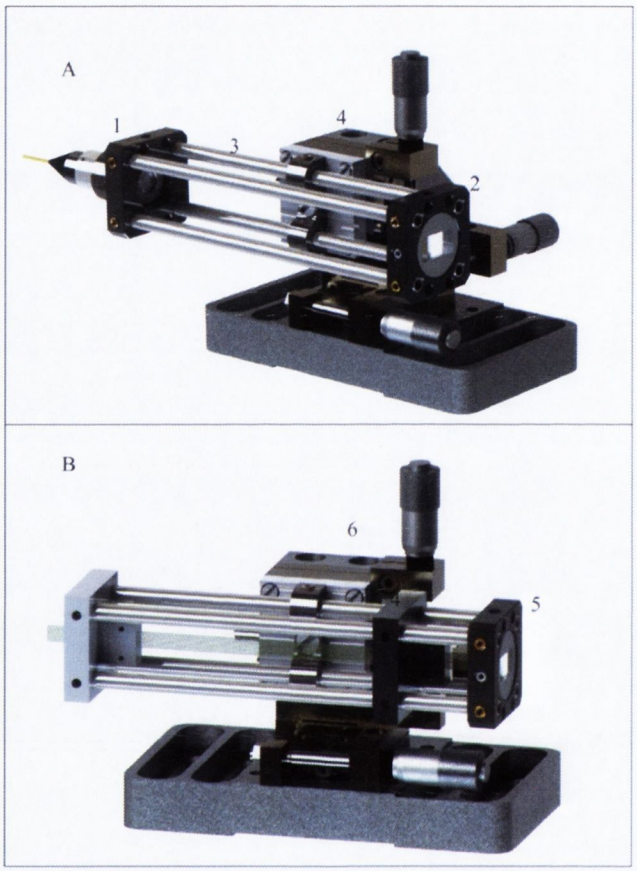


Figure 3.3: (A) Device input optics. (1) A pig tailed laser diode accompanied by a collimator and mounted in a 16 mm cage plate (Thorlabs) provides a collimated laser beam to the system. (2) A convex cylindrical (f =20 mm) is used to focus the collimated laser beam into a line across the cantilever array. The lens is held in a 16 mm cage plate using a custom designed mount. (3) The optical axis is maintained using a 16 mm cage system. (4) The cage system is mounted on an XYZ micro translation stage (New focus) to enable fine positioning of the focused laser line on the cantilever array. (B) Device output optics. (4) Eight optical fibres with an outer diameter of 0.5 mm and a core diameter of 0.2 mm are held in a line using a custom designed holder. (5) A concave cylindrical lens (f = -7.7 mm) directs the deflected light from each cantilever in the array into the matching corresponding optic fibre. (6) The output optical axis is maintained using a 16 mm cage system.

### 3.2.2 Piezoelectric Mount

In order to actuate the cantilever with sufficient amplitude to enable measurement of resonance frequencies and to ensure that the array was not tilted, a mount containing a piezoelectric ceramic was fabricated (Figure 3.4). The piezoelectric ceramic (EBL #2, EBL Products Inc., CT, USA) has a length, width, and thickness of 15 mm, 15 mm, and 1 mm respectively. To apply a voltage to the ceramic, copper wires (diameter = 0.1 mm) were glued to the positive and negative plates using an electrically conductive silver epoxy (EPO-TEK ® E4110, Epoxy Technology Inc., MA, USA). The ceramic is glued between two pieces of machinable glass ceramic (Macor®) and is held in place using an epoxy adhesive (EPO-TEK ® 377). The cantilever array is mounted in a PolyEther Ether Ketone (PEEK) holder and is held in place using a copper beryllium clip. The PEEK mount is sandwiched between two pieces of machined aluminium, the bottom of which is glued to the top macor piece using the previously mentioned epoxy adhesive.

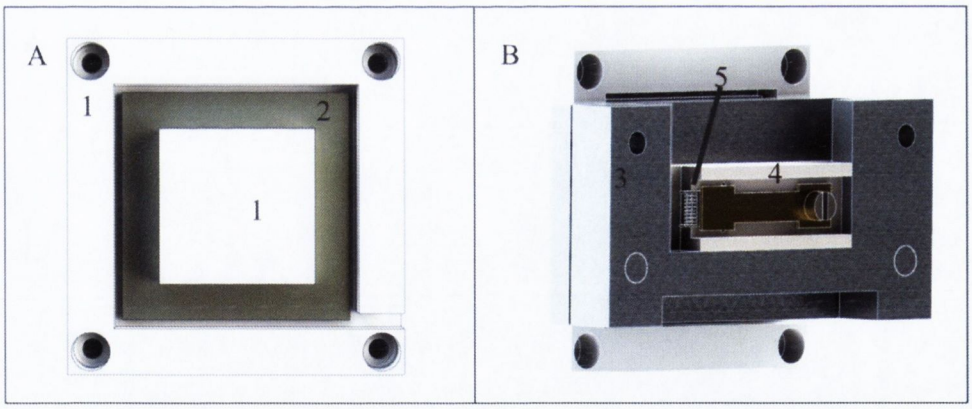


Figure 3.4: (A) Machinable glass ceramic (Macor®) (1) sandwiching a piezoelectric ceramic (2) with a length, width, and thickness of 15 mm x 15 mm x 1mm. An epoxy adhesive is used to hold the piezoelectric in place. (B) Two pieces of machined aluminium (3) hold a PEEK (4) mount which holds the cantilever array (5) in place with the aid of a copper beryllium clip. The setup provides sufficient actuation of the cantilever array for measurement of resonance frequencies.

### 3.2.3 Environmental Chamber

The device is housed in a custom designed environmental chamber (5500-8139 A; Electro Tech Systems Inc. PA, USA) (Figure 3.5) which is used to regulate temperature and humidity. Access to the chamber is via two small side doors and one main front door. Two 8 inch iris ports on the front of the environmental chamber allow for device manipulation without any major interruption of the environmental conditions. The roof of the chamber is slanted to prevent droplets of condensation landing on the fibre optic device below. Temperature is generated using a heating element housed inside the chamber. Humid air is pumped into the chamber using an ultrasonic humidification system (5472-3; Electro Tech Systems Inc.; PA USA). Humidity and temperature are regulated using a temperature-compensated humidity sensor (554; Electro Tech Systems Inc., PA, USA) in conjunction with a microprocessor controller (5200 441-431; Electro Tech Systems Inc., PA, USA). This system allows humidity and temperature to be kept within ± 0.25 % and ± 0.15 °C of the desired set points respectively (Figure 3.6). Humidity and temperature are independently logged using a HygroClip-SC05 sensor (Rotronic, Switzerland) placed next to the measurement device.

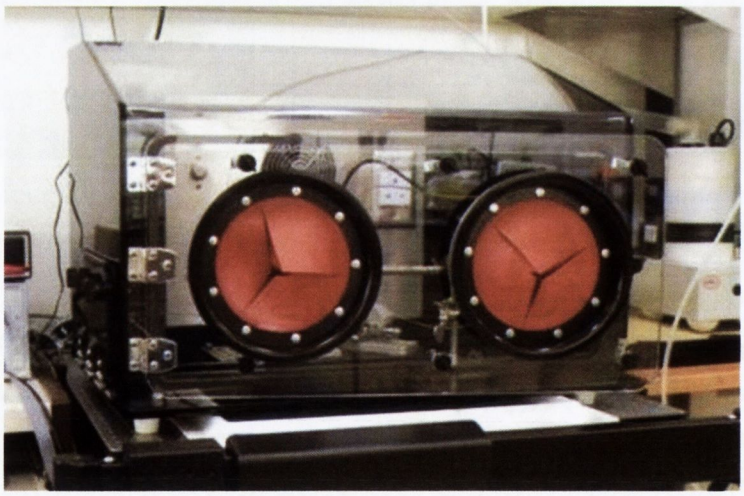

Figure 3.5: Environmental Chamber. The optical device is housed inside this chamber. Temperature control is via a heating element located inside the chamber. Humidity regulation is via an external nebuliser system.

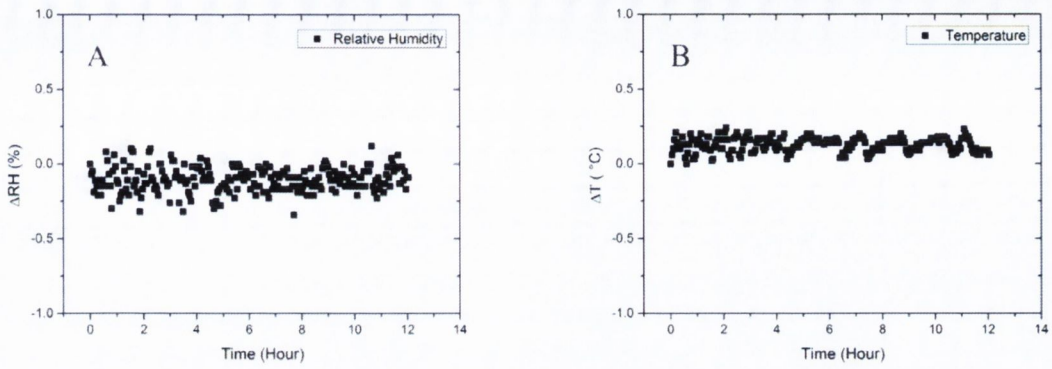


Figure 3.6: (A) Humidity stability at experimental conditions (94% RH, 30 °C). (B) Temperature stability at experimental conditions (94% RH, 30 °C). Humidity and temperature are kept within ± 0.25 % and ± 0.15 °C of the desired set points respectively.

### 3.2.4 Dynamic Mode Operation

Automated control of the device is via the visual programming language LabVIEW. Discussion of LabVIEW can be found in Chapter 4. It is not discussed here as the device control programme was written by a previous group member before I began working on this project.

Two PCI boards are used to generate and record frequencies. A waveform generation board (NI PCI-5412, 100 MS/s, 14-Bit Arbitrary Waveform Generator; National Instruments, TX, USA) provides a sinusoidal frequency signal to the piezoelectric actuator. Excitation of the cantilever occurs at a number of frequencies in a linear range. Upon excitation at one of its resonance frequencies the movement of the cantilever causes a modulation of the intensity of the light entering the pick-up fibres. The modulating light intensity results in a modulating current signal produced by a photo detector. The rate of change of this signal represents the resonance frequency of the cantilever. The modulating signal is pre amplified (SR560 Low-Noise Preamplifier; Stanford Research Systems, CA, USA) before being digitised (High Speed Digitiser; National Instruments, TX, USA) and converted into amplitude spectra by the LabVIEW programme. The amplitude of the recorded resonance peak is proportional to the difference between the maximum and minimum intensities of the optical signal reaching the photo detector through the pick-up fibres. The above is repeated for each cantilever in the array in a time multiplexed fashion.

One modification made to the LabVIEW code is that control of the laser diode output is possible. Control is provided via a multifunctional input/output PCI board (NI PCI-6010, 16-Bit, 200 kS/s, 16 Analog Input Multifunction DAQ; National Instruments, TX, USA). When performing a measurement the laser diode turns on 1 minute before a frequency measurement is taken and turns off between measurements to limit any heating effects on the biological sample.

### 3.2.5 Operation Procedure

The operation of this fibre optic device is outlined below. The procedure for the successful alignment of an agarose coated cantilever array is included. As agarose coated sensors are sensitive to relative humidity changes it is essential to have one uncoated reference sensor in the array. This procedure should be performed before all growth detection measurements. After agarose functionalisation the resonance frequencies of the sensors in the array are measured using a Multimode™ AFM (Digital Instruments, Santa Barbara, CA, USA). The array is mounted into the PEEK holder and then into the piezo actuator. Using the micro translation stage the focused laser line is positioned at the free end of the cantilevers. An infra-red viewing card can be used to aid this procedure by using it to monitor the reflection from the array. When correctly aligned and focused the reflection from the cantilever array should be a series of 8 lines of light with equal spacing between each line.

Alignment of the blank cantilever to the desired pick up fibre is performed (*i.e.* cantilever number eight to pick-up fibre number eight) at room conditions. The previously measured resonance frequencies are used to identify which sensor is directed towards which pickup fibre. The alignment tab shown in Figure 3.7 (A) allows for continuous actuation at an individual resonance frequency. Using this tab, fine positioning of the pickup fibres via the micro translation stage (Figure 3.3 (B)) can be performed to ensure a signal with good signal to noise is recorded. The optimal position for maximum signal to noise is when one end of the reflected line from a cantilever is aligned to the pickup fibre. If the centre of the reflected beam is positioned on the fibre there is insufficient modulation of the light intensity.

(A) Alignment Tab

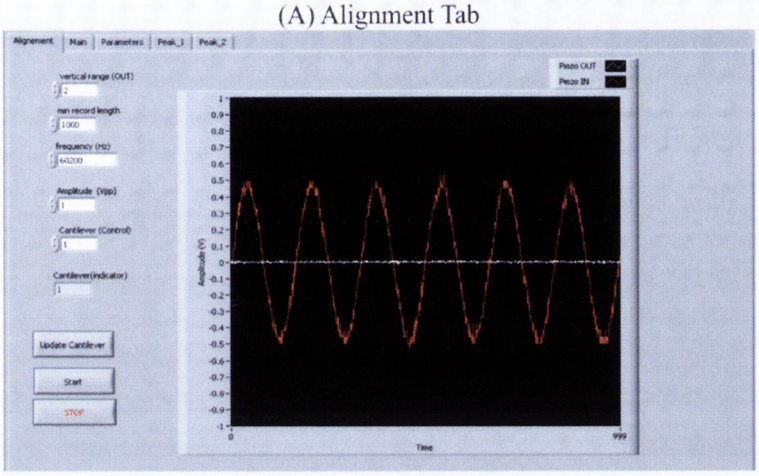


(B) Measurement Tab

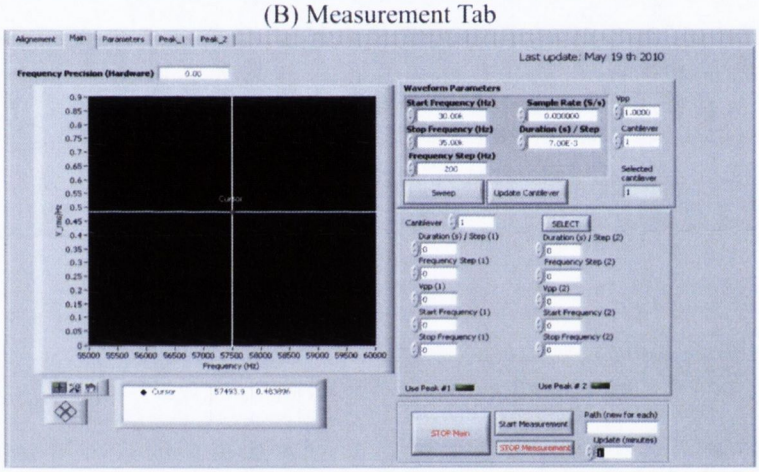


Figure 3.7: (A) Alignment Tab. An individual resonance frequency is generated by the waveform generator and the response of the cantilever is displayed. Alignment of the optic fibres to the position of maximum signal modulation can be monitored using this tab. The largest peak to peak amplitude indicates the optimal position for resonance frequency measurement. (B) Measurement tab. For each cantilever the start and stop frequencies for the frequency range of interest are defined along with the number of data points to be recorded. The peak to peak voltages to be supplied to the piezoelectric actuator by the waveform generator for each cantilever are also defined. Other parameters such as sampling time per data point and sampling rate are also defined.

When the blank sensor is aligned correctly then the rest of the sensors in the array are also aligned. The resonance frequency of each sensor is then recorded. At this point the conditions in the environmental chamber are elevated to experimental conditions (typically 94% RH and 30 °C). The resonance frequency of each cantilever in the array is then recorded again. Any cross talk can be eliminated by adjustment of the distance between the concave cylindrical lens and the optic fibres. At this point the device is fully aligned. Using

the iris ports the PEEK holder and cantilever array can be removed via a side door and microorganism deposition can be performed. It is vital that the cantilever remains in the PEEK holder during deposition. Removal requires performance of the above alignment procedure again. After microorganism deposition the PEEK holder is put back into position in the device and any fine adjustment, if required, is performed. Using the measurement tab (Figure 3.7 (B)) the waveform parameters for the measurement are defined. For each cantilever the start and stop frequencies for the frequency range of interest are defined along with the number of data points to be recorded. The peak to peak voltages to be supplied to the piezoelectric actuator by the waveform generator are also defined. Other parameters such as sampling time per data point and sampling rates are also entered. The sampling rate is set to $10^7$ sample second$^{-1}$ to satisfy Nyquist's theorem and avoid aliasing. The time interval at which to record resonance frequencies is also defined using this tab (typically 30 minutes). Once all parameters are set the measurement is started.

## 3.3 Measurements Performed using Fibre Optic Device

In this section measurements performed using this device and the accompanying results are described and discussed. First the ability of the device to monitor resonance frequency changes due to the adsorption of water by agarose functionalised sensors is discussed. Next a measurement showing the detection of *A. niger* is described and the cantilever response is discussed.

### 3.3.1 Resonance Frequency Measurement

Figure 3.8 shows the fundamental mode frequency spectrum of 2 µm and 7 µm thick cantilevers at room conditions. The plots demonstrate the ability of this home built fibre optic based readout device to measure resonance frequencies of cantilevers. The above spectra were recorded at 30 °C. The peak positions correspond to those predicted by theory. In comparison to the previous version of this device, the measurement of resonance frequencies of several cantilevers is possible in an automated and time multiplexed

fashion. The measurement of resonance peaks is greatly aided by the use of a preamplifier (SR 560, Stanford Research Systems) which is a new addition to the device.

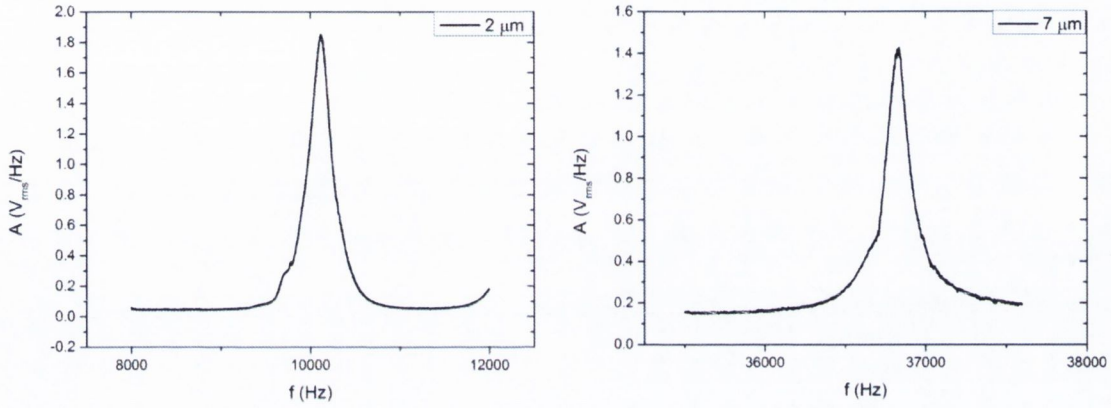


Figure 3.8: Fundamental mode frequency spectrum of a 2 μm and 7 μm thick cantilever at room conditions. The x axis shows frequency (f) in Hertz while the y axis shows amplitude ($V_{rms}$/Hz).

### 3.3.2 Response of Agarose Functionalised Cantilevers

The aim of this experiment was to confirm that an agarose coated cantilever is sensitive to changes in humidity. The effect of agarose layer thickness on sensitivity and noise in the measured signal was investigated. Two 7 μm thick cantilevers arrays ((i) and (ii)) were prepared. More details about the agarose coating and chemistry are described in Chapter 2 and protocols are provided in the Appendix. In the case of array (i), cantilevers were exposed to the agarose solution for 1 second. In the case of array (ii), cantilevers were exposed to the agarose solution for 1, 5, or 10 seconds to obtain a different agarose thickness on each cantilever.

The fundamental resonance frequencies of cantilevers in array (i) were tracked as humidity was increased from room conditions to 94% RH. Environmental conditions were then kept stable for several hours before the regulation of relative humidity was stopped. The resonance frequency spectra were measured by sweeping 2100 frequency steps in a 2.1 kHz range. A spectrum was recorded for each cantilever in the array every 2 minutes. The same test was performed for array (ii). In this case 1000 data points were taken in a 1 kHz range.

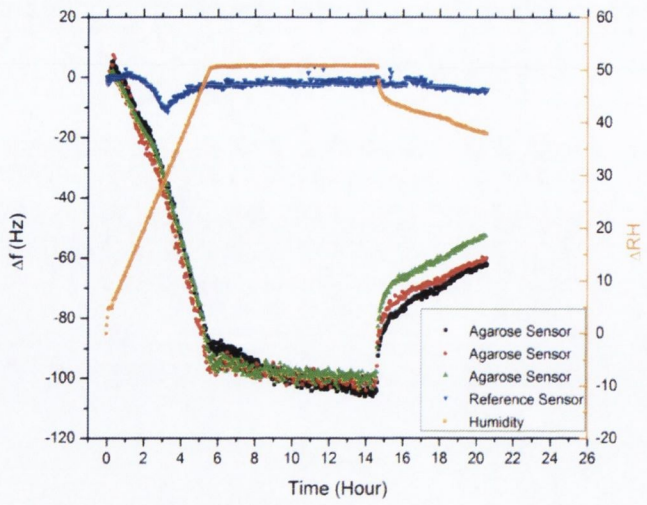


Figure 3.9: Resonance frequency response of agarose functionalised cantilevers (red, green and blue data points). The response of a blank silicon cantilever is also shown in blue. The corresponding change in relative humidity is shown (orange data points). Agarose functionalised cantilevers show an increased response to changes in humidity due to an increase in mass on the cantilevers surface. Zero point on right hand axis corresponds to 44% RH.

Figure 3.9 and Figure 3.10 show the resonance frequency response of cantilevers from array (i) and (ii) to changes in humidity respectively. Agarose functionalised cantilevers show an increased response to changes in humidity. This is due to an increase in mass on the cantilever surface caused by the absorption of water by the agarose layer. Increasing the incubation time in agarose solution during functionalisation results in a thicker layer and hence a greater response to humidity fluctuations (Figure 3.10). There is seen to be a correlation between frequency noise levels in the device and the incubation time of the cantilevers in the agarose solution during functionalisation. For incubation times of 0, 1, 5, and 10 seconds noise levels are found to increase from approximately 4 - 10 Hz. Fluctuations in humidity are responsible for noise in frequency measurement and thus a thicker agarose layer results in increased noise levels. The average mass responsivity of an agarose functionalised cantilever in array (i) when operated in its first resonance mode is ~ 51 ± 1 pg/Hz. Taking a noise level of 4 kHz this results in a minimal detectable mass of ~ 200 pg.

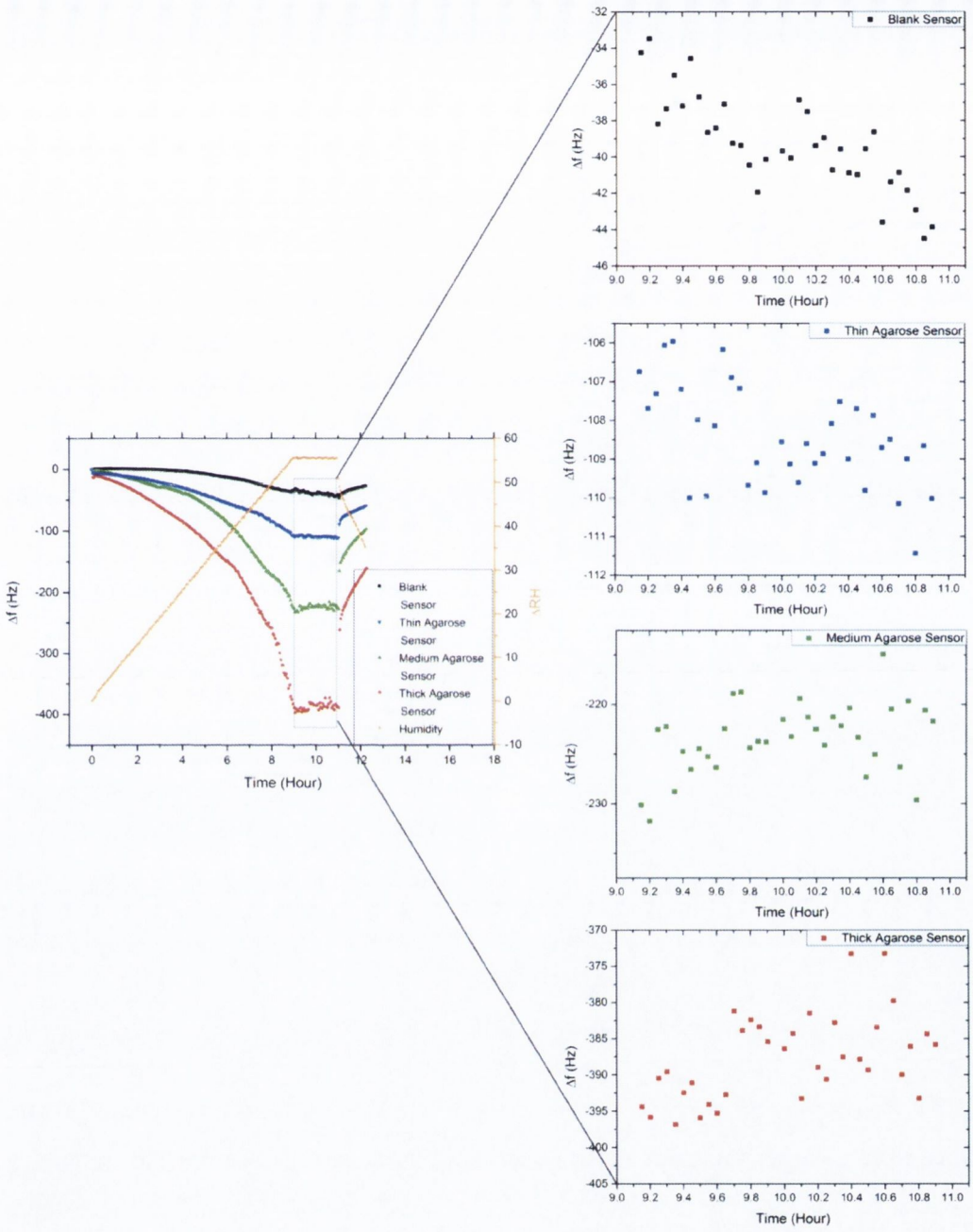


Figure 3.10: Resonance frequency response of agarose functionalised cantilevers. The thin, medium, and thick agarose sensors correspond to 1, 5, and 10 second incubation times during functionalisation respectively. The response to humidity changes increases with increasing layer thickness. The plots on the right show expanded views of the resonance frequency plots when environmental conditions are stable. Frequency noise levels are also seen to increase slightly with increasing layer thickness. The zero point on the right hand axis corresponds to 36% RH.

## 3.4 *Aspergillus niger* Growth Detection

The aim of this measurement is to demonstrate the ability of this device to detect the growth of *A. niger* spores faster than conventional growth detection methods. The growth of spores on the cantilevers surface results in a net increase in mass due to water adsorption and thus a decrease in resonance frequency. An agarose functionalised cantilever array was prepared as described in Chapter 2. The nutritional soaking of the agarose layer in malt extract (ME) broth and deposition of *A. niger* spores on the cantilever was performed in parallel using glass capillaries as described in Chapter 2. Two cantilevers from array A were immersed in the spore suspension for 10 min. The *in situ* reference cantilever was immersed in 10% ME broth without spores for 10 min. The array was immediately placed inside the test chamber at 94% RH and 30 °C. A resonance frequency spectrum was recorded for each cantilever every 15 minutes to avoid inhibition of growth due to oscillation of the cantilevers. For each spectrum 2000 data points were taken in a frequency range of 4 kHz. Figure 3.11 shows resonance frequency shift ($\Delta f$) versus time for two *A. niger* spore coated cantilevers. The observed shift is a result of spores starting to germinate and spread hyphae along the cantilever. Water adsorption on the new hyphae results in an increased mass on the cantilever. The detection of vital fungal growth is possible in less than 15 hours. This is an order of magnitude faster than currently used detection methods where detection takes up to 5-14 days.

The use of the new automated system allowed experiments to be run over longer periods of time (> 48 h) which has provided further insights into the dynamics of mycelium growth. Approximately 28 h after the start of the experiment an increase in resonance frequency was observed. The effect of adsorbate mass, stiffness, and its position along the cantilever have been reported in [4-6]. This effect is discussed in detail in Chapter 5 but for the purpose of this discussion the effect will be summarised. For a cantilever operated in its fundamental resonance mode the adsorbate mass dominates when positioned at the cantilevers free end resulting in a negative shift in resonance frequency. When positioned at the cantilevers clamped end the effect of the adsorbate stiffness dominates and a positive shift in resonance frequency is observed. Figure 3.12 shows images of the front and back of the two cantilevers (A and B) at the end of the measurement while image C shows an

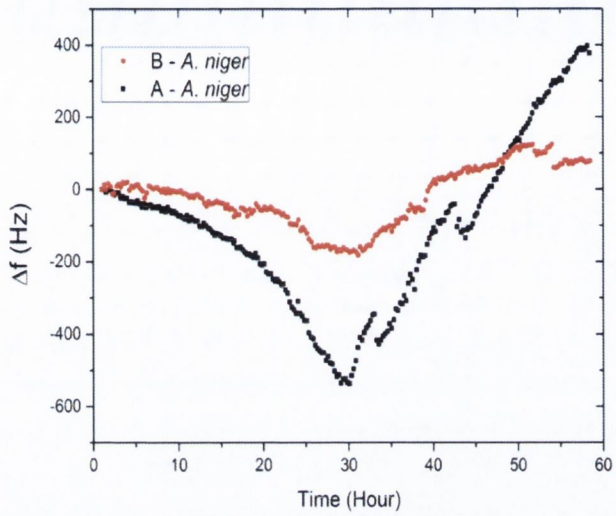


Figure 3.11: Frequency response of cantilevers due to *A. niger* spore growth. The detection of vital fungal growth is possible in less than 15 hours. As the spread of hyphal filaments propagates past the cantilevers mid-point we begin to see a positive shift in resonance frequency. Plots marked A and B correspond to images marked A and B in Figure 3.12.

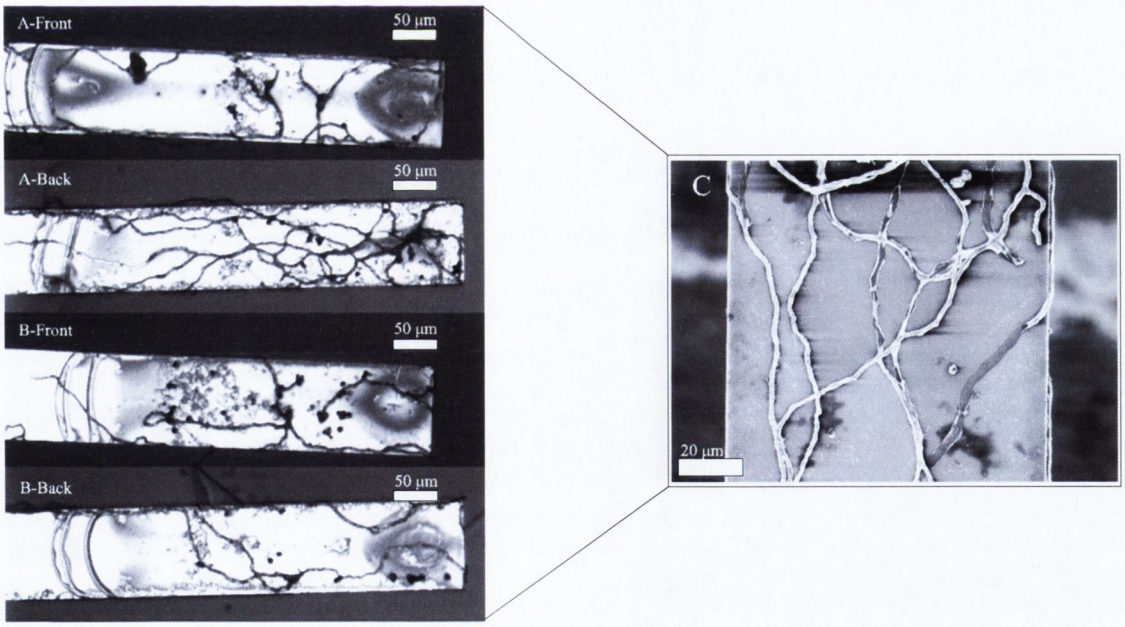


Figure 3.12: Images of the front and back of the two cantilevers (A and B). Image C shows an SEM image of hyphae on a cantilever. It can be seen that the position of spores is predominantly in the front half of the cantilever in both cases. Images marked A and B correspond to plots marked A and B in Figure 3.11

SEM image of hyphae on a cantilever. It can be seen that the position of spores is predominantly in the front half of the cantilever in both cases. As spores begin to swell and subsequently germinate a decrease in resonance frequency is observed. As the spread of hyphal filaments propagates past the cantilevers mid-point we begin to see a positive shift in resonance frequency. We believe the jumps in resonance frequency observed at ~33 and 42 h for the cantilever with the denser spore coating (Figure 3.11; black curve) is due to a hypha which has been growing off the cantilevers surface and then reattaches itself. This is further examined in Chapter 5 where online imaging of the cantilever during a growth experiment is performed. Different magnitudes of response can be linked to a higher number of viable spores on one cantilever than the other as can be seen in Figure 3.12. One point to note is the rate of growth is the same on both cantilevers as the individual sensor response seems to scale with the number of viable spores deposited.

## 3.5 Conclusions: Issues with the Device

The development of a fibre optic based readout device for the measurement of the flexural resonance frequencies of cantilevers in an array has been described. The tracking of the resonance frequency of cantilevers in dynamically changing environmental conditions has been demonstrated. The detection of the growth of viable *A. niger* spores has also been reported in less than 15 hours using this device. However, there are several issues with the device described above which warrant discussion.

The required measurement of the cantilevers resonance frequencies using an extra instrument (AFM) adds a step in experimental preparation. The alignment of the device is also extremely time consuming and requires an experienced user.

Whilst the device is capable of the readout of resonance frequencies of multiple cantilevers in an array, the situation of no cross talk is not easily attainable when trying to perform measurements using eight sensors. When using blank silicon arrays the readout of all eight sensors without cross talk is possible, however once functionalisation has taken place there is sufficient diffusion of the reflected optical signal to convolute some of the optical signals picked up by the optic fibres. To overcome this issue every second cantilever in the array was removed. This removed any cross talk and enabled the measurement of the intended cantilever's resonance frequency in the corresponding optic fibre. This provision allowed

for successful measurements to be performed but at the cost of half of the sensors available.

The next challenge deals with device sensitivity; it has been shown that operation of cantilevers at higher modes leads to a linear increase in mass sensitivity with the square of the mode number [7]. The use of optic fibres to detect cantilever oscillation requires modulation of the signal entering the optic fibres. Maximum deflection of the laser beam occurs at the nodes of vibration; hence the focused laser line should be positioned at the resonance nodes. Whilst the amplitude of vibration in the fundamental resonance mode can produce sufficient modulation of the optical signal this is not the case for higher order resonance modes. Using a focused line to illuminate the array makes flexible positioning on each cantilever difficult. Therefore measurement of higher vibrational modes was severely hindered and the sensitivity of the device was limited to that of the fundamental resonance mode.

Due to the requirement that the array must be kept in the PEEK holder during functionalisation limits the use of available techniques. Deposition of growth medium and cells on the sensor's surface attenuates the optical signal, therefore increasing noise levels, and in some cases renders the sensor unreadable. Deposition of micro droplets on the backside of the sensor using the ink-jet printing technique is a solution to this problem but cannot be performed due to the alignment procedure for this instrument. In order to resolve these issues a new device consisting of a movable input optical system and a PSD for frequency measurement was developed and is discussed in Chapter 4.

## 3.6 References


1. Binnig, G., C.F. Quate, and C. Gerber, *Atomic Force Microscope.* Physical Review Letters, 1986. **56**(9): p. 930-933.
2. Neuman, K.C., et al., *Characterization of Photodamage to Escherichia coli in Optical Traps.* Biophysical journal, 1999. 77(5): p. 2856-2863.
3. Newport,*GaussianBeamOptics.*URL: http://www.newport.com/store/genContent.aspx/Gaussian-Beam-Optics/144899/1033, Accessed 17/09/2010.
4. Tamayo, J., et al., *Effect of the adsorbate stiffness on the resonance response of microcantilever sensors.* Applied Physics Letters, 2006. **89**(22): p. -.
5. Ramos, D., et al., *Origin of the response of nanomechanical resonators to bacteria adsorption.* Journal of Applied Physics, 2006. **100**(10): p. 106105-3.
6. Ramos, D., et al., *Detection of bacteria based on the thermomechanical noise of a nanomechanical resonator: origin of the response and detection limits.* Nanotechnology, 2008. **19**(3): p. 035503.
7. Murali Krishna, G. and et al., *Higher modes of vibration increase mass sensitivity in nanomechanical microcantilevers.* Nanotechnology, 2007. **18**(44): p. 445502.

# Chapter 4

# Dual Translation Stage Device

In this chapter the development of a device capable of the measurement of multiple flexural resonance modes is described. All of the issues present in the previous fibre optic based device (Chapter 3) were taken into consideration during its design and development.

The motivations behind the development of this device were:

1. Eliminate the need for predetermination of cantilever resonance frequencies using an external instrument (AFM).

2. Increase achievable sensitivity by facilitating the measurement of higher order resonance modes.

3. Remove restrictions regarding the use of functionalisation techniques as was the case for the fibre optic based device (Chapter 3).

4. Eliminate cross talk between adjacent sensors and hence the required removal of sensors from a cantilever array.

The device presented uses the laser beam deflection method to sequentially readout the resonance frequencies of cantilevers in an array. The device consists of a piezoelectric ceramic mount used for cantilever actuation, a 2D laser optics positioning system, and a position sensitive detector (PSD). The range of motion of the 2D system is 5 x 5 mm with a positional accuracy of 50 nm. We continue to read out the cantilever arrays with eight sensors with a footprint of 2.5 x 2.8 mm as described previously. Automated control of the device is provided using LabVIEW and several national instruments PCI boards (National Instruments, TX, USA). All of the above is housed in the custom designed environmental chamber (described in Chapter 3) to provide a humid and temperature stabilised environment which is required for accurate growth detection measurements.

## 4.1 Instrumentation

Several components used in this device were recycled from the fibre optic based device however they are listed here for clarity. Where a component has been recycled it is highlighted using italics.

### 4.1.1 Optics and Positioning System

All optical components were purchased from Thorlabs (Cambridgeshire, UK) unless otherwise stated. A single wavelength ($\lambda$ = 830 nm) *pigtailed laser diode* (LPS-830-FC) accompanied by a *collimator* is used to provide a parallel laser beam (beam diameter = 3.45 mm) to the system. The laser diode is driven with an external module (*ITC502-Benchtop Laser Diode and Temperature Controller*) and is temperature controlled (*TCLDM9-TE-Cooled Mount*) to increase output stability. The laser beam is attenuated by neutral density filters to avoid PSD saturation. The number of filters used can be varied to obtain the desired sum signal of 2-4 V from the PSD. A convex lens (f = 30 mm) is utilised to focus a laser spot on the cantilever. The resultant laser spot has a diameter and depth of focus of ~ 9 μm and ~ 425 μm respectively. The input optical axis is maintained using a 16 mm cage system comprised of several components; *cage plates* (SP03), *cage rods* (SR3), quick release cage mounts (QRC05A), collimator adaptor (AD1109F), *cage mounting bracket* (SMB1), and *several retaining rings* (SM05RR).

Two automated translation stages (M-110K043; Physik Instrumente (PI), Bedford, MK43 0AN, UK) were manufactured on request by PI and are modified versions of the M110.1DG translation stage (PI). This modification was not available during the fibre optic device development, hence the use of the focused line in the device described in Chapter 3. In order for the stage to operate at high relative humidity levels (~ 94 %) the encoder has been insulated from the environment. These stages have a travel range of 5 mm and when arranged orthogonal to each other (one horizontal and one vertical) allow for rapid movement of the laser spot along and across the cantilever array (max travel speed 1.5 mm/s). A minimum incremental motion of 50 nm accompanied with a unidirectional repeatability of 0.1 μm ensures that the laser spot is returned to the desired position and that no additional noise is added to dynamic mode measurements. The vertical translation

stage acts as the mount for the optical cage system providing the focused laser beam for the device. The cage system is attached to the translation stage via a custom designed aluminium piece. A modified XYZ micro translation stage (Gothic arch 9061-XYZ; Newport, CA 92606, USA) is mounted on the horizontal translation stage and acts as the mount for the vertical translation stage.

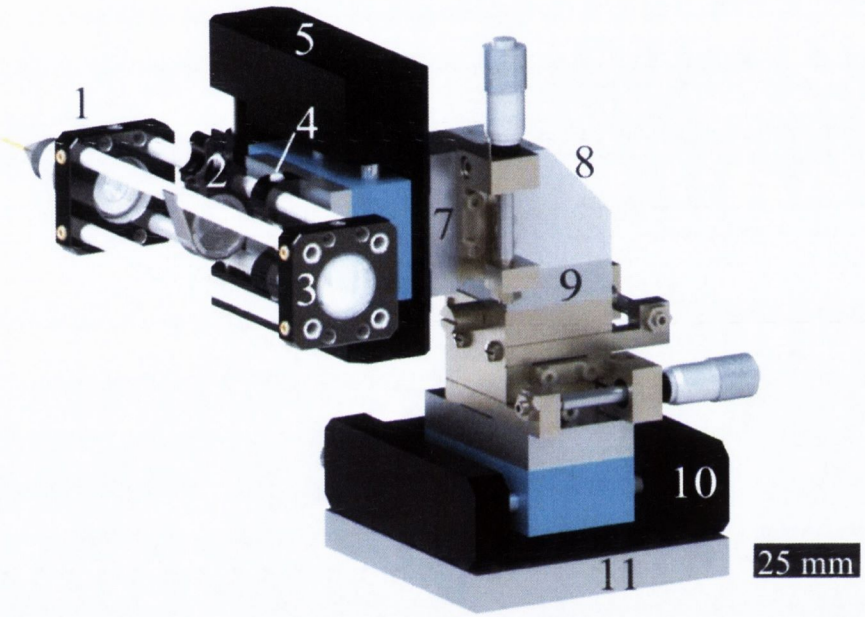


Figure 4.1: Input optical system. A pigtailed laser diode accompanied by a collimator provides a collimated laser beam ($\lambda$ = 830 nm) to the system. The intensity of the light is attenuated using several neutral density filters. A convex lens with a focal length of 30 mm focuses the laser into a spot. The optical axis of the system is maintained using a 16 mm cage system. Two automated translation stages are arranged orthogonal to each other (one horizontal and one vertical). The vertical stage facilitates the movement of the laser spot from cantilever to cantilever. The horizontal translation stage facilitates movement along cantilevers. The stages are mounted on an XYZ micro translation stage with facilitates fine alignment of the laser spot on the cantilever at the start of an experiment. (1) Cage plate holding collimator. (2) Quick release cage mount containing neutral density filters. (3) Cage plate holding convex lens. (4) Mounting bracket and custom aluminium piece facilitating attachment to vertical translation stage. (5) Vertical translation stage. (7) Vertical translation stage mount on XYZ translation stage. (8) XYZ micro translation stage. (9) Height extender piece. (10) Horizontal translation stage. (11) Piece facilitating attachment to breadboard.

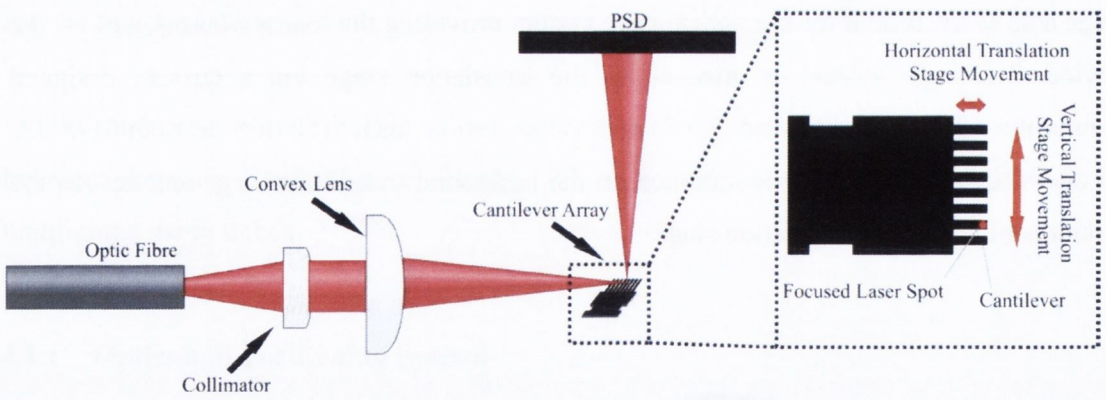


Figure 4.2: Illustration of device optics. A convex cylindrical lens is used to focus a laser spot onto the cantilevers in an array. Motion of the deflected laser beam is monitored using a PSD. Movement of the laser spot is via two automated translation stages positioned horizontal to each other. The vertical stage facilitates movement of the laser spot to adjacent cantilevers in the array while the horizontal stage facilitates movement of the laser spot along the cantilevers longitudinal axes.

Attachment of the XYZ micro translation stage to the automated translation stages is via custom designed aluminium pieces. The height of the XYZ translation stage has also been increased using an aluminium insert to facilitate the vertical translation stage. The micro XYZ translation stage is utilised for initial positioning of the laser spot onto cantilevers. An illustration of the dual translation stage system is shown in Figure 4.1 whilst an illustration of the device optics and laser spot movement on the cantilever array is shown in Figure 4.2.

### 4.1.2 Position Sensitive Detector

A Position Sensitive Detector (PSD) is a photo detector, typically a PIN diode, where upon exposure to a spot of incident light a current is generated at contacts on either side of the sensing area due to the formation of carriers in the depletion region. In this device a 1-dimensional PSD (Figure 4.3 (A)) with accompanying signal processing circuitry (SPC) on its backside (1L10-10-A_SU65_SPC02, Sitek, Sweden) (Figure 4.3 (B)) is utilised to determine the position of the laser spot deflected by the cantilever. The SPC is fabricated on a 20.5 x 20.5 mm ceramic substrate. The entire structure is housed in a Dual in Line Package (DIL) with 16 pins to facilitate measurement of the generated electrical signals.

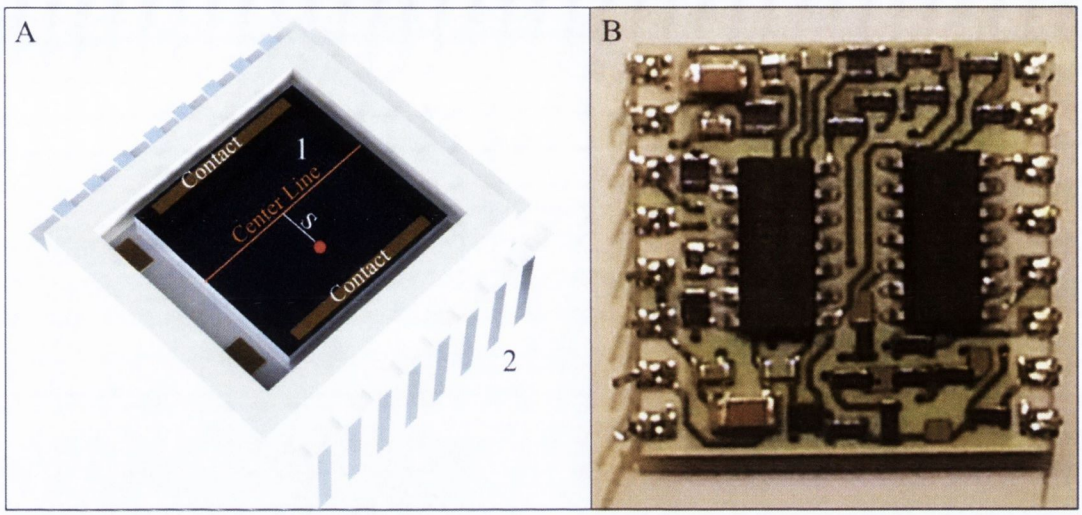


Figure 4.3: (A) Position sensitive detector (PSD). The active area of the PSD has dimensions of 10 x 10 mm. 16 pins facilitate the measurement of the generated electrical signals. (1) PSD active area. (2) DIL pins (B) Image of signal processing circuitry (SPC) on ceramic substrate attached to the backside of the PSD. The PSD-SPC device is operated under reverse bias (15 V) and has a functional bandwidth of 400 kHz.

The photo detector has an active sensing area of 10 x 10 mm and is sealed from the humid environment in the environmental chamber using a glass cover slip. The PSD-SPC device is operated under reverse bias (15 V) and has a functional bandwidth of 400 kHz. The PSD currents generated by an incident light spot are output as bipolar voltages representing the total intensity ($I_1$+$I_2$) and differential position ($I_1$-$I_2$) by the SPC. Using these values the normalised position ($s$) of the laser spot relative to the centreline of the sensors active area can be calculated using the following equation [1],

$$s = \frac{I_1 - I_2}{I_1 + I_2} \frac{l_{PSD}}{2} \qquad 4.1$$

where $I_1$ and $I_2$ correspond to the current generated at the contacts on either side of the sensing surface and $l_{PSD}$ to the distance between the contacts. The spot position is independent of the light intensity as long as the intensity is below the saturation level of the PSD. Position determination is centre of gravity weighted and is thus independent of the spot shape as long as it is smaller than the sensing area.

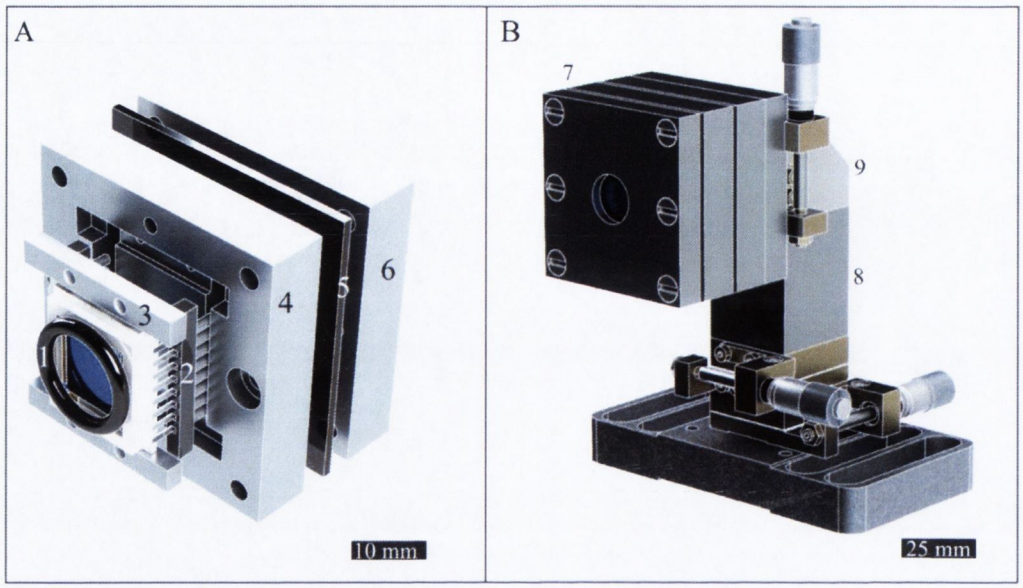


Figure 4.4: (A) Expanded view of PSD-SPC holder. The PSD is mounted into an aluminium holder consisting of three pieces. The DIL pins on the PSD are inserted into IC sockets (2), which are held in place using aluminium clamps (3). To ensure sufficient isolation from the environment, gasket sealer (5) is sandwiched between the individual aluminium pieces (4, 6). An O-ring (1) is used to seal the gap between the PSD and the circular opening in the top aluminium piece (not shown) to allow incident light to reach the sensing area. (B) Assembled holder mounted on XYZ micro translation stage. This allows for the movement of the PSD so that the incident laser spot is initially positioned on the centreline of the sensing area. (7) Assembled PSD holder. (8) Extender used to adjust height. (9) XYZ micro translation stage.

As the PSD-SPC is required to operate at humid environmental conditions outside of its specifications it is housed in a custom designed aluminium holder to prevent damage to the SPC. An expanded view of the holder assembly is shown in Figure 4.4 (A) while the assembled holder mounted on a XYZ micro translation stage (Gothic arch 9061-XYZ; Newport, CA, USA) is shown in Figure 4.4 (B). The linear translation stage allows for fine positioning of the laser spot on the PSD active area. The DIL pins on the PSD-SPC are inserted into IC sockets which are held in place using screwed down aluminium clamps. Wires are soldered to the pin side of the IC socket to allow measurement of electrical signals. A gasket sealer is used to seal the holder and an O-ring is used to seal the round opening which allows the incident light to reach the PSD active area. The linearity and stability of the response across the length of the PSD active area is excellent as shown in Figure 4.5. Here a laser spot was moved in incremental steps across the PSD active area.

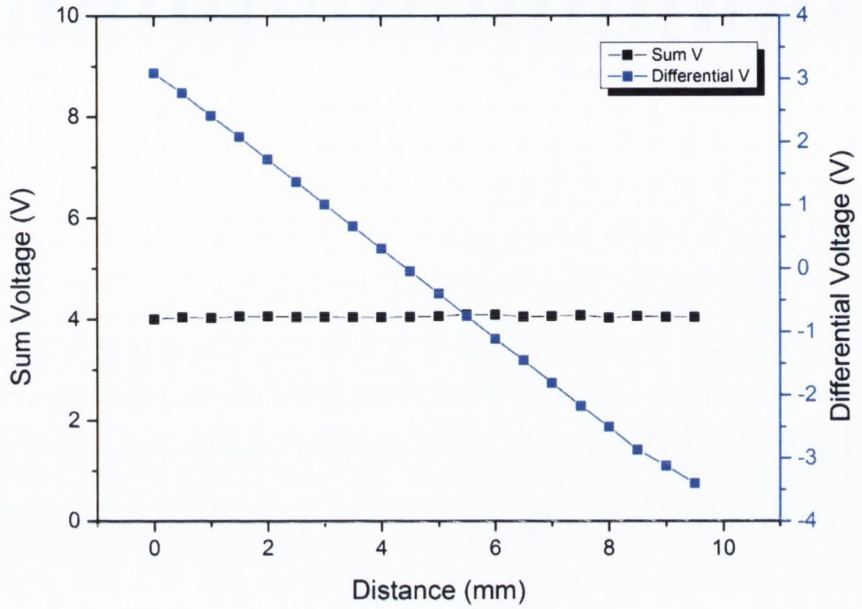


Figure 4.5: PSD response. A laser spot was moved in incremental steps across the PSD active area. The sum voltage ($I_1$+$I_2$) is seen to be constant indicating that light intensity measurement is independent of position on the PSD. The differential voltage ($I_1$-$I_2$) is seen to vary linearly across the PSD active area.

### 4.1.3 Piezoelectric Actuator

In order to provide sufficient actuation of the cantilever array for measurements of higher flexural resonance modes and also to provide access to the backside of the sensors during functionalisation a new actuator mount was fabricated. Two piezoelectric pieces with dimensions of 5x6 mm sandwich one smaller piece with dimensions of 5x5 mm. The three-stack is held together using an electrically conductive silver epoxy (EPO-TEK E4110, Epoxy Technology Inc., MA, USA). Electrical connections for the stack are made using copper wire with a diameter of 0.1 mm. The wires are glued to the piezoelectric ceramics using the same electrically conductive epoxy listed above. The piezo stack is sandwiched between two pieces of macor using an optically transparent epoxy (EPO-TEK 301, Epoxy Technology Inc., MA, USA). The macor is used to insulate the piezoelectric stack from any metal components in the stage. The piezoelectric macor stack is housed in a PEEK holder. The stack is sealed from the environment using Torrseal® resin. A stainless steel platform is used to hold the cantilever array in position. A two sided trough machined into

the stainless steel platform is utilised to ensure that the cantilever array is kept orthogonal to the axis of the vertical translation stage. A PEEK clamp screwed to the stainless steel platform holds the cantilever in position. Figure 4.6 shows an expanded (A) and assembled view (B) of the actuator. Two pins from an IC socked are glued to the piece onto which the whole actuator is attached. Copper wires from the piezo stack are attched to the IC pins (not shown in image). This allows the thin wires attached to the piezoelectric stack to be held in position free from any external forces which might cause them to break and render the entire assembly unusable.

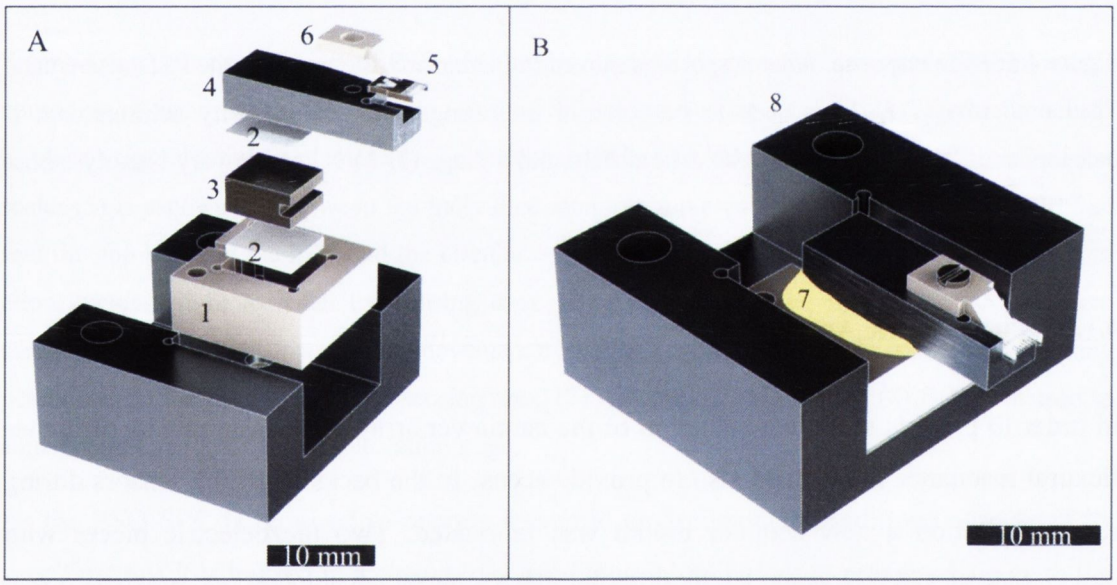


Figure 4.6: (A) Expanded view of piezoelectric actuator. A piezoelectric three-stack is sandwiched between two pieces of macor. A stainless steel platform with a PEEK clamp holds the cantilever in position. (1) PEEK housing for stack. (2) Macor. (3) Piezoelectric stack. (4) Stainless steel platform for cantilever array. (5) Cantilever array. (6) PEEK clamp. (B) Assembled piezoelectric actuator. The piezoelectric/macor stack is housed in a PEEK holder and insulated using Torrseal®. The assembled actuator is screwed to a piece of machined aluminium. An IC socket is glued to this piece as a stress reliever for the wires attached to the piezo stack (not shown in image). (7) Torrseal®. (8) Machined aluminium piece.

### 4.1.4 Environmental Control

Environmental control is provided using the same system that is described in Chapter 3.

## 4.2 Assembled Device

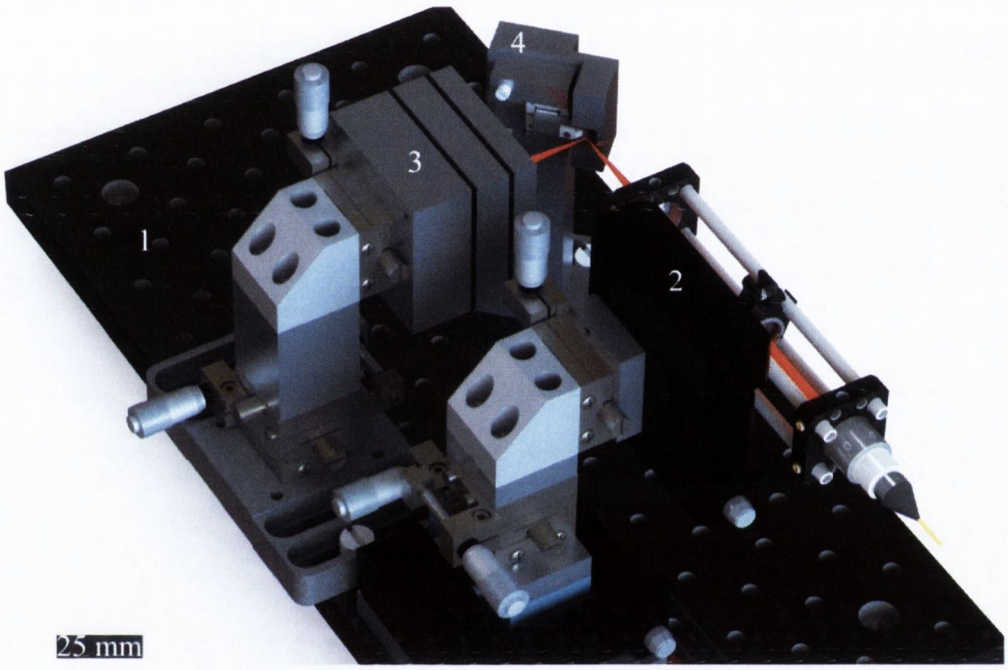


Figure 4.7: Dual translation stage device. (1) Optical breadboard. (2) Input optics and positioning system. (3) Insulated PSD system. (4) Piezoelectric mount with wind protection.

An image of the assembled device is shown in Figure 4.7. All of the optical components are arranged on an optical breadboard (MB1530, Thorlabs). The custom pieces used to attach the components to the breadboard have been designed to ensure that the distance from the convex cylindrical lens to the cantilever array is approximately 30 mm. The XYZ micro translation stage is used for fine adjustment of this position. The distance from the cantilever array to the position sensitive detector is ~ 23 mm. When in the device the cantilever is held at 45 ° to the input optical beam resulting in a 90 ° change in the optical path after deflection. When mounted in the new piezoelectric actuator mount the cantilevers in the array protrude over the edge of the platform. It has been observed that the force of air flow generated by a fan located in the back of the chamber affects the measurement of resonance frequencies and the growth of microorganisms. In order to

overcome this issue the mount which holds the cantilever array in the optical path has been designed with a wind shield.

The optical device is housed in the environmental chamber described in Chapter 3. Ports located in the side walls of the chamber provide access for cables. The chamber is placed on an optical table (Newport, CA, USA) to isolate it from external vibrations. The pig tailed laser diode and temperature controlled mount are also located on this table. The optical table is grounded to earth to avoid the build-up of any static charges.

The PC, environmental microprocessor controller, and PSD power supply are located to the left side of the optical table. To the right the humidifier is located below the water reservoir from which humid air is generated. Items such as the laser driver and amplifier (SR560 Low-Noise Preamplier; Stanford Research Systems, CA 94089, USA) are located below the optical table (Figure 4.8).

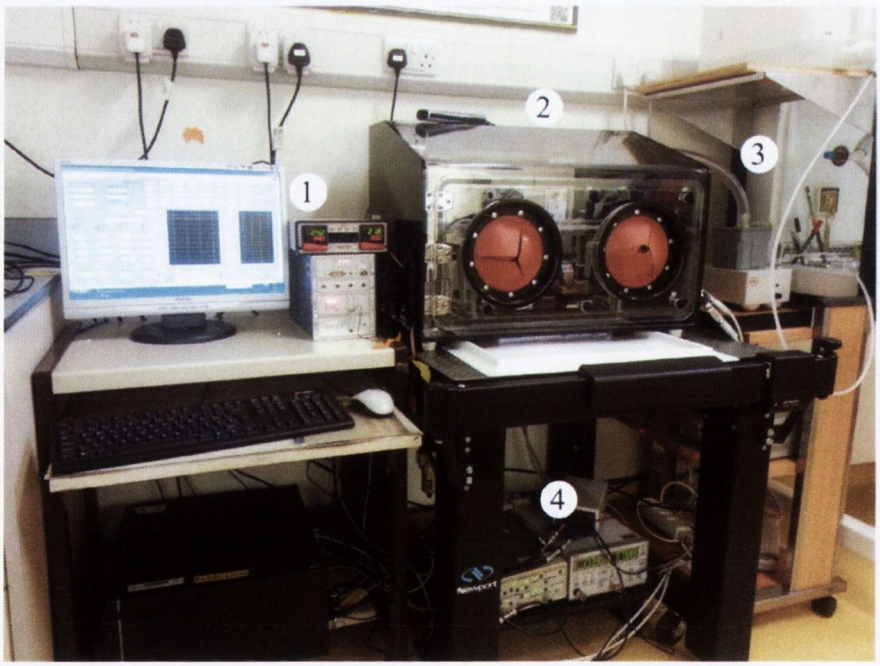


Figure 4.8: Photograph of entire device. (1) Device PC, PSD power supply, and environmental microprocessor controller. (2) Environmental chamber housing optical device on optical table. (3) Humidifier and water reservoir. (4) Laser driver and preamplifier.

## 4.3 LabVIEW Programming

LabVIEW (Laboratory Virtual Instrumentation Engineering Workbench) is a development environment for the dataflow programming language "G", which is developed by National Instruments. Each LabVIEW programme or virtual instrument (VI) consists of a "front panel" and "block diagram." The front panel is the user interface where controls (which allow the user to enter information) and indicators (which display data to the user) are placed. The block diagram contains the VI graphical source code where data is passed between different nodes by connecting them with wires. Items placed on the front panel also appear in the block diagram. Hence, each LabVIEW VI can be thought of as an electronic device where the front panel represents the user controls and the block diagram represents the electronics inside the device. Each VI can be run as a standalone routine or placed into another VI as a subroutine allowing for the construction of complicated instruments. Multithreading allows multiple tasks to be performed in parallel leading to greater system automation. The main benefit of LabVIEW is the wide catalogue of instrumentation hardware and drivers which allow interfacing with the outside world.

### 4.3.1 Device Virtual Instrument

Figure 4.9 shows a schematic outlining the operating procedure of the device. All functions of the device (except environmental regulation) are controlled using one LabVIEW VI, which is comprised of several sub VIs. The front panel of the main VI is shown in Figure 4.10. The front panel is comprised of several tabs each displaying information relating to the different functions of the device. The alignment tab shown is the only tab where user control is required. Using this tab the waveform parameters for four non adjacent frequency spectra for each cantilever in the array can be entered. Alignment of the laser spot to positions along the cantilevers longitudinal axis with the best signal to noise ratio (this may not be the same for each cantilever) is also performed using this tab. The environmental conditions tab displays real time plots of the conditions in the chamber allowing fluctuations to be monitored. The waveform parameters tab displays the parameters (pre-determined using the alignment tab) for each frequency spectrum to be recorded. Tabs entitled "peak 1" to "peak 4" correspond to the four different frequency spectra which can be recorded. Each of these tabs contains eight sub tabs for each

cantilever in the array displaying amplitude and phase spectra recorded throughout an experiment allowing the measurement to be monitored. The ability to record four frequency spectra means that four flexural resonance modes can be recorded for each cantilever in the array. As each cantilever can have a different substance deposited on its surface for growth measurements it is sometimes necessary to use different waveform parameters for each frequency spectrum to be recorded. A detailed discussion of VI opertion and measurement of dynamic and static signals can be found in Appendix 7.

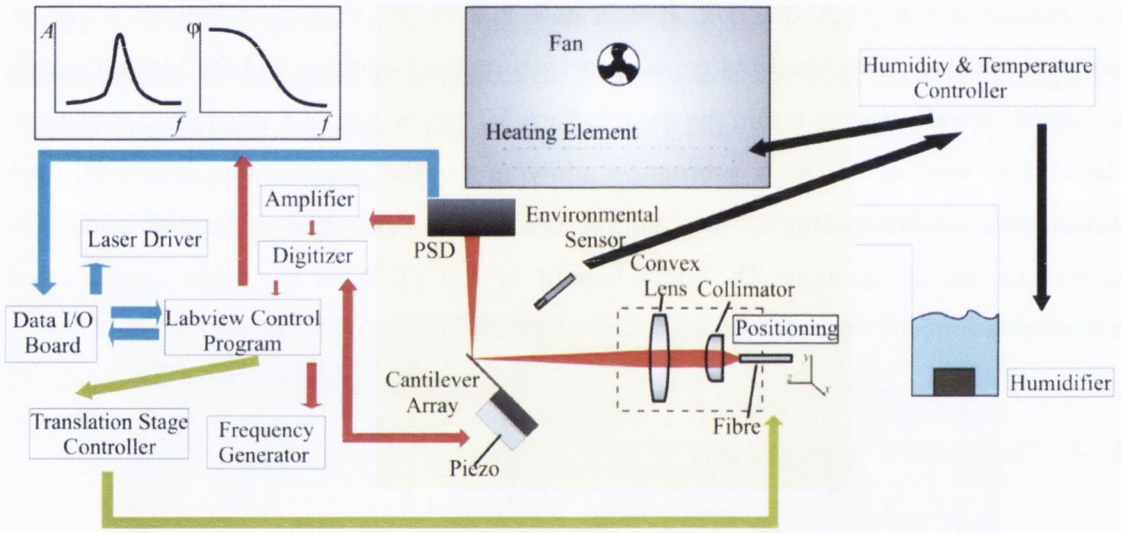


Figure 4.9: Schematic of dual axis PSD device. A LabVIEW program is used to control the operation of this device and the recording of data. Environmental control is via a microprocessor controller which operates a heating element inside the environmental chamber and a humidifier outside it (black lines). Motion control of two automated translation stages (M-110K043) by the LabVIEW program is via a PCI board (green lines). For measurement of the dynamic signal (red lines) the laser spot is moved to the desired position. A waveform generator sends a sinusoidal chirp dependant on the selected waveform parameters to the piezoelectric actuator. A PSD is used to record the motion of the cantilever. The differential voltage of the PSD is pre-amplified before being digitised by a PCI digitiser board for processing by the LabVIEW control program. Further analysis is performed to produce amplitude and phase spectra. For measurement of the static signal (blue lines) the laser spot is moved to the tip of the cantilever where the difference and sum voltages of the PSD are recorded by a PCI DAQ board. These values are then processed to give the static deflection of the cantilever.

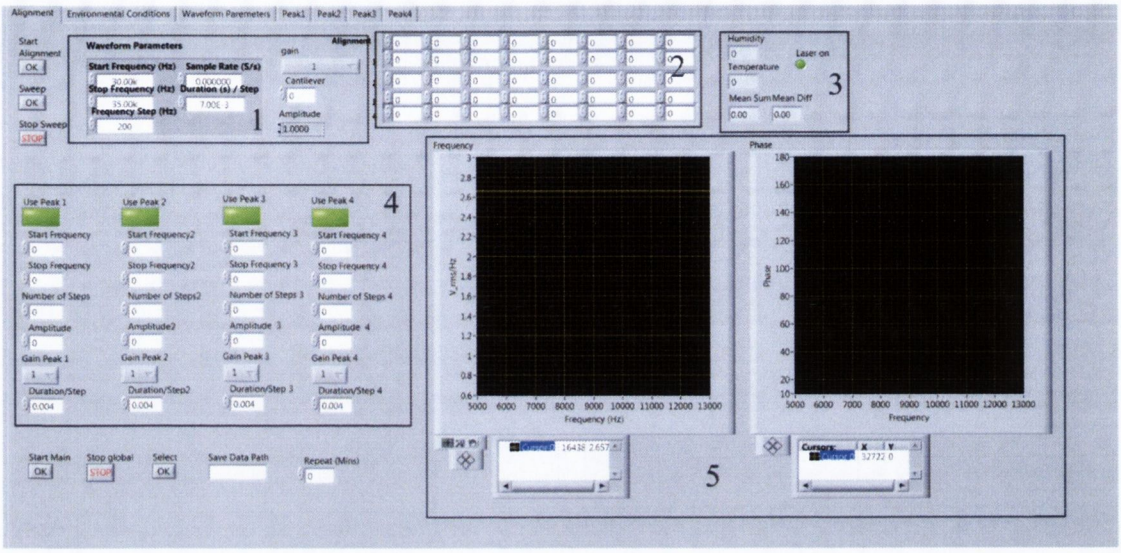


Figure 4.10: Front panel of the device VI. The front panel is the interface which allows the user to operate the device. It contains several tabs dedicated to alignment, environmental conditions, selected waveform parameters, and the display of recorded amplitude spectra. The alignment tab shown is the only tab where user input is required. (1) Waveform parameters and amplification factors are entered here for alignment optimisation. (2) Distances to move along each cantilever are entered here. The first row is used during alignment and also is the position for measurement of the static signal. The remaining rows are used to enter the desired positions along each cantilever for the four "peaks" or higher resonance modes which can be recorded. (3) Displays current temperature, humidity, sum voltage, differential voltage, and on/off of laser. (4) Optimised waveform parameters for each "peak" are entered here and written to an array using the select Boolean. If a "peak" is not to be recorded for a selected cantilever it can be deselected using the "use peak" Boolean. (5) Displays amplitude and phase spectra during optimisation of waveform parameters.

## 4.4 Results and Discussion

The development of this new device has resulted in a vast improvement in the ability to track flexural resonance frequencies when compared to the fibre optic device discussed in Chapter 3. The main changes made are to the optics system of the device. The focused line from the fibre optic device has been replaced by a focused laser spot. A dual translation stage system has been implemented for automated control of the laser spot position, thus allowing motion to individual cantilevers and also along the cantilevers length. As the laser spot is used to illuminate only one cantilever at a time the issue of cross talk is non-existent

in this device. The ability to position the laser spot at nodes of vibration on each cantilever allows for the optimal measurement of up to four flexural resonance modes for each cantilever in the array. The measurement of only one resonance mode was possible with the fibre optic device and due to alignment and cross talk issues this was only possible for a maximum of four cantilevers in the array (the remainder having to be broken off).

The implementation of a PSD to replace the pick-up fibres has vastly reduced the time required to align the system. Previously the alignment required fine positioning of the pick-up fibres to the deflected laser beam from the cantilever array. Now alignment simply requires the positioning of the PSD (active region of 10 x 10 mm) in the path of the deflected laser beam. The newly designed piezoactuator also facilitates easy functionalisation of cantilevers while the array is still mounted in the holder. Clamping of the cantilever in the new piezoactuator is via a screw clamp as opposed to copper beryllium clip used on the actuator described in Chapter 3. This improved clamping facilitates an improved transduction of the oscillating stages kinetic energy into the cantilever array allowing for actuation at higher resonance frequencies and thus improving the achievable sensitivity of the system.

In the subsequent sections the performance of this device for the measurement of cantilever dynamic signals is discussed. The cantilevers used are either blank silicon or coated on both sides with an agarose hydrogel as they are functionalised with microorganism growth detection in mind. Since they are coated symmetrically with the agarose hydrogel the static deflection data does not provide extra information. The analysis of the static mode could provide information when microorganisms are deposited on one side only. Within the scope of this work we did not have time to analyse this further and propose such experiments for subsequent studies.

### 4.4.1 Multimode Frequency Spectrum

The resonance frequency spectrum, with accompanying phase shift, of a 2 μm cantilever is shown in Figure 4.11. Peaks for the first four flexural resonance modes are shown in the frequency range of 0 – 400 kHz (bandwidth of the PSD). This spectrum consists of 2000 data points and took 4 seconds to record. In order to visualise the fundamental resonance mode (presented in the expanded view) a higher voltage must be applied to the

piezoelectric actuator. Movement of the laser spot to the individual resonance nodes allows for optimisation of the deflected laser signal thus allowing multiple resonance modes to be recorded for each cantilever in an array. By utilising the ability to record 4 non-adjacent frequency spectrums it is possible to reduce the frequency span required for the

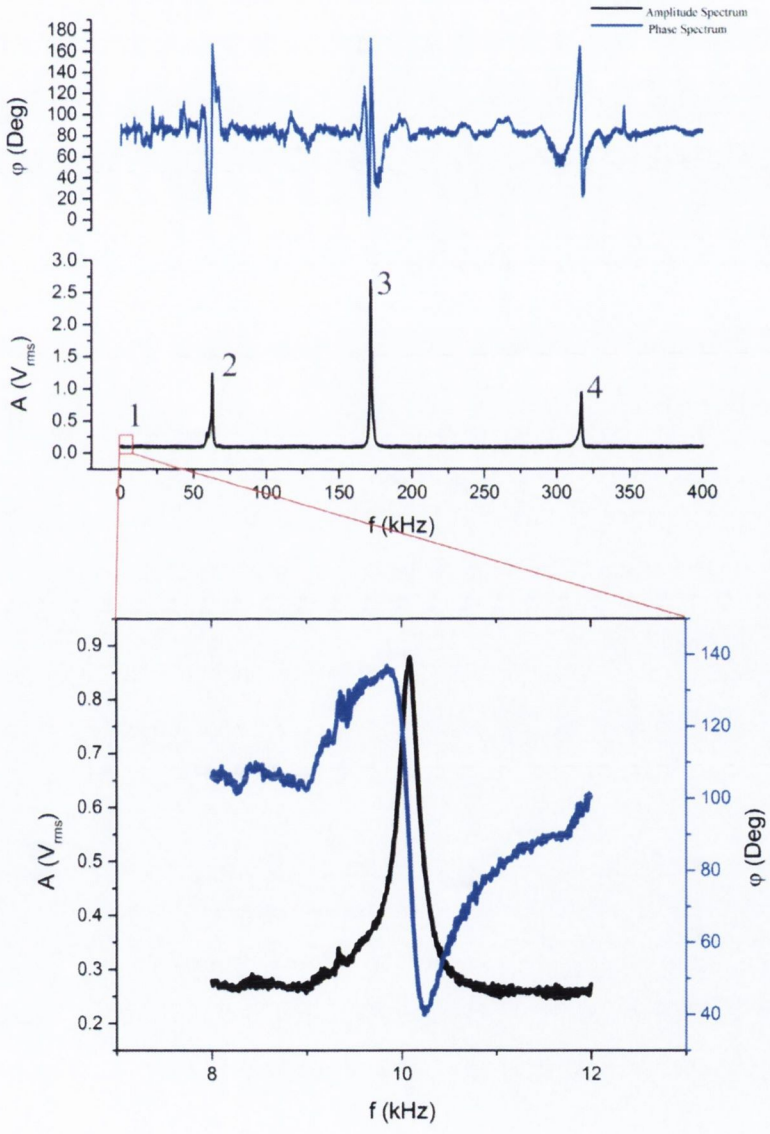


Figure 4.11: The resonance spectrum, with accompanying phase shift, of a 2 μm cantilever. The first four flexural resonance modes are shown. Due to the design of the piezoelectric actuator a higher voltage (4 $V_{peak\text{-}peak}$) must be applied in order to visualise the fundamental resonance mode shown in the expanded view.

measurement of each resonance peak. This enhances the frequency resolution of the measurement system. For example, the frequency resolution of the plot shown in Figure 4.11 is 5 Hz. This can be reduced by using a smaller frequency span. It has been observed that the measurement of multiple modes in the one frequency spectrum is not always possible using functionalised sensors, hence the development of a system with the ability to recorded individual non-adjacent frequency spectra with independent laser spot positioning along each cantilever.

### 4.4.2 Measurements with Agarose Functionalised Cantilevers

This device is designed to measure the resonance frequencies of agarose functionalised cantilevers at elevated relative humidity conditions. The tests outlined below have been performed using cantilevers with thicknesses of 2 or 7 μm.

**Measurement:** The cantilever arrays were cleaned by exposure to oxygen plasma and the agarose functionalisation was performed as described in Chapter 2.

The 2 μm agarose functionalised cantilever array was mounted onto the piezo actuator and the laser system was aligned. The temperature in the chamber was set to 30 °C and allowed to stabilise for 30 minutes. The relative humidity was ramped slowly from ~ 75% to ~ 90% and then held at this final value for several hours. Resonance frequency data was recorded for the first four resonance modes. For each mode 2000 data points were recorded with a sampling time of 2 ms per data point. A full scan of the array was repeated every 3 minutes.

The 7 μm thick agarose functionalised cantilever array was placed in the chamber and the temperature was set to 30 °C. RH levels were ramped from 86% to 96 % and allowed to return to 86% at a period of ~ 25 minutes. The response of the first flexural resonance mode was recorded. 400 data points were taken per sweep with a sampling time of 6 ms per data point. A full scan of the array was taken every 2 minutes.

**Results:** The change in flexural resonance frequency of the first four modes for the 2 μm cantilever is shown in Figure 4.12. Changes in resonance frequency are due to the absorption of water from the surrounding humid environment by the agarose layer on the cantilever. The black, red, green, and blue plots correspond to the fundamental, second,

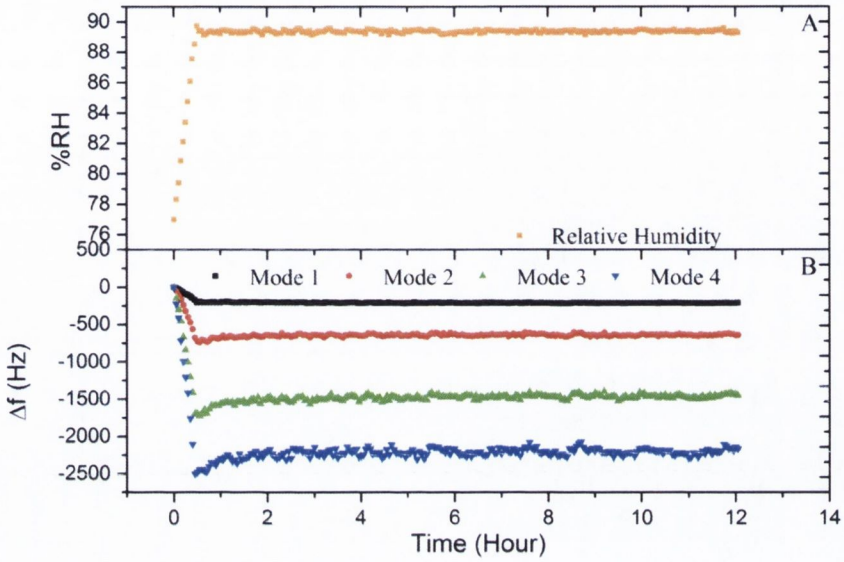


Figure 4.12: (A) Relative humidity. (B) Flexural resonance frequency response of the first four modes of a 2 μm thick agarose functionalised cantilever. Use of higher resonance modes increases device sensitivity by a factor of 13 when compared to the fundamental resonance mode.

third, and fourth resonance modes respectively. The figure shows that there is a direct correlation between humidity levels (Figure 4.12 (A)) and the resonance frequency of an agarose coated cantilever (Figure 4.12 (B)).

Plots of the same format can be shown for more than one cantilever in the array but they are omitted for clarity. Slight variances in the agarose layer on each cantilever produces different magnitudes of frequency response. This is more pronounced for higher resonance modes which would result in the convolution of the figure shown. For the specific cantilever shown its mass responsivity ($R_m$) (mass sensitivity $(S)^{-1}$) is found to be 38.8 ± 0.8, 10.3 ± 0.1, 4.3 ± 0.1 and 2.9 ± 0.1 pg/Hz for the fundamental, second, third, and fourth flexural resonance modes respectively assuming a uniform coverage of agarose on the cantilever's surface. Figure 4.13 shows inverse mode number squared ($n^{-2}$) versus mass responsivity. There is a linear relationship between square of mode number and sensitivity which is in agreement with data published in [2]. Here it is assumed that any damping caused by the viscoelastic agarose layer is negligible. As mentioned in Section 1.3.2 an increase in mass on the cantilevers surface results in an increase in $Q$ factor. This increase

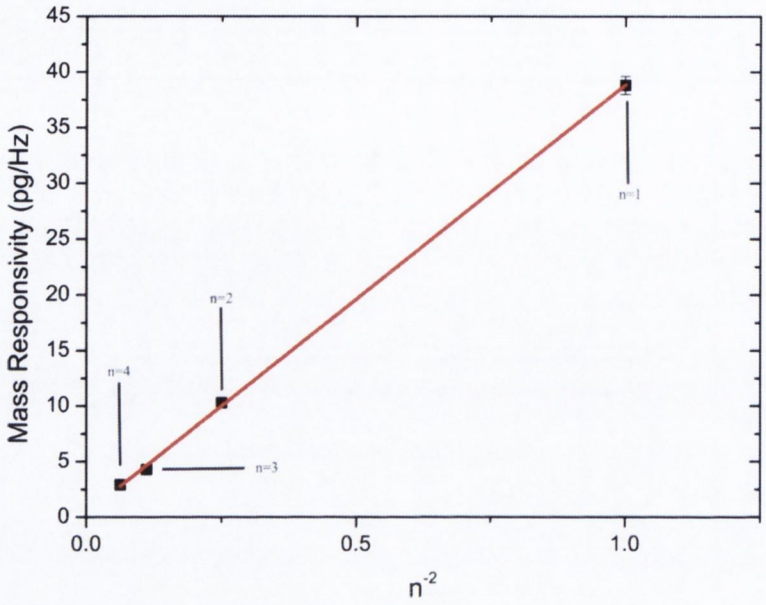


Figure 4.13: Plot of $n^{-2}$ versus mass responsivity. There is a linear increase in sensitivity with mode number squared.

is due to an increase in total stored vibrational energy ($W_s$). Any significant energy losses caused by the viscoelastic agarose layer would result in a decrease in $Q$ factor. The total increase in mass due absorption of water by the agarose layer is found to be ~ 7.6 ± 1.9 ng. The corresponding increases in $Q$ factor for modes 1-4 are shown in Table 4.1. As only increases in $Q$ factor are observed for all modes any damping caused by the viscoelastic agarose layer are deemed to be negligible. The ability of this device to accurately record the multimodal resonance frequency response of cantilevers in an array has been demonstrated. The ability to record the fourth resonance mode has increased the sensitivity of the device by a factor of 13 when compared to that achievable using the fundamental resonance mode. When using the fibre optic device the sensitivity would be limited to that of the first resonance mode due to device limitations. It should be noted that the mass

Table 4.1: Change in $Q$ factor for modes 1-4. The increase in mass on the cantilever due to the absorption of water by the viscoelastic agarose layer produces an increase in $Q$ factor thus indicating that any damping caused by the agarose layer is negligible.

| **Mode** | **1** | **2** | **3** | **4** |
|---|---|---|---|---|
| $\Delta Q$ | 11 | 29 | 60 | 74 |

responsivity is determined by the dimensions and functionalisation of the sensor used. A device capable of measurement of higher resonance modes allows the achievable mass responsivity to be realised.

The data shown in Figure 4.12, between the time points of 2 and 12 hours, demonstrates the excellent stability of environmental control provided by the environmental chamber. This is essential for accurate growth detection measurements. It should also be noted that there is no frequency drift over time for all modes. Noise levels, due to fluctuations in environmental conditions, are seen to increase with mode number.

Figure 4.14 shows an induced periodic fluctuation of humidity (A) and the corresponding first mode response of one blank Si cantilever and 3 agarose coated cantilevers on a 7 μm array (B). A direct correlation can be seen between humidity levels in the environmental chamber and the resonance frequency response of cantilevers. The figure demonstrates; (i) water absorbed by an agarose layer is immediately lost as humidity levels surrounding the

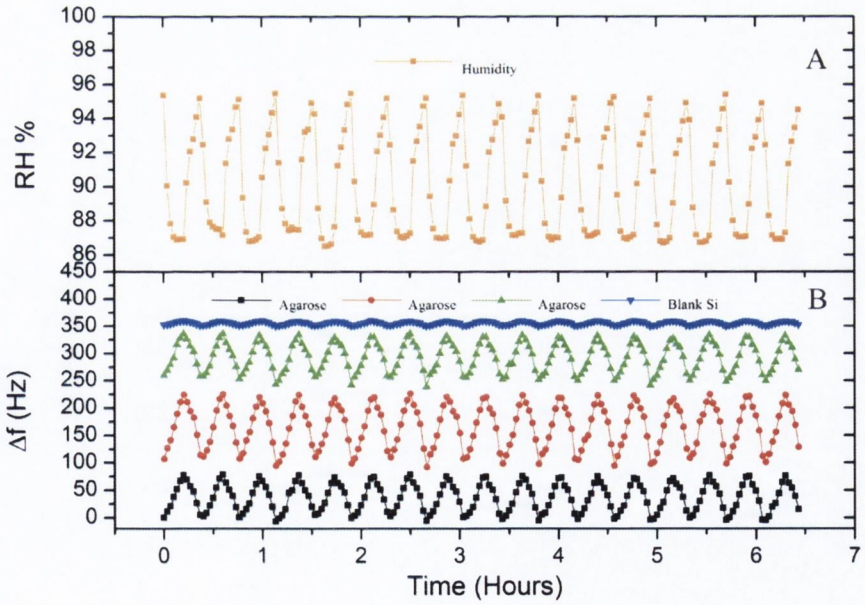


Figure 4.14: (A) Induced periodic fluctuation of humidity. (B) Fundamental mode response of one blank Si cantilever (blue) and 3 agarose coated cantilevers on a 7 μm array (green, red, black). A direct correlation can be seen between humidity levels in the environmental chamber and the resonance frequency response of cantilevers.

cantilevers decrease resulting in a positive resonance frequency shift. (ii) The device is capable of measuring resonance peaks of cantilevers with dynamic surface conditions.

The results described in this section indicate that this new device is capable of recording resonance spectra for multiple flexural resonance modes in dynamic conditions. The rates of change shown here are several times faster than those observed during microorganism growth measurements. This indicates the devices suitability for these measurements. Operation of this device has also been demonstrated, without issue, at the high humidity levels required for microorganism growth measurements.

## 4.5 References

1. Andersson, H., *Position sensitive detectors - device technology and applications in spectroscopy.* Ph.D. Thesis. Electronics Design Division in Dept. of Information Technology and Media, Mid Sweden University, Sweden., 2008.
2. Murali Krishna, G. and et al., *Higher modes of vibration increase mass sensitivity in nanomechanical microcantilevers.* Nanotechnology, 2007. **18**(44): p. 445502.

# Chapter 5
# Single Spore Growth Detection and Interpretation of Cantilever Response

In this chapter the resonance frequency response of cantilevers due to the spreading of fungal hyphae along their longitudinal axis is investigated. Multimodal growth measurements are presented where the growth of a single *A. niger* spore is detected. The subsequent spread of hyphal filaments produces different changes in the frequency response of the cantilever dependent on the resonance mode being tracked. Data is presented for cantilevers with thicknesses of 7 and 2 μm, where the thickness of the latter is smaller than the thickness of the hypha on its surface. The use of a 2 μm thick cantilever array allows for a higher number of modes to be tracked (due to bandwidth limitations of the PSD used) as opposed to using a 7 μm thick cantilever array. Hence, this provides more information on the dynamics of hyphal growth along a cantilever's longitudinal axis.

## 5.1 Introduction

When operated in dynamic mode cantilevers have traditionally been thought of as "mass sensors." Adsorption of a particle generates a negative frequency shift ($\Delta f$) dependant on the mass of the particle ($m$), its adsorbed position ($x$), and the resonance mode of operation. This relationship is summarised in Equation 5.1 [1]

$$\frac{\Delta f_n}{f_n} = -\frac{\psi_n(x)^2}{2}\frac{m_a}{m_b} \qquad 5.1$$

where $\psi_n(x)$ is the amplitude of the $n^{th}$ mode of vibration at a position $x$ along the cantilever's longitudinal axis (see Figure 5.1) and $f_n$ is the $n^{th}$ mode flexural resonance frequency of the unloaded cantilever. The subscripts $a$ and $b$ denote the adsorbed particle and cantilever beam respectively (this notation is maintained for the remainder of this chapter). Thus the magnitude of frequency shift ($\Delta f_n$) due to particle adsorption at a position ($x$) is proportional to the square of the amplitude ($\psi_n(x)^2$) at that position.

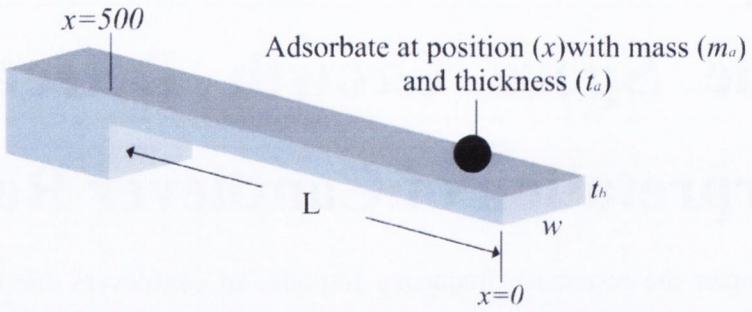


Figure 5.1: Schematic of cantilever with an adsorbed particle at a position $x$ along cantilever's longitudinal axis. $x$=0 corresponds to the cantilever's free end while $x$=500 corresponds to the clamped end. $L$, $w$, and $t_b$ correspond to the length, width, and thickness of the cantilever respectively. $m_a$ and $t_a$ correspond to the mass and thickness of the adsorbed particle respectively.

The amplitude of vibration for a given mode ($n$) is given by

$$\psi_n(x) = C_{1n}cos(\beta_n x) - C_{1n}cosh(\beta_n x) - C_{2n}sin(\beta_n x) + C_{2n}sinh(\beta_n x). \quad 5.2$$

The values of the eigenvalues $\beta_n$ and constants $C_{1n}$ and $C_{2n}$ for the first four flexural resonance frequency modes are shown in Table 5.1 [1]. It has also been shown that the adsorption of particles on cantilever beams can produce a positive shift in resonance frequency at certain positions ($x$) [2]. It is proposed that the stiffness of the adsorbed particle alters the flexural rigidity ($D^F$) of the cantilever according to the following equation [3]

$$D^F(x) = \frac{w}{12} \times \left( \frac{E_b^2 t_b^4 + E_a^2 t_a^4(x) + 2E_b E_a t_b t_a(x)\left(2t_b^2 + 2t_a^2(x) + 3t_b t_a(x)\right)}{E_b t_b + E_a t_a(x)} \right) \quad 5.3$$

where $w$ corresponds to the width of the cantilever. $t$ and $E$ correspond to thickness and Young's modulus respectively.

Table 5.1: Values for $\beta_n$ and constants $C_{1n}$ and $C_{2n}$ for the first four resonance modes.

| $n$ | $\beta_n$ | $C_{1n}$ | $C_{2n}$ |
|---|---|---|---|
| **1** | 1.8751 | 1 | 0.734096 |
| **2** | 4.69409 | 1 | 1.01847 |
| **3** | 7.85476 | 1 | 0.999224 |
| **4** | 10.9955 | 1 | 1.00003 |

A model based on Rayleigh's method, where a work-energy balance during an oscillation cycle, is used to determine the resonance frequency due to adsorption at a specific position $x$, as shown in Equation 5.4 [3]

$$f_n^2 = \frac{\int_0^L D^F(x)\left(\frac{d^2\psi_n(x)}{dx^2}\right)^2 dx}{\rho_c w t_b \int_0^L \left(1+\frac{\rho_a}{\rho_b}\frac{t_a}{t_b}\right)\psi_n(x)^2 dx} \qquad 5.4$$

where $\rho_b$ and $\rho_a$ correspond the densities of the cantilever and adsorbate respectively. Using this model the resonance frequency response due to adsorption of bacterial cells [3, 4] and gold patches [5] has been investigated. Work has also been published where the position and mass of the adsorbed particle can be determined based on the multimodal resonance frequency response of a cantilever [6-8]. Some of these works however assume no contribution due to the stiffness of the adsorbed mass.

An extended equation for the resonance frequency shift due to the adsorption of a particle on a beam that accounts for both the mass, stiffness, and position of the particle is [1],

$$\frac{\Delta f_n}{f_n} = \left(\frac{3}{2}\frac{1}{\beta_n{}^4}\frac{d^2\psi_n(x)^2}{d(x)^2}\frac{E_a}{E_b} - \frac{1}{2}\psi_n(x)^2\frac{\rho_a}{\rho_b}\right)\frac{V_a}{V_b} \qquad 5.5$$

where $E$, $\rho$, and, $V$ correspond to Young's modulus, density, and volume respectively. Examination of Equation 5.5 reveals that the effect of the adsorbate stiffness is proportional to the square of the curvature ($d^2\psi_n(x)^2/d(x)^2$) of the vibrational mode at the position of adsorption $x$. Figure 5.2 shows plots of mode shape ($S$) above plots of responsivity/sensitivity ($R$) due to the mass (red) and stiffness effect (blue) for the first four flexural resonance modes. For the subsequent discussion the cantilever's free end corresponds to $x$=0 while the clamped end corresponds to $x$=500 μm as illustrated in Figure

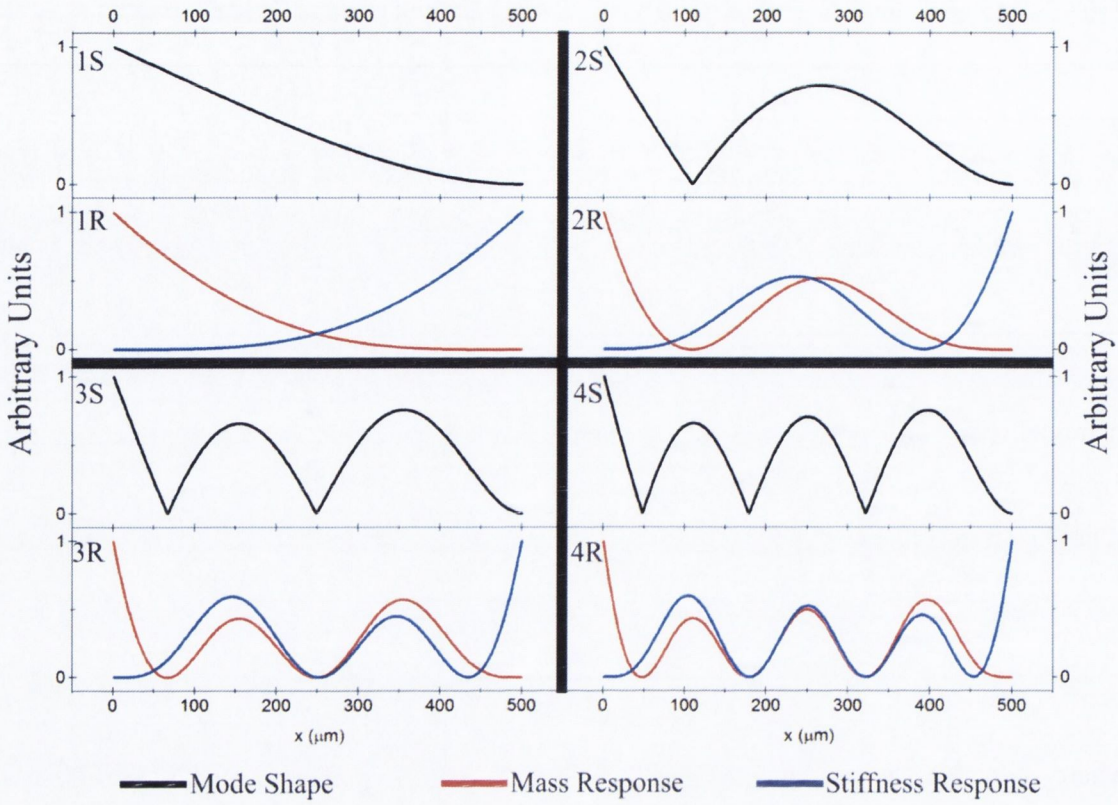


Figure 5.2: Mode shape ($S$) and Responsivity ($R$) due to the mass (red) and stiffness effect (blue) for the first four flexural resonance modes. $x$ corresponds to length along the cantilever's longitudinal axis where 0 corresponds to the cantilevers free end and 500 to the clamped end. These curves are plots of $\psi_n(x)$, $\psi_n(x)^2$, and $d^2\psi_n(x)^2/d(x)^2$ which represent vibrational amplitude, proportionality to mass sensitivity (amplitude squared), and proportionality to stiffness sensitivity(curvature squared) respectively.

5.1. From Figure 5.2 it is evident that uncoupling of the mass and stiffness effect is only possible at certain regions along the cantilever's longitudinal axis. For all modes the mass and stiffness effects are dominant at the free and clamped ends of the cantilever respectively. A fungal spore placed at the cantilever's free end results in the spreading of hyphal filaments across the cantilever's surface. Changes in frequency response will be observed as the hyphae cross different regions of the cantilever dependent on the vibrational mode shape of the resonance mode being tracked. The models discussed above deal only with point masses or masses which are small compared to the length ($L$) of the cantilever. In the case of a growing spore hyphae eventually spread along the cantilever's length but cannot be treated as a uniformly distributed layer because their width (3-6 μm) is significantly smaller than the cantilever beam (100 μm). In the subsequent sections the

hyphal growth from individual spores is monitored using multiple flexural resonance modes with accompanying video analysis. The equations presented here are pushed to the limits of their intended use to try to model the observed frequency responses.

## 5.2 Instrumentation

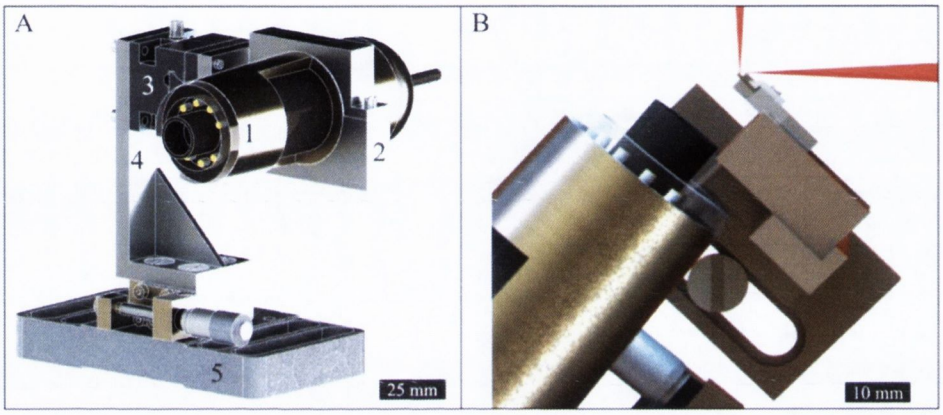


Figure 5.3: (A) Mounted USB digital camera. (1) USB digital camera. (2) Custom designed camera mount. (3) Dual axis (YZ) micro translation stage. (4) Extender mount. (5) Linear (X) translation stage. (B) Close up of USB camera location in device. The camera provides a magnification of x460 and at a working distance of 7.9 mm.

Measurements are performed using the device described in Chapter 4. In order to enable imaging of spores on the cantilever a USB digital camera (AM7013MZT4; Dino-Lite Europe, Netherlands) with high magnification (x460), long working distance (7.9 mm), and sufficient field of view (0.86 x 0.65 mm) is utilised. The camera is mounted onto a dual axis (YZ) micro translation stage via a custom designed mount. The dual axis micro translation stage is mounted via a custom designed mount on a linear translation stage (New Focus, Santa Clara, CA, USA) which provides motion in the X direction. This is shown in Figure 5.3 (A). In order to enable imaging of the backside of the cantilever during measurements the wind shielding mount (discussed in Chapter 4) used to protect the cantilever array was replaced with the mount shown in Figure 5.3 (B). In order to prevent adverse effects due to the wind generated by the fan in the back wall of the environmental chamber a Perspex box was fabricated to house the entire breadboard onto which the optical components are mounted. Air flow into the Perspex box is via small inlets on the front and sides which allows for a stable environment to be maintained.

Camera specific software (Dinocapture 2 Dino-Lite Europe, Netherlands) is used to turn on/off the camera for recording of images at designated time intervals. The software controls the output of LEDs on the camera used for illumination of the field of view. It is possible to turn off the LEDs when measuring resonance frequencies to prevent saturation of the PSD.

## 5.3 Materials and Methods

Two cantilever arrays were plasma cleaned, silanised, and agarose functionalised as described in Chapter 2. The arrays chosen had thickness of 2 and 7 μm, with lengths and widths of 500 and 100 μm respectively.

Individual *A. niger* spores were placed on cantilevers using the glass needle technique as described in Chapter 2. Spores were deposited on three cantilevers in the 7 μm array and two in the 2 μm array. Prior to spore deposition the arrays were soaked in Roswell Park Memorial Institute medium broth (RPMI – 1640, Sigma Aldrich) (supplemented with 0.165 M MOPS and 0.2% glucose) for 10 minutes in order to load the agarose layer with nutrition.

## 5.4 Measurement

For both measurements the environmental conditions inside the device chamber were set to 94% RH and 30 °C and allowed to equilibrate for >30 minutes. After spore deposition, the cantilever array was mounted on the piezoelectric actuator and placed into the device. The digital camera was aligned for imaging of the test cantilevers at 30 minute intervals.

### 5.4.1 7 μm Experiment

Frequency spectra were recorded for the first two resonance modes. For the fundamental resonance mode 400 data points were recorded in each spectrum at a sampling rate of 8 ms per data point. For the second resonance mode 800 data points were recorded at a sampling rate of 4 ms per data point. Spectra were recorded every 30 minutes for 6 cantilevers (3 test and 3 reference) in the array.

### 5.4.2 2 μm Experiment

Frequency spectra were recorded for the first four resonance modes. For the fundamental mode 400 data points were recorded in each spectrum at a sampling rate of 8 ms per data point. For the second resonance mode 800 data points were recorded in each spectrum at a sampling rate of 4 ms per data point. For the third and fourth resonance modes 2000 data points were recorded in each spectrum at a sampling rate of 2 ms. Spectra were recorded every 30 minutes for 5 cantilevers (2 test and 3 reference) in the array.

Measurement intervals of 30 minutes (video and frequency) were chosen in both experiments (7 and 2 μm). *A. niger* is a slow growing species, so more frequent (or even continuous) data and video acquisition would exceed PC storage capacity due to the length of time required for growth to be observed.

## 5.5 Results and Discussion

### 5.5.1 7 μm Experiment

Data is presented for two of the test cantilevers. The 3$^{rd}$ cantilever shows the same qualitative results however condensation of a water droplet on the sensor during this experiment makes image analysis difficult. Figure 5.4-5.7 show plots for the fundamental and second mode differential resonance frequencies for two cantilevers (A and B). All frequency plots shown have been reference corrected using the frequency response of agarose functionalised sensors. Black data points correspond to the measured relative resonance frequency shift ($\Delta f/f$). The blue data points correspond to the percentage of the cantilevers surface occupied by hyphal filaments. Measurement of hyphal area was performed using National Instruments IMAQ VIs. Data before 5 hours is omitted as camera alignment issues resulted in a disruption of the environmental regulation and fluctuations in resonance frequency were observed. No growth had occurred before this time point, therefore their exclusion is justified. Figure 5.4 – 5.7 also display selected images of the cantilevers recorded during the growth measurement. The times at which the images were recorded are indicated in the figures. The cantilever's free end ($x$=0), clamped

end ($x$=500), and any significant vibrational nodes are indicated in the images where necessary.

A resonance frequency shift is observed in all plots shown in Figure 5.4 - 5.7 indicating the detection of single *A. niger* spore growth after 15 hours. This detection time is an order of magnitude faster than that which is achievable using conventional culturing techniques [9]. This detection time is also comparable to times reported in [10, 11] and in the experiments described in Chapter 3 where the detection of multiple spores is reported using a single resonance mode. The ability to detect the growth of single spores within a short time is advantageous, especially in a clinical setting, as it allows for a reduction in the number of spores/cells required. In the subsequent sections a detailed examination of the frequency plots and corresponding recorded images is performed.

#### 5.5.1.1 Fundamental Resonance Mode

Through examination of Figure 5.4 and Figure 5.5 it can be seen that the rate of change of the resonance frequency varies over time (black). However the corresponding plots of cantilever coverage by hyphal filaments (blue) do not always show the same trends. This would indicate that hyphae are propagating along the cantilevers length and thus entering regions where sensitivities to mass and stiffness differ.

**Cantilever A**

Figure 5.4 displays data obtained for cantilever A. The pink segment (highlighted in the plot) shows a small negative shift in resonance frequency. Images 1 and 2 (which correspond to the start and end point of the pink segment) show a significant swelling of the spore. The increase in spore size, due to intake of water by the cytoplasm, results in increased water adsorption on the spore's hydrophilic outer wall. Swelling occurs prior to generation of the germ tube [12, 13] which leads the way for hypha formation. The start of the yellow segment highlights the time at which hypha start to protrude from the spore. An increasing rate of frequency change is observed in the yellow segment. Image 3 shows that

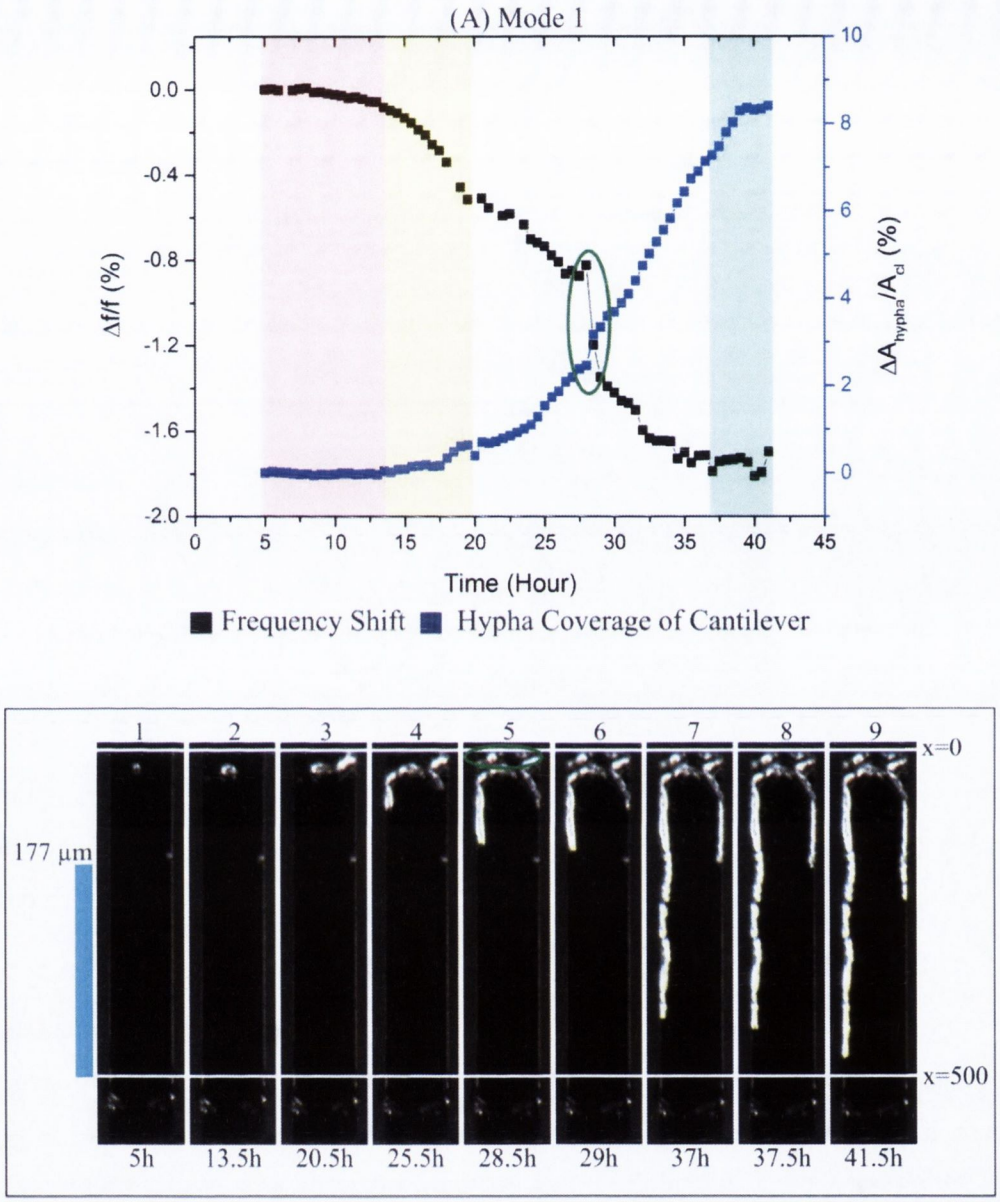


Figure 5.4: Fundamental mode experimental data for cantilever A. The plot shows relative resonance frequency shift (black) and percentage coverage of cantilever by hyphae (blue) with respect to time. The coloured segments identify specific growth events which are discussed in the text. The images show the surface of the cantilever with fungal growth at different time points during the experiment. Areas of mass insensitivity are marked in blue to the left of the image.

a hypha is growing towards the cantilever's free end. In this case the hypha is experiencing higher amplitudes of vibration ($\psi_n(x)$); hence according to Equations 5.1 and 5.5 an increasing rate of frequency shift change is observed as growth propagates towards the

cantilever's free end. Although not visible in Image 3 hyphal growth continues off cantilever when the free end is reached (yellow segment end).

At 20.5 hours (Image 3) additional germination occurs and two new hyphae emerge from the spore. These hyphae grow towards either side of the cantilever and then towards the clamped end as shown in Image 4. Growth of these new hyphal structures towards the cantilever's clamped end results in the observed linear decrease in resonance frequency. The hypha circled in green (Image 5) which was previously growing off cantilever has relocated onto the cantilever's surface at the free end between two scanning steps. Its relocation in between frequency measurements is the cause of the large frequency shift which is circled in the frequency plot. The large shift observed indicates that off cantilever growth has a reduced effect on the cantilever's resonance frequency. It is postulated that when a hypha is located on the cantilever's surface a larger water layer is adsorbed on the hypha's outer wall than that which adsorbs when the hypha is off cantilever. The reason for the relocation of this hypha and the termination of its growth afterwards is unknown. Examination of the area plot at this time point (28 – 28.5 hours) also shows a small jump in cantilever coverage which is attributed to the relocation of this hypha. Its relocation at the free end of the cantilever, where $\psi_n(x)$ is maximal, produces a large negative frequency shift because this is the point on the cantilever where mass sensitivity is greatest.

The hyphae on either side of the cantilever continue to grow towards the clamped end of the cantilever. After 37 hours the rate of frequency change is seen to decrease to zero. The decrease in the rate of frequency change is not reflected in the rate of change of hyphal area which remains constant until 39 hours indicating the cessation of growth. The decrease in the rate of resonance frequency change indicates that growth has propagated into a region of the cantilever which is not sensitive to mass loading. As growth is occurring at different rates on each side of the cantilever it is difficult to ascertain the distance from the cantilever's free end where mass sensitivity is null. Image 7 shows the extent of hyphal propagation at this time point. The hypha on the left side of the cantilever has nearly reached the cantilever's clamped end and according to Equation 5.5 (and Figure 5.2 R1) its mass should have no effect on resonance frequency. There is no observable increase in resonance frequency in the region where stiffness should dominate (towards the clamped end), which would indicate that the stiffness of this hypha is not sufficient to produce a positive frequency shift. It can be assumed then that the length of the

shorter/slower hypha on the right side of the cantilever can be used to determine the point at which mass has no measureable effect. Therefore for the fundamental resonance mode the position at which hyphal growth is no longer detectable is approximately 177 ± 5 μm from the cantilevers free end. The non-mass sensitive region for the fundamental mode is shown in blue on the left hand side of the images in Figure 5.4. The error in the length measurements is based on the ability to accurately determine the end of the hypha position. An error of ± 3 % is assumed based on a standard error in position determination of 3 pixels during image analysis.

**Cantilever B**

Figure 5.5 displays data obtained for cantilever B. After spore swelling (pink segment on plot, Images 1-2) hyphal filaments begin to spread towards the cantilever's clamped end. This spreading is reflected in an initial linear decrease in resonance frequency observed in the white segment. Growth continues to proceed at a linear rate until 26 hours. Through examination of Images 4 and 5 it can be seen that there is a reduction in the size of the water layer surrounding the hypha circled in green. This is mirrored by a decrease in the hyphal coverage of the cantilever (blue data points) and a positive resonance frequency shift which is circled in green also. Partial drying appears to affect this specific hypha while the rest of the fungal structure appears to retain its full water layer. It is postulated that this drying is due to the secretion of proteins known as hydrophobins. Hydrophobins form amphipathic monolayers at hydrophobic–hydrophilic interfaces which reduce the surface tension of the medium or the substrate in/on which fungi grow [14]. This reduction in surface tension ensures that hyphae can form structures such as aerial hyphae or fruiting bodies [15]. The hydrophilic side of the hydrophobin is facing the hypha cell wall whereas the hydrophobic rodlet-decorated surface is exposed to the air [15]. The hypha on the discussed cantilever fails to emerge into the air but it is no longer able to assimilate nutrition from the moist environment. From the remaining images shown it can be seen that the growth of this hypha ceases after this point. We observed aerial hyphae in several experiments where they can grow more than one hundred microns and also bridge the distance (150 μm) between cantilevers (data not shown here).

A second hypha protrudes from the spore as shown in Image 3 and propagates towards the cantilever's clamped end. A third hypha also protrudes from the spore and propagates

towards the cantilever's left side as shown in Image 7. Both of these hyphal filaments are propagating at different rates and in different directions, again making it difficult to

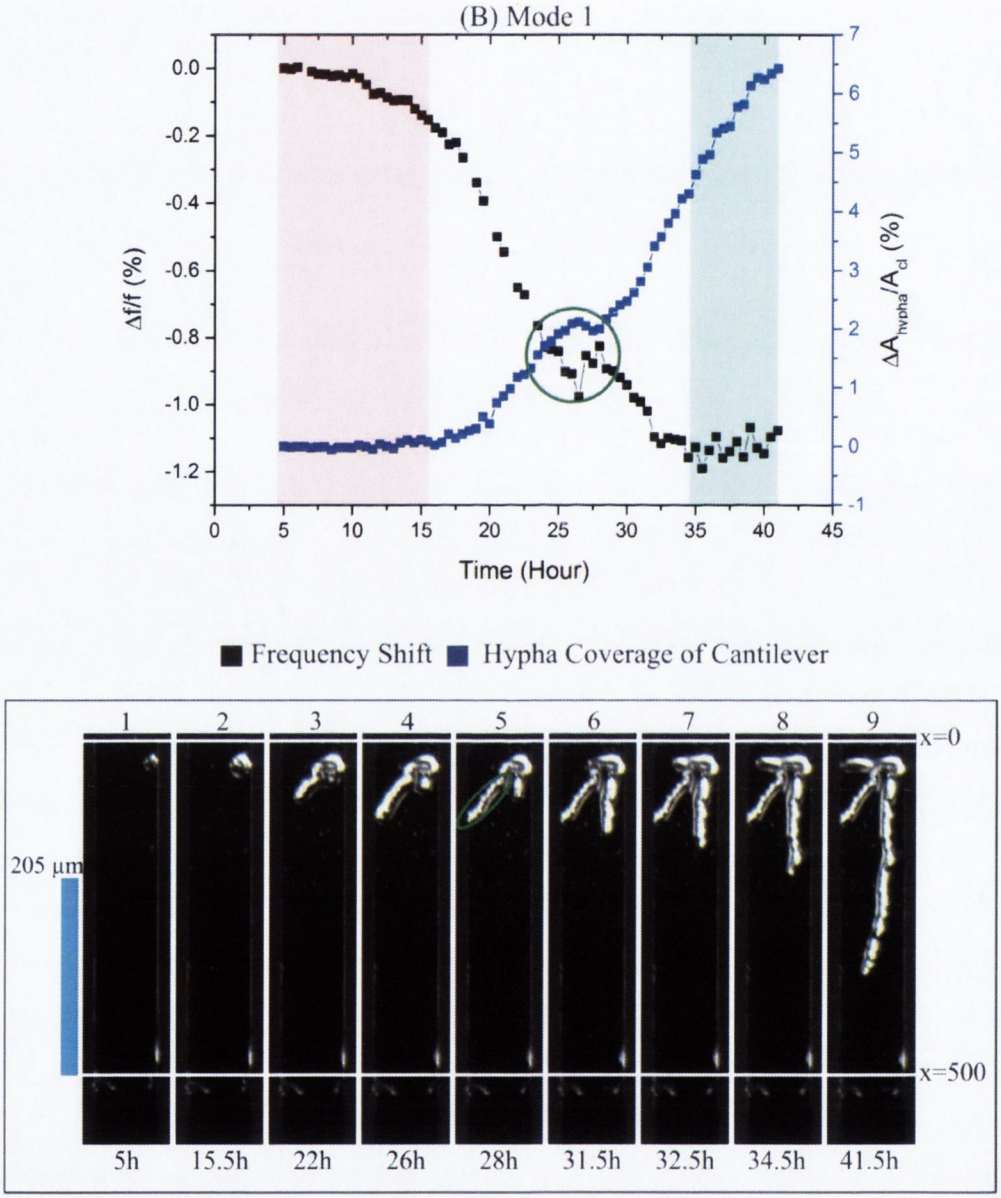


Figure 5.5: Fundamental mode experimental data for cantilever B. The plot shows relative resonance frequency shift (black) and percentage coverage of cantilever by hypha (blue) with respect to time. The coloured segments identify specific growth events which are discussed in the text. The images show the surface of the cantilever with fungal hypha growth at different time points during the experiment. Areas of mass insensitivity are marked in blue to the left of the images.

ascertain where along the cantilevers length mass sensitivity is null. The start of the green segment highlighted on the plot in Figure 5.5 shows the point where resonance frequency changes cease. Again it can be observed that at this point there is no reduction in growth rate as indicated by the plot of hyphal coverage. Image 8 corresponds to the end of frequency changes. Analysis of this image indicates that the hypha growing towards the cantilever's clamped end has no effect on resonance frequencies approximately 205 ± 6 μm from the cantilever's free end. When compared to cantilever A this distance is slightly longer. The longer distance in the case of cantilever B could be due to two factors; (i) the hypha propagating towards the cantilever's clamped end is visually larger than the hypha on the right side of cantilever A (Figure 5.4 Image 8) which was used to determine the value of 177 ± 5 μm. This larger size/mass results in measureable frequency shifts closer to the cantilever's mid-point. (ii) In the case of cantilever B there is a hypha growing towards the left hand side of the cantilever as the hypha propagating towards the clamped end is reaching the mass insensitive region. This makes it difficult to identify the start point of the mass insensitive region as the hypha propagating towards the left of the cantilever is also contributing to the observed resonance frequency shift.

#### 5.5.1.2 Second Resonance Mode

Changes in the rate of frequency shift can also be observed in the second mode resonance frequency plots shown in Figure 5.6 and Figure 5.7 for cantilevers A and B respectively. These are examined in detail in the subsequent sections.

**Cantilever A**

Figure 5.6 shows data obtained for cantilever A when operated at its second flexural resonance mode. Spore swelling (Image 1- 2) and growth of the hypha towards the front of the cantilever (Image 3) is again highlighted in pink and yellow on the plot, as was the case in the fundamental resonance mode discussed previously. At 20.5 hours a linear decrease in resonance frequency is observed indicating the start of growth towards the clamped end of the cantilever (Image 4). The green segment (25.5 hours) highlights the segment where growth enters the mass insensitive region located around the node of vibration marked in the images as 'node'. The tip of the hypha on the left of the cantilever (Image 4) is used to

identify this region, which is found to start ~69 ± 2 µm from the cantilever's free end. This region of the cantilever has lower vibrational amplitude therefore masses located at this position produce small/no resonance frequency shifts as indicated by Figure 5.2 R2 (and

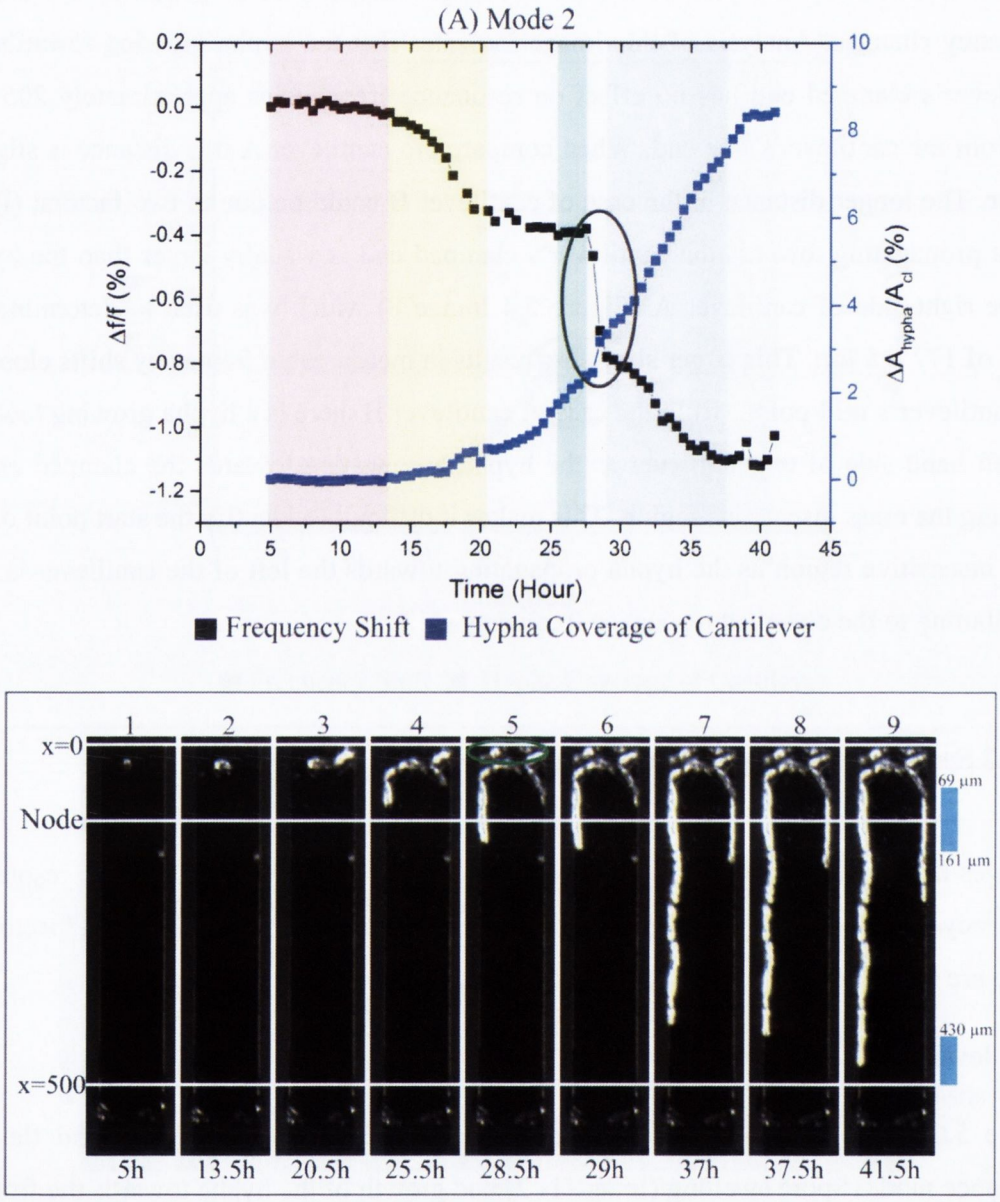


Figure 5.6: Second flexural resonance mode experimental data for cantilever A. The plot shows the relative resonance frequency shift (black) and the percentage coverage of cantilever by hypha (blue) with respect to time. The coloured segments identify specific growth events which are discussed in the text. The images show the surface of the cantilever with fungal growth at different time points during the experiment. Areas of mass insensitivity are marked in blue to the right of the image.

Equation 5.5). As the curvature of the mode shape ($d^2\psi_n(x)/d(x)^2$) begins to increase at this point a positive shift in resonance frequency might be expected dependant on the value of the Young's modulus of the adsorbate ($E_a$). As no rise in resonance frequency is observed it is evident that the stiffness of the hypha is not sufficient to produce a measureable frequency shift.

The rapid change in resonance frequency at 28.5 hours (circled in green on plot) is due to the relocation of off cantilever growth onto the cantilever as discussed previously. At 29 hours the hypha on the left of the cantilever emerges from the mass insensitive region resulting in the observed decrease in resonance frequency (grey segment). In the grey segment masses are experiencing amplitudes of vibration ($\psi_n(x)$) which are sufficient to produce measureable changes in resonance frequency. From Image 6 the end of the mass insensitive region occurs ~ 161 ± 5 μm from the cantilever's free end. The region around the node (69 – 161 μm) of vibration where there is no mass sensitivity is marked in blue beside the images.

At this point growth continues in a linear fashion. At 37.5 hours (Image 8) the rate of frequency change decreases to 0. This indicates that growth has again entered a region of the cantilever which is insensitive to mass loading. Using the tip of the hypha on the left of the cantilever this position is found to occur ~ 430 ± 13 μm from the cantilevers free end. After this time point there are observed fluctuations in the resonance frequency. This may be due to a possible positive frequency shift caused by the hypha on the left of the cantilever as it approached the clamped end of the cantilever. At the clamped end the 'stiffness effect' dominates as shown in the responsivity plots shown at the beginning of this chapter (Figure 5.2). The hypha on the right is growing in the mass sensitive region of the cantilever. Hence, the 'mass effect' and 'stiffness effect' are competing after 37.5 hours resulting in the observed fluctuation.

**Cantilever B**

Figure 5.7 displays the data obtained for cantilever B when operated at its second flexural resonance mode. At 15.5 hours (Image 2) hyphal filaments begin to spread after spore swelling (pink segment) resulting in the observed linear decrease in resonance frequency (yellow segment). The rate of resonance frequency change decreases (white segment) and then increases again (green segment).

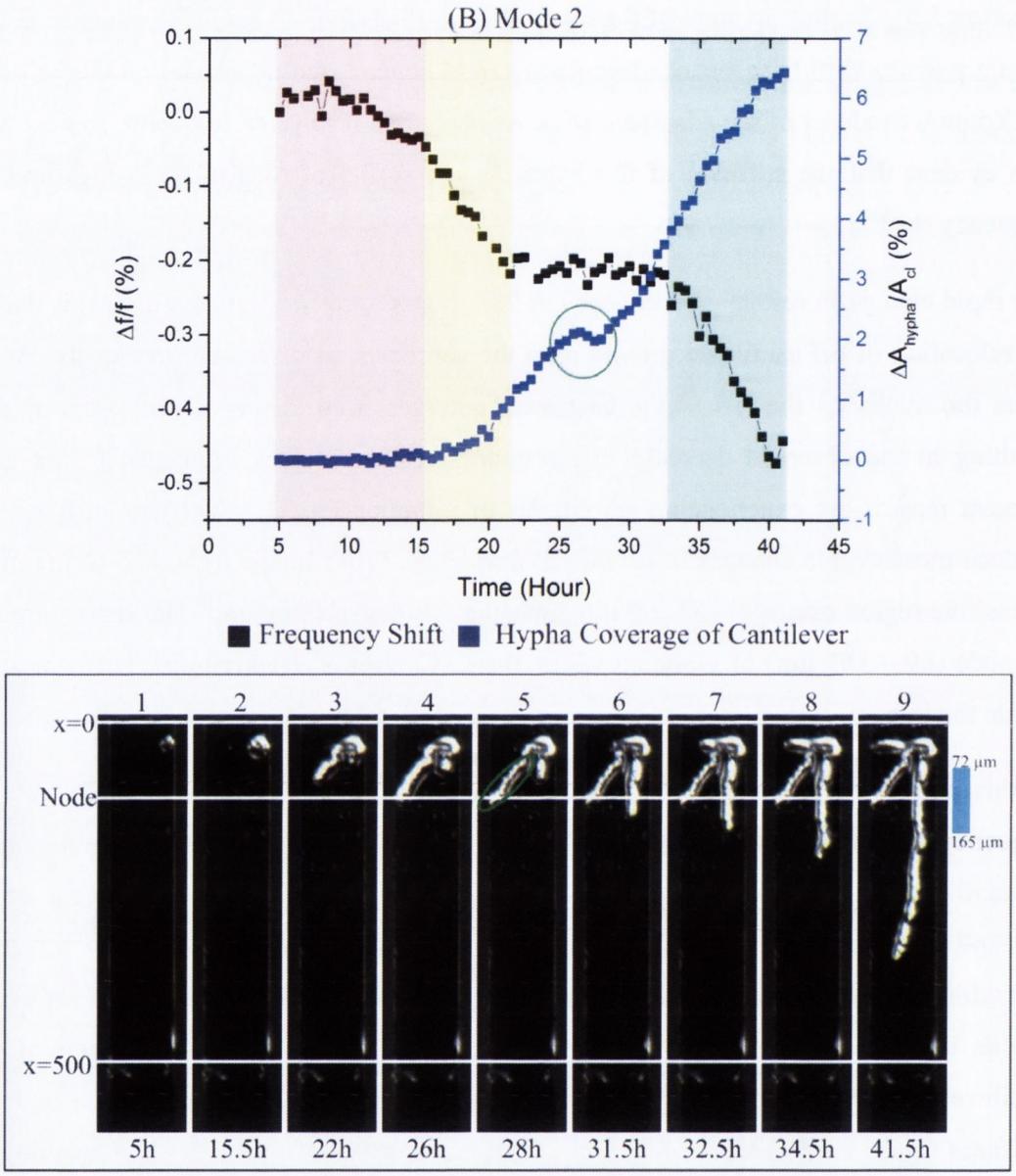


Figure 5.7: Second flexural resonance mode experimental data for cantilever B. The plot shows the relative resonance frequency shift (black) and the percentage coverage of cantilever by hypha (blue) with respect to time. The coloured segments identify specific growth events which are discussed in the text. The images show the surface of the cantilever with fungal growth at different time points during the experiment. Areas of mass insensitivity are marked in blue to the right of the image.

The start of the white segment at 22 hours highlights the point where resonance frequency change ceases, indicating that growth has entered a mass insensitive region. Through examination of Image 3 it can be seen that there are two hyphae protruding from the spore. Here the tip of the shorter hypha is used to identify the starting position of the mass

insensitive region. If the longer hypha identified the position of the mass insensitive region at this time point then growth of the smaller hypha past its position shown (Image 3), would be expected to produce a measureable resonance frequency shift. As this is not the case the use of the shorter hypha is justified. Hence, the start of the mass insensitive region is found to occur ~72 ± 2 μm from the cantilever's free end.

The beginning of the green segment at 32.5 hours highlights a negative frequency shift indicating that the hypha has emerged from the mass insensitive region. From Image 7 this occurs ~ 165 ± 5 μm from the cantilever's free end. Thus for cantilever B the mass insensitive region is found to be located between 72-165 μm from the cantilevers free end as highlighted in blue to the right of the images.

The drying of the hypha circled in green (Image 4), due to the production of hydrophobins, does not produce a positive frequency shift as was observed in the fundamental mode frequency plots (Figure 5.5). Examination of Image 4 reveals that this hypha is located in the mass insensitive region and thus the mass loss is not detected.

Tracking of two resonance modes provides information regarding the position ($x$) of the hypha tip on the cantilevers longitudinal axis while also providing a qualitative growth detection result. It has been observed that growth through regions of low vibrational amplitude result in a decreased mass sensitivity. Evaluation of the resonance frequency allows for the position of the hyphal tip to be determined. For example, in the case of the fundamental resonance mode a reduction in mass sensitivity is observed as the hyphal tip approaches the mid-point of the cantilever's longitudinal axis. At the same time in the case of the second resonance mode mass sensitivity decreases around the vibrational node as predicted. Hence, measurement of both modes reveals that hyphal propagation has passed the mass sensitive region around the node of vibration ($2^{nd}$ mode), but has yet to reach the mass insensitive region closer to the mid-point of the cantilever ($1^{st}$ mode). As growth is occurring in multiple directions at the same time it is not possible to accurately determine the exact position of the hyphal tip. An accurate estimation of growth rate cannot be given without video analysis as hyphae are propagating in multiple directions. From the recorded images the hypha on the left of the cantilever in Figure 5.6 is found to have the fastest growth rate of ~ 41 μm per hour according to image analysis.

#### 5.5.1.3 Predictions and Simulation

Comparisons to theoretical equations and finite element modelling (FEM) were performed in order to verify the experimental observations made. Theoretical modelling was performed using Mathematica (Wolfarm research). Equation 5.5 is used to determine the frequency shift due to the growth of a single hypha from the cantilever's free end towards the clamped end. The cantilever was assumed to have a length, width, and thickness of 500, 100, and 7 μm respectively. The cantilever was assumed to have a density ($\rho_b$) of 2330 kg/m$^3$ and a Young's modulus ($E_b$) of 131 GPa. The hypha was modelled as consecutive rectangular blocks with a width, height, and length of 5, 5, and 10 μm respectively. Due to its high water content (> 90%) the hypha was assumed to have a density ($\rho_a$) of 1000 kg/m$^3$ and a Young's modulus ($E_a$) of 0.2 GPa [16]. The resonance frequency shift was calculated at positional intervals ($x$) of 10 μm. After each interval the mass of the hypha was added to that of the cantilever's to ensure that the entire mass of the hypha is considered as its length increases. The same was not applied to the Young's modulus as the effect of the stiffness contribution of an elongated mass on a cantilever's resonance frequency is not easily determined (due to its irregular shape on the surface of the sensor) or accounted for in Equation 5.5. It should be noted that Equation 5.5 is intended for modelling frequency changes due to adsorbed point masses. Its application here is pushing the limits of its intended use.

FEM was performed using Comsol. The same hyphal material properties used for theoretical modelling are assumed and a Poisson ratio ($\upsilon$) of 0.5 is also applied [17]. The length of the hypha was increased from 10-500 μm at 10 μm intervals starting at the cantilever's free end. An extra fine free tetrahedral mesh was used.

**Fundamental Mode**

Figure 5.8 (B) shows the relative frequency shifts obtained from modelling using Equation 5.5 and simulation. Both methods produce the same result as expected. Part A of this figure shows the mode shape and corresponding square of amplitude and curvature plots which are proportional to the mass and stiffness responsivities. Both methods show a decrease in resonance frequency until the cantilever's mid-point where the rate of frequency change decreases to zero. If compared to the experimental plots (Figure 5.4 and Figure 5.5) it can

be seen that there is a qualitative agreement once effects due to off cantilever growth, hydrophobin production, and growth towards the cantilever's free end are ignored. From this information it is possible to conclude that the stiffness of the hypha is having a small/negligible effect on frequency response.

Experimentally, mass insensitivity was found to occur on average 191 ± 6 μm from the cantilevers free end. This value is significantly shorter than that predicted by theory. There are several reasons for this; (i) Modelling does not account for noise levels present due to humidity fluctuations. As the mid-point of the cantilever is approached the mass of the hypha appears to be insufficient to produce a measureable frequency shift. (ii) The hypha is modelled as a rectangular block with a uniform composition. While this allows for easy modelling to be performed, in reality the hypha is cylindrical in shape and does not have a uniform composition but a complex internal structure containing several intracellular components and a cytoskeleton.

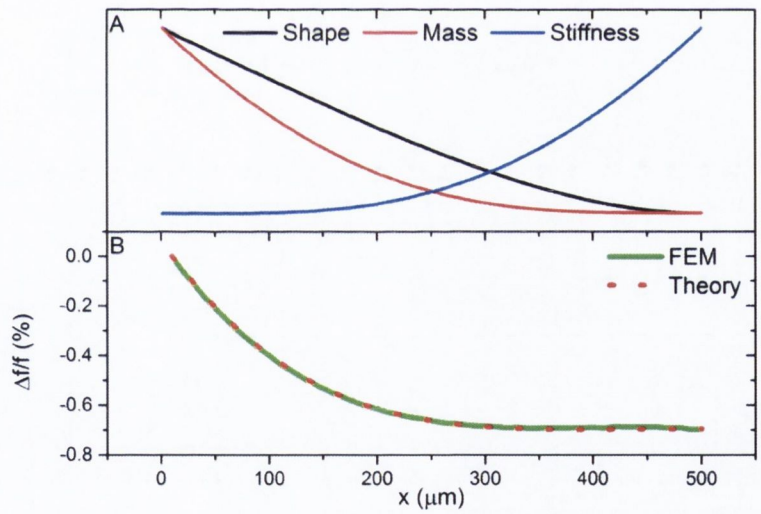


Figure 5.8: Fundamental mode relative frequency shift predictions due to hyphal growth. (A) Normalised plots of mode shape ($\psi_n(x)$), $\psi_n(x)^2$ ($\propto$ mass responsivity), and $d^2\psi_n(x)^2/dx^2$ ($\propto$stiffness responsivity). (B) Relative resonance frequency shift due to hyphal growth along a cantilever according to FEM (green) and Equation 5.5 (red). The hypha is modelled as a rectangular block with length, width, and thickness of 10, 5, and 5 μm respectively. The length of the hypha is increased in steps of 10 μm.

**Second Mode**

Figure 5.9 (B) shows the relative frequency shifts obtained from modelling using Equation 5.5 and simulation. Part A of this figure shows the mode shape and corresponding mass and stiffness responsivities. Again both techniques produce the same result. When compared to the experimental data in Figure 5.6 and Figure 5.7 it can be seen that the same trends in resonance frequency shift can be observed when effects due to swelling, growth towards the cantilever free end, off cantilever growth, and drying are ignored.

Figure 5.9 shows that there is no resonance frequency shift in between 80 – 140 μm and 420-500 μm. Experimentally these values are found on average to be between (70 ± 2) – (163 ± 5) μm and (430 ± 13) – 500 μm. The size of the predicted second region of mass insensitivity agrees with that measured experimentally. The first region of mass insensitivity, around the node of vibration at 112 μm, is found to be smaller than that calculated experimentally. The reasons listed in the previous section apply here again.

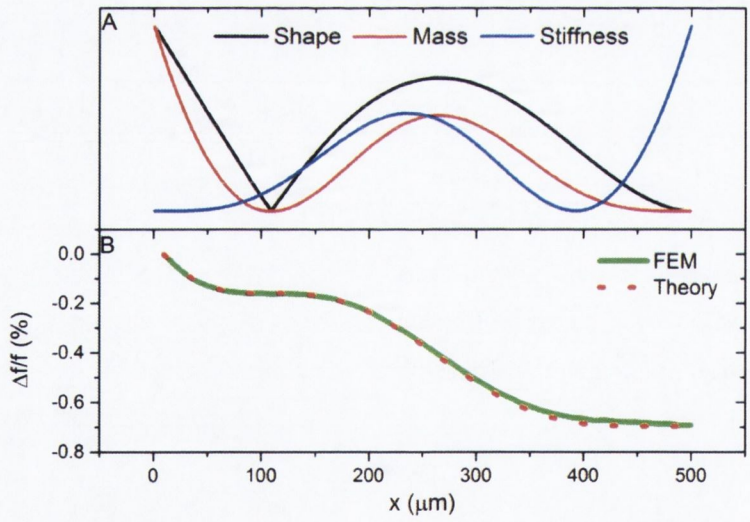


Figure 5.9: Second flexural resonance mode relative frequency shift predictions due to hyphal growth. (A) Normalised plots of mode shape ($\psi_n(x)$), $\psi_n(x)^2$ ($\propto$ mass responsivity), and $d^2\psi_n(x)^2/dx^2$ ($\propto$stiffness responsivity). (B) Relative resonance frequency shift due to hyphal growth along cantilever according to FEM (green) and Equation 5.5 (red). The hypha is modelled as a rectangular block with length, width, and thickness of 10, 5, and 5 μm respectively. The length of the hypha is increased in steps of 10 μm.

### 5.5.2 2 μm Experiment

Data is presented for one of the test cantilevers. The other test cantilever is omitted as growth proceeded onto the cantilever's top side and off the cantilever's surface once germination began rendering it unsuitable for video analysis.

Figure 5.10 shows the relative frequency shift for the fundamental resonance mode during the course of the growth experiment. Growth of a single spore has been detected after ~ 24 hours. This is slower than growth detection times previously reported. This may be an indication of the health of the spore, which may be influenced by the measurement of 4 modes (6 cantilevers × 4 modes each = 24 scans/30 minutes). The increased 'shaking' as a result of measurement of multiple resonance modes may be the cause of the increased lag time observed prior to spore germination. At higher modes spores are exposed to higher forces due to acceleration which may be detrimental to spore viability. It should be noted however that the displacement experienced by the spore, due to oscillation of the cantilever, at higher modes is significantly reduced when compared to that of the fundamental resonance mode. At higher modes displacement is only a fraction of spore diameter and hence forces due to acceleration can possibly be neglected. Further investigation is required in this area.

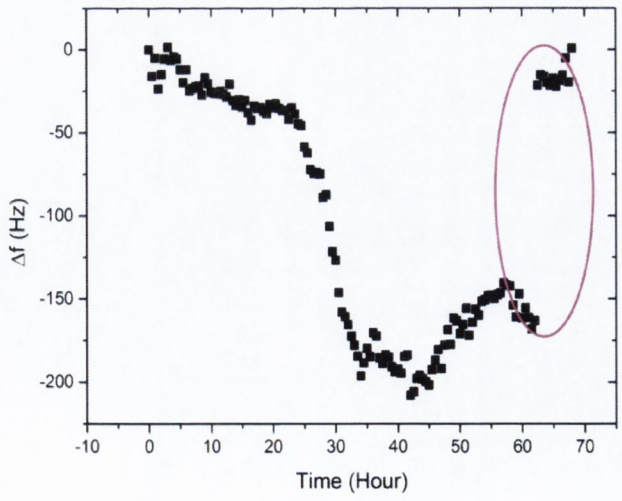


Figure 5.10: Resonance frequency shift versus time for the fundamental resonance mode. Raw data is shown. Growth is detected after ~ 24 hours. The drift up to this point is present in all sensors. The circled jump in resonance frequency is assumed to be due to the secretion of hydrophobins.

The increased growth detection time may also be due to variations in growth rates between different spores. The higher vibrational modes provide the same qualitative growth detection time (data not shown). However, the detection time is not of concern here but the frequency response of the cantilever as hyphae propagate along its length. Figure 5.11 shows images of the cantilever at the start (1) of the measurement and once hyphal growth has reached the clamped end (2). Image (3) shows an image where there has been significant drying of the hypha which is the cause of the rise in resonance frequency circled in purple in Figure 5.10. This rise is not seen in the case of the reference sensors (not shown) and therefore, cannot be attributed to a change in environmental conditions. It is assumed that the observed drying is a result of hydrophobin secretion as discussed in Section 5.5.1.

Figure 5.12 – 5.15 (B) show plots of differential relative frequency shift ($\Delta f/f$) versus hyphal tip distance ($x$) from the cantilever's free end for the fundamental, second, third, and fourth resonance modes respectively. Normalised plots of mode shape ($\psi_n(x)$), $\psi_n(x)^2$ ($\propto$

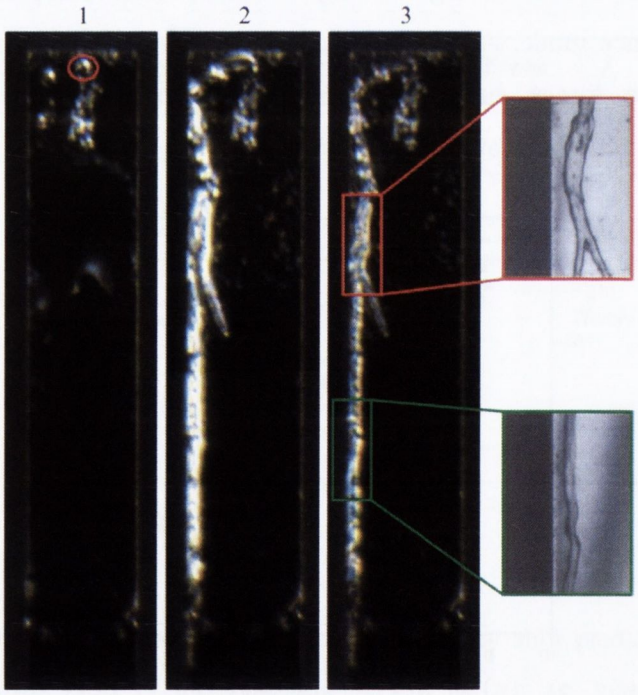


Figure 5.11: Image of hyphal growth on a 2 μm thick cantilever. Spore position at start of experiment (1). Hypha has reached the cantilevers clamped end (2). Reduction in hypha diameter indicating drying (3). The zoomed images illustrate the differences in hyphal diameter before (red) and after branching (green). There is a reduction in size of ~ 50%.

mass responsivity), and $d^2\psi_n(x)^2/dx^2$ ($\propto$stiffness responsivity) are shown in part A of these figures. For these plots data points are only shown for the spreading of hyphal filaments. Data points recorded before germination occurred have been omitted as have those once hyphal growth has reached the cantilever's clamped end. As mentioned previously a standard error of ±3% is assumed for all length measurements. Through examination of the resonance frequency shift versus distance plots it can be seen that there are positive and negative shifts in resonance frequency as the hypha extends along the cantilever's longitudinal axis. The positions at which these shifts occur indicate that the mass and stiffness of the hypha are having an effect on the cantilever's resonance frequency. For the fundamental mode (Figure 5.12) it is observed that as the hypha begins to propagate from the initial spore position (~15 μm) negative frequency shifts are observed. The rate of resonance frequency change begins to decrease around 150 ± 5 μm from the cantilever's free end and remains relatively stationary until ~ 275 ± 8 μm where a positive resonance frequency shift is observed. This rise in resonance frequency indicates that hyphal stiffness is having an effect on the resonance frequency. Thus once a rise in resonance frequency is observed (after ~ 44 hours) it is possible to conclude that hyphal growth has propagated past the cantilever's mid-point.

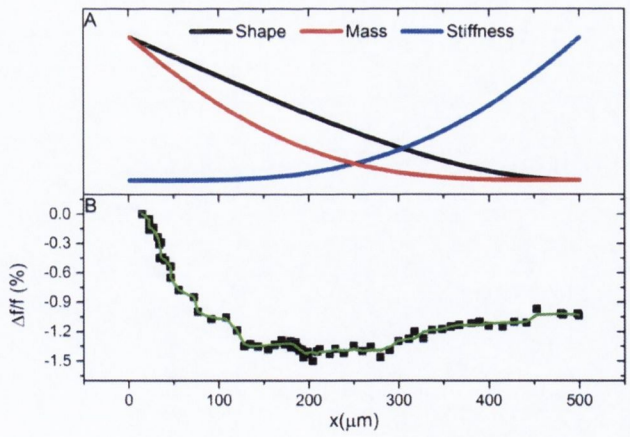


Figure 5.12: Fundamental mode relative frequency shift versus distance ($x$) along cantilevers longitudinal axis. (A) Normalised plots of mode shape ($\psi_n(x)$), $\psi_n(x)^2$ ($\propto$ mass responsivity), and $d^2\psi_n(x)^2/dx^2$ ($\propto$stiffness responsivity). (B) Relative frequency with respect to hyphal tip distance ($x$) from the cantilever's free end. The first data point corresponds to the start of hyphal propagation. The data points have been fitted with a smoothed curve (percentile filter) shown in green.

Examination of the higher vibrational modes (Figure 5.13-5.15) reveals that a positive shift in resonance frequency followed by a stationary frequency is observed between adjacent vibrational nodes and antinodes. Between adjacent antinodes and nodes a negative shift in resonance frequency followed by a stationary frequency is observed. In the case of mode 3 (Figure 5.14) and 4 (Figure 5.15) there is a decrease in the magnitude of the positive frequency shift as the distance from the cantilever's free end increases. It can be seen from part A in these figures that stiffness sensitivity at antinodes decreases with distance ($x$) from the cantilever's free end, while the opposite is observed for mass sensitivity.

Through closer examination it has been observed that the point where a negative frequency shift is observed, prior to a positive or stationary frequency shift, corresponds closely to the points where the slope ($m$) of the tangent to the curve of the curvature ($d^2\psi_n(x)^2/dx^2$) is zero. This observation holds only for positive peaks on the stiffness curve. This is not observed for the fundamental resonance mode as $m$=0 for the tangent to the curve of $d^2\psi_n(x)^2/dx^2$ does not occur.

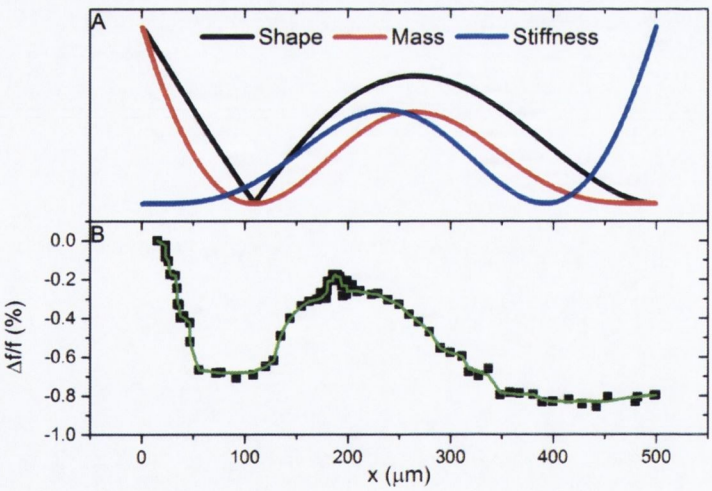


Figure 5.13: Second flexural mode relative frequency shift versus distance ($x$) along cantilevers longitudinal axis. (A) Normalised plots of mode shape ($\psi_n(x)$), $\psi_n(x)^2$ ($\propto$ mass responsivity), and $d^2\psi_n(x)^2/dx^2$ ($\propto$stiffness responsivity). (B) Relative frequency with respect to hyphal tip distance ($x$) from the cantilever's free end. The first data point corresponds to the start of hyphal propagation. The data points have been fitted with a smoothed curve (percentile filter) shown in green.

Thus, it should be possible to determine the position of the hyphal tip by the variation of the frequency response over time. Figure 5.16 displays smoothed plots of $\Delta f/f$ versus time. Data is shown for the second, third, and fourth resonance modes. The points where negative frequency shifts are observed are highlighted with their corresponding time points. Table 5.2 shows the time points and corresponding hyphal tip position from the cantilever's free end ($x$), where these negative frequency shifts are observed. The 3rd column in this table displays the positions where the slope ($m$) of the tangent to the curve of $d^2\psi_n(x)^2/dx^2$ is zero. It can be seen that these values agree closely.

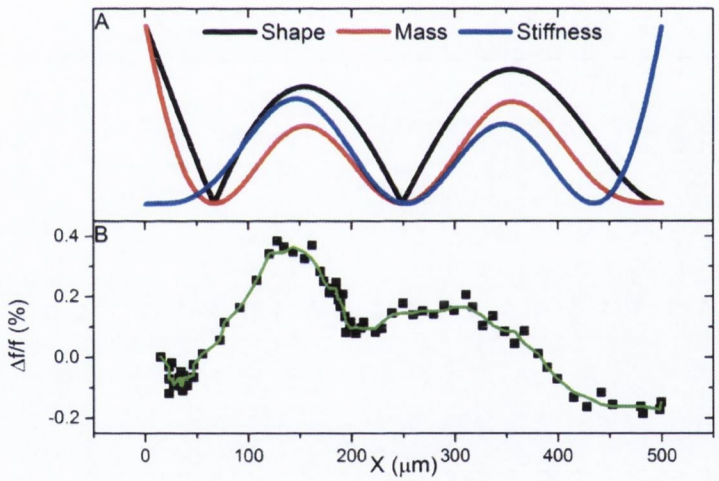


Figure 5.14: Third flexural resonance mode relative frequency versus distance ($x$) along cantilevers longitudinal axis. (A) Normalised plots of mode shape ($\psi_n(x)$), $\psi_n(x)^2$ ($\propto$ mass responsivity), and $d^2\psi_n(x)^2/dx^2$ ($\propto$stiffness responsivity). (B) Relative frequency with respect to hyphal tip distance ($x$) from the cantilever's free end. The first data point corresponds to the start of hyphal propagation. The data points have been fitted with a smoothed curve (percentile filter) shown in green.

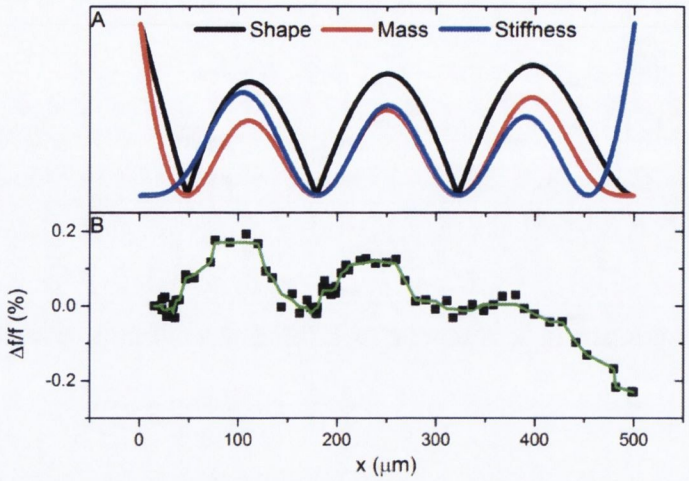


Figure 5.15 Fourth flexural resonance mode relative frequency versus distance ($x$) along cantilevers longitudinal axis. (A) Normalised plots of mode shape ($\psi_n(x)$), $\psi_n(x)^2$ ($\propto$ mass responsivity), and $d^2\psi_n(x)^2/dx^2$ ($\propto$stiffness responsivity). (B) Relative frequency with respect to hyphal tip distance ($x$) from the cantilever's free end. The first data point corresponds to the start of hyphal propagation. The data points have been fitted with a smoothed curve (percentile filter) shown in green.

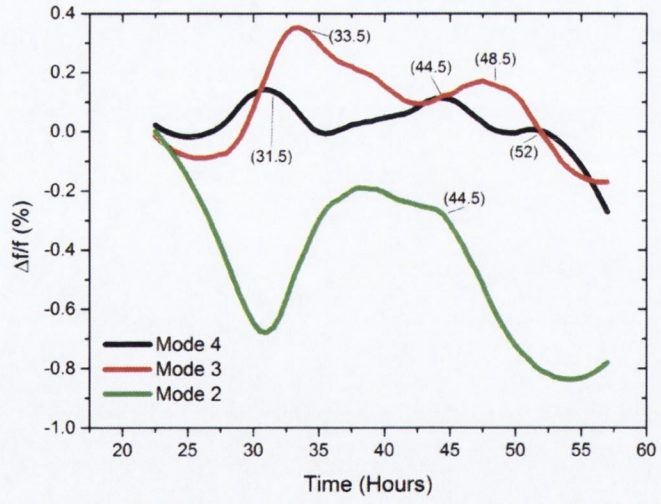


Figure 5.16: Relative frequency shift versus time due to hyphal growth. Smoothed curves are shown to enable easy visualisation of features of all modes in the one plot. The times indicated on each curve show points where a decrease in resonance frequency is observed following a rise in resonance frequency.

Table 5.2: Table of time points where decreases in resonance frequency are observed. The second column displays the position $x$ determined from images.The third column displays positions where the slope ($m=0$) of the tangent to the curve of $d^2\psi_n(x)^2/dx^2$ is zero.

| Time (Hour) | Observed $x$ (μm) | $x$ at $m$=0 (μm) |
|---|---|---|
| **31.5** | 108 ± 3 | 105 |
| **33.5** | 144 ± 4 | 146 |
| **44.5** | 229 ± 7 | 236 |
| **45** | 239 ± 7 | 252 |
| **48.5** | 311 ± 9 | 347 |
| **52** | 381 ± 11 | 391 |

#### 5.5.2.1 Predictions and Simulation

FEM simulation was performed using Comsol. The same cantilever parameters are used as listed in section 5.5.1.3 (new thickness 2 μm). In order to simulate what is occurring the start of the block was positioned 15 μm from the cantilever's free end. Initially the block representing the hypha was given a length, width, and thickness dimensions of 10, 5, and 5 μm respectively. At 145 μm from the cantilever's free end the hypha splits in two, with the resulting hypha having half the thickness of the original. At this point the width and thickness of the hypha are changed to 2.5 μm. The zoomed images shown in Figure 5.11 show the different hyphal thicknesses. The block representing the hypha is placed at the side of the cantilever as was observed during growth. The length of the block was increased by 10 μm between simulations. The same values of density ($\rho_a$) and Poisson ratio ($v$) previously outlined are used. The value for the hypha's Young's modulus ($E_a$) was difficult to determine. A value of 0.2 GPa from [16] was initially used however the plots for the 2 μm sensors produced were similar to those obtained in the simulations performed in Section 5.5.1. This value was deemed too low as it is clear from the experimental data that the stiffness of the hypha is not negligible.

Figures 5.17-5.20 show the relative frequency shifts obtained when a value of 1 GPa was assumed for $E_a$. This value is a factor of five larger than values found in literature where measurements are typically performed using AFM on hyphal cell walls. Anisotropic

Young's modulus has been reported in plant cell walls (comparable to hyphal cell walls) where values for Young's modulus are seen to increase by a factor of ~ 4 in some directions [18]. The Young's modulus of DNA filaments has also been found to be in the order of 1 GPa using optical tweezers measurements [19]. As structures similar to this are present in the hypha this assumed value is not totally unfounded.

Examination of the simulated plots reveals similar trends to those measured experimentally however positive and negative frequency shifts are occurring at slightly different positions along the cantilever's length. These discrepancies can be attributed to the use of an over simplified model as growth is not occurring in a straight line and hyphal splitting is also not accounted for. There is clearly a difference between the spores used for this experiment and those used in Section 5.5.1. The reason for this could not be determined. It is possible that this is a normal variation present in fungal populations. Modelling performed using Equation 5.5 did not provide the same qualitative results as simulation. Whilst it is possible to account for the total mass of the hypha on the cantilever using this model, it is not possible to account for the stiffness effect of an elongated structure along the cantilever's length.

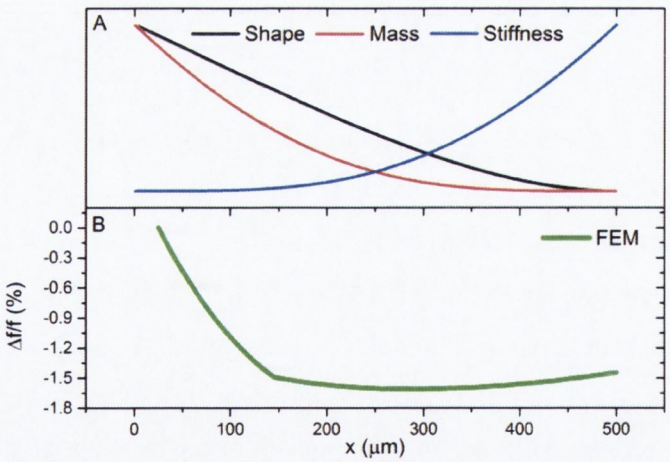


Figure 5.17: Fundamental mode relative frequency shift predictions due to hyphal growth. (A) Normalised plots of mode shape ($\psi_n(x)$), $\psi_n(x)^2$ ($\propto$ mass responsivity), and $d^2\psi_n(x)^2/dx^2$ ($\propto$stiffness responsivity). (B) Relative resonance frequency shift due to hyphal growth along cantilever according to FEM (green).

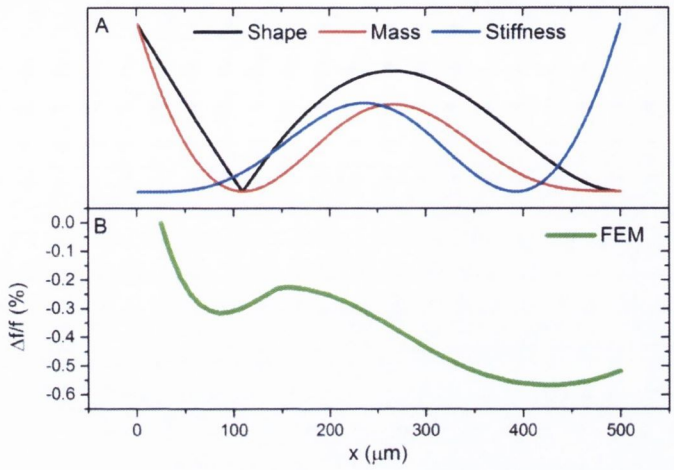


Figure 5.18: Second mode relative frequency shift predictions due to hyphal growth. (A) Normalised plots of mode shape ($\psi_n(x)$), $\psi_n(x)^2$ ($\propto$ mass responsivity), and $d^2\psi_n(x)^2/dx^2$ ($\propto$stiffness responsivity). (B) Relative resonance frequency shift due to hyphal growth along cantilever according to FEM (green).

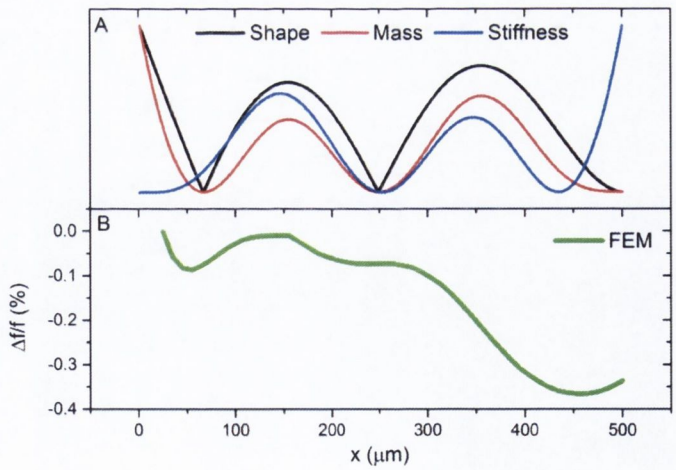


Figure 5.19: Third mode relative frequency shift predictions due to hyphal growth. (A) Normalised plots of mode shape ($\psi_n(x)$), $\psi_n(x)^2$ ($\propto$ mass responsivity), and $d^2\psi_n(x)^2/dx^2$ ($\propto$stiffness responsivity). (B) Relative resonance frequency shift due to hyphal growth along cantilever according to FEM (green).

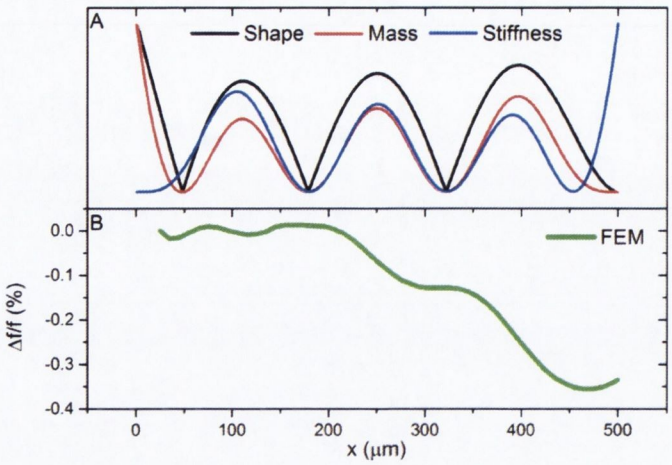


Figure 5.20: Fourth mode relative frequency shift predictions due to hyphal growth. (A) Normalised plots of mode shape ($\psi_n(x)$), $\psi_n(x)^2$ ($\propto$ mass responsivity), and $d^2\psi_n(x)^2/dx^2$ ($\propto$stiffness responsivity). (B) Relative resonance frequency shift due to hyphal growth along cantilever according to FEM (green).

From simulation it was noted that there is a visible change in mode shape observed for modes 3 and 4 as shown in Figure 5.21 and Figure 5.22. As the hyphal thickness is larger than the thickness of the cantilever this is to be expected. The degree to which mode shape is changed varies with increasing hyphal length and it thus different for each frequency measurement made. Due to this fact it is not practical to calculate the effect this has.

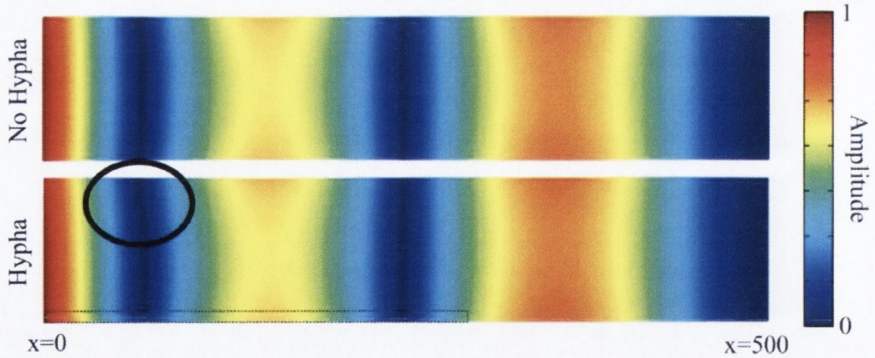


Figure 5.21: Simulated third mode vibration shape of a 2 μm cantilever. The top image is the mode shape of an unloaded beam. The bottom image shows mode shape for a cantilever with a hypha (dashed rectangle). There is a visible change in mode shape (circled) due to added mass. $x$=0 and 500 correspond to the cantilever's free and clamped ends respectively.

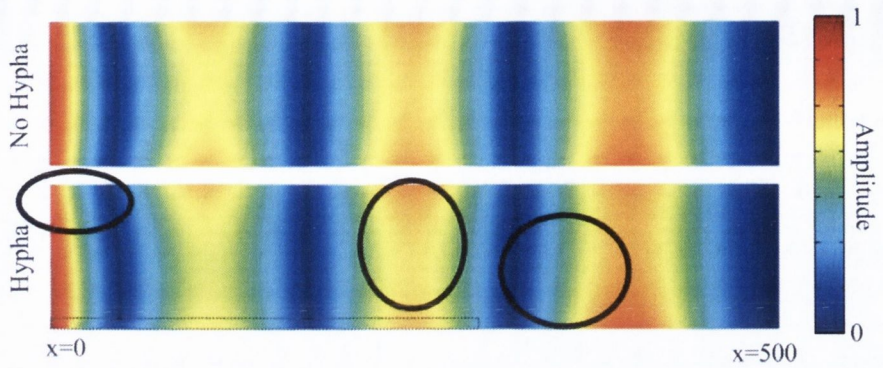


Figure 5.22: Simulated fourth mode vibration shape of a 2 μm cantilever. The top image is the mode shape of an unloaded beam. The bottom image shows mode shape for a cantilever with a hypha (dashed rectangle). There is a visible change in mode shape (circled) due to the hypha. $x$=0 and 500 correspond to the cantilever's free and clamped ends respectively.

## 5.6 Conclusion

Detection of the growth of single *A. niger* spores has been shown using multiple resonance modes. Detection times as low as 15 hours have been achieved. This is an order or magnitude faster than conventional growth detection techniques. These growth detection times are also in agreement with work previously published, where single mode detection was performed [10, 11]. The detection of this minimal amount of fungal material indicates the suitability of this method for growth detection in any setting. The ability to detect the growth of single spores within a short time is advantageous, especially in a clinical setting as it allows for a reduction in the number of isolates required.

The use of higher vibrational modes does not provide any reduction in detection time. However, it does provide a quantitative measurement of the progression of growth along the cantilever's longitudinal axis. The increased sensitivity provided by the use of higher vibrational modes will allow for the detection of smaller microrganisms such as bacteria and yeast. It has been demonstrated that it is possible to determine the extent to which growth has proceeded along the cantilever's length, even when growth is occurring in multiple directions. In the case where growth is proceeding in a linear fashion towards the cantilever's clamped end we show that a more accurate determination of hyphal tip position can be performed. Events occurring on the cellular level such as the secretion of hydrophobins can also be detected. The measurement of such biological processes

highlights the advantages which are gained through the use of cantilevers for the measurement of microbial growth as opposed to the use of only optical methods. While optical inspection allows for viable spore growth to be detected it provides no information on the mechanical properties of newly grown hyphae. The use of cantilevers for antibiotic susceptibility testing (as demonstrated in Chapter 6) can provide information on the effects that antifungal drugs have on the mechanical properties of the cell membrane. Measurement of multiple modes also allows for the positions at which these processes are occurring to be determined. Monitoring of $Q$ factor as well as resonance frequency may allow additional mechanical information to be obtained from the viscoelastic components of the growing hyphal filaments. This analysis is deemed outside the scope of this work due to its high difficulty. Such analysis has been performed on uniformly adsorbed protein layers on a quartz crystal microbalance [1].

## 5.7 References


1. Tamayo, J., et al., *Biosensors based on nanomechanical systems.* Chemical Society Reviews, 2013. **42**(3): p. 1287-1311.
2. Tamayo, J., et al., *Effect of the adsorbate stiffness on the resonance response of microcantilever sensors.* Applied Physics Letters, 2006. **89**(22): p. -.
3. Ramos, D., et al., *Detection of bacteria based on the thermomechanical noise of a nanomechanical resonator: origin of the response and detection limits.* Nanotechnology, 2008. **19**(3): p. 035503.
4. Ramos, D., et al., *Origin of the response of nanomechanical resonators to bacteria adsorption.* Journal of Applied Physics, 2006. **100**(10): p. 106105-3.
5. Lee, D., et al., *Effects of gold patterning on the bending profile and frequency response of a microcantilever.* Journal of Applied Physics, 2009. **106**(2): p. 024310-7.
6. Dohn, S., et al., *Position and mass determination of multiple particles using cantilever based mass sensors.* Applied Physics Letters, 2010. **97**(4).
7. Dohn, S., et al., *Mass and position determination of attached particles on cantilever based mass sensors.* Review of Scientific Instruments, 2007. **78**(10): p. 103303-3.
8. Ramos, D., et al., *Measurement of the Mass and Rigidity of Adsorbates on a Microcantilever Sensor.* Sensors, 2007. **7**(9): p. 1834-1845.
9. Nugaeva, N., et al., *Micromechanical cantilever array sensors for selective fungal immobilization and fast growth detection.* Biosensors and Bioelectronics, 2005. **21**(6): p. 849-856.
10. Nugaeva, N., et al., *An antibody-sensitized microfabricated cantilever for the growth detection of Aspergillus niger spores.* Microscopy and Microanalysis, 2007. **13**(1): p. 13-17.
11. Maloney, N., et al., *Fibre Optic Readout of Microcantilever Arrays for Fast Microorganism Growth Detection.* Journal of Sensors, 2012. **2012**.
12. Tsukahara, T., *Electron microscopy of swelling and germinating conidiospores of Aspergillus niger.* Medical Mycology, 1968. **6**(3): p. 185-191.
13. Gottlieb, D. and R.K. Tripathi, *The Physiology of Swelling Phase of Spore Germination in Pencillium Atrovenetum.* Mycologia, 1968. **60**(3): p. 571-590.
14. Bayry, J., et al., *Hydrophobins—Unique Fungal Proteins.* PLoS Pathog, 2012. **8**(5): p. e1002700.
15. Wösten, H.A.B., et al., *How a fungus escapes the water to grow into the air.* Current Biology, 1999. **9**(2): p. 85-88.
16. Ma, H., et al., *Surface ultrastructure and elasticity in growing tips and mature regions of Aspergillus hyphae describe wall maturation.* Microbiology, 2005. **151**(Pt 11): p. 3679-88.
17. Nikiyan, H., A. Vasilchenko, and D. Deryabin, *Humidity-Dependent Bacterial Cells Functional Morphometry Investigations Using Atomic Force Microscope.* International Journal of Microbiology, 2010. **2010**.
18. Wei, C.F., L.S. Lintilhac, and P.M. Lintilhac, *Loss of stability, pH, and the anisotropic extensibility of Chara cell walls.* Planta, 2006. **223**(5): p. 1058-1067.
19. Hegner, M., S.B. Smith, and C. Bustamante, *Polymerization and mechanical properties of single RecA–DNA filaments.* Proceedings of the National Academy of Sciences, 1999. **96**(18): p. 10109-10114.

# Chapter 6
# Antibiotic Susceptibility Testing

In this chapter antibiotic susceptibility tests are performed using cantilever arrays. First an introduction is given to current methods used for the determination of minimum inhibitory concentrations. Next experiments are described where the susceptibility of *A. niger* to fluconazole and *A. fumigatus* to amphotericin B are described.

## 6.1 Introduction

In the past three decades the incidence of fungal infection has increased dramatically. In a clinical setting the determination of the minimum inhibitory concentration (MIC) is required to ensure accurate administration of antimicrobial agents. Because of a rapid increase in acquired resistance to most antimicrobials the empiric therapy of microbial infections is increasingly untrustworthy. For this reason antimicrobial susceptibility testing (AST) is performed [1].

MIC is defined as the minimum concentration of an antibiotic that is able to prevent the further growth of an infectious organism *in vitro* [2]. This value is determined by letting the microorganism grow in the presence of known concentrations of drugs. Various dilution techniques in broth, agar, and gradient tests are available for defining breakpoint concentrations which will categorise the microbial isolates into susceptible (S), intermediate susceptible (I), and resistant (R) [3]. When resistance, pharmacokinetic, and pharmacodynamic information are taken into account the information derived from AST MIC can be used for therapy of the infected patient [1].

There is currently no standardised ISO (International Organisation of Standards) procedure for antifungal MIC determination. Recommendations are from the EUCAST subcommittee on Antifungal Susceptibility Testing (EUCAST AFST) [4]. In this document a 96-well micro-titre plate containing two-fold dilution series of antimicrobials is utilised. After preparation of suitable inocula fungal spores are incubated in RPMI medium in the presence of the desired antifungal drug. Accuracy of test results is monitored by the use of

control strains with a known stable drug susceptibility pattern. MICs for control strains should ideally be close to the middle of the range of the two-fold series tested. The range of concentrations should encompass the breakpoint, when one exists, as well as the expected results for the quality control strains. Test plates are read after 24-48 hours of incubation either manually or using automated systems based on optical density measurements. Interpretation of mould MICs is challenging and interpretative breakpoints have yet to be established [5].

The primary target of antifungal drugs is ergosterol and its biosynthetic pathway. Ergosterol is found in fungal membranes and is essential for growth of fungi [6]. Three main classes of antifungal drugs, namely polyenes, allylamines, and azoles directly target ergosterol itself or enzymatic steps of its biosynthetic pathway [6]. Azoles target the biosynthetic pathway of ergosterol via the inhibition of the lanosterol 14-alpha demethylase enzyme and are the most commonly used antifungals in clinical settings, thus their modes of action have been widely studied [7]. In the 1990s fluzonazole was the gold standard used by clinicians for the treatment of fungal infections. Its advantages are that it is hydrosoluble and is completely adsorbed through the gastrointestinal tract. Its over-prescription however has led to an increase in resistance to azole drugs [7]. The polyene amphotericin B targets ergosterol in the cell membrane. Its amphiphilic structure allows it to bind to ergosterol in the lipid bilayer and to form pores. This results in plasma membrane destabilisation and leakage of intracellular components such as $K^+$ ions responsible for cell lysis [8]. Resistance to amphotericin B is rare and as it posesses a large range of activity it has become widely used for the treatment of systemic fungal infections [9]. The main issue with the use of amphotericin B for treatment is its toxicity resulting in liver and kidney damage [7, 9].

Here, it is proposed to use dynamic operation of cantilevers to determine the susceptibility of fungi to different antifungal drugs. Through the use of cantilever arrays it is possible to perform tests on different concentrations of antifungal drugs in parallel. As a proof-of-concept experiment the antifungal effect of fluconazole and amphotericin B is shown on *A. niger* and *A. fumigatus* respectively. In the initial experiments reported here two concentrations of antifungals were tested. 0.03 μg/mL represents a low concentration of the growth inhibiting drug, while 128 μg/mL represents a high concentration of the tested drug as determined from the EUCAST-AST recommended drug dilution series.

## 6.2 Materials and Methods

All chemicals and reagents are of analytical grade and were purchased from Sigma-Aldrich (Arklow, Ireland), unless otherwise stated.

### 6.2.1 Cantilever Preparation

Two 7 μm cantilevers were cleaned using oxygen plasma as described in Chapter 2. Silanisation and agarose coating was also carried out as outlined in Chapter 2.

### 6.2.2 Susceptibility of *A. niger* to Fluconazole

*A. niger* spore suspensions listed in Table 6.1 were prepared following the adapted protocol from EUCAST-AST described in Appendix 6.

One droplet of spore suspensions was deposited on cantilevers using the ink-jet printing technique described in Chapter 2. A 50 μm pipette nozzle diameter was used. The solution deposited on each cantilever is shown in Table 6.2. After deposition the array was placed in the environmental chamber at experimental conditions (94% RH, 30 °C). Amplitude spectra for the fundamental and second resonance modes were recorded at intervals of 30 minutes. For both modes 4000 data points were recorded in a 10 kHz frequency range.

Table 6.1: Table outlining constituents of each prepared sample.

| Tube | Spore Concentration (Spore/mL) | Fluconazole Concentration (μg/mL) | Spore Condition | Suspension Name |
|---|---|---|---|---|
| **A** | $1.5x10^6$ | NA | Dead | Dead Spore |
| **B** | $2.3x10^6$ | NA | Live | Live Spore |
| **C** | $2.0x10^6$ | 0.03 | Live | Lo Flu |
| **D** | $1.8x10^6$ | 128 | Live | Hi Flu |

Table 6.2: Table outlining solution deposited on each cantilever and spotting order.

| Cantilever | Functionalisation | Spotting Order |
|---|---|---|
| **1** | Agarose | NA |
| **2** | High Flu | 4 |
| **3** | High Flu | 4 |
| **4** | Dead Spores | 1 |
| **5** | Low Flu | 3 |
| **6** | Live Spores | 2 |
| **7** | Dead Spores | 1 |
| **8** | Blank | NA |

### 6.2.3 Susceptibility of *A. fumigatus* to Amphotericin B

*A. fumigatus* spore suspensions listed in Table 6.3 was prepared following the adapted protocol from EUCAST-AST described in Appendix 6.

One droplet of spore suspension was deposited on cantilevers using the ink-jet printing technique described in Chapter 2. A 50 µm pipette diameter was used. The solution deposited on each cantilever is shown in Table 6.4. After deposition the array was placed in the environmental chamber at experimental conditions (100% RH, 30 °C). Amplitude spectra for the fundamental and second resonance modes were recorded at intervals of 30 minutes. For the fundamental mode 500 data points were recorded in a 10 kHz range. For the second resonance mode 1000 data points were recorded in a 40 kHz range.

Table 6.3: Table outlining constituents of each prepared sample.

| Tube | Spore Concentration (Spore/mL) | Amphotericin B Concentration (µg/mL) | Spore Condition | Suspension Name |
|---|---|---|---|---|
| **A** | $2.1x10^6$ | NA | Dead | Dead Spore |
| **B** | $3.7x10^6$ | NA | Live | Live Spore |
| **C** | $3.6x10^6$ | 0.03 | Live | Amp B |

Table 6.4: Table outlining solution deposited on each cantilever and spotting order.

| Cantilever | Functionalisation | Spotting Order |
|---|---|---|
| **1** | Amp B | 3 |
| **2** | Live Spore | 2 |
| **3** | Dead Spore | 1 |
| **4** | Amp B | 4 |
| **5** | Amp B | 3 |
| **6** | Live Spore | 2 |
| **7** | Dead Spore | 1 |
| **8** | Blank | NA |

## 6.3 Results

### 6.3.1 Susceptibility of *A. niger* to Fluconazole

The fundamental mode frequency response of all cantilevers in the array is shown in Figure 6.1. The plot shows that growth has been detected on the cantilevers where live spores and spores in the presence of 0.03 μg/mL of fluconazole have been deposited. The growth of spores has been detected within 12 hours where no antifungal drugs are present, this value is in agreement with values previously published and is an order of magnitude faster than conventional growth detection methods [10]. Where spores have been inoculated with fluconazole at a concentration of 0.03 μg/mL (Low Flu, green), there is an increase in the time required for growth to be detected. After approximately 25 hours a decrease in resonance frequency is observed indicating an increase of mass on the sensors surface due to fungal growth. Thus, at a concentration of 0.03 μg/mL fluconazole is seen to partially inhibit the growth of *A. niger*. In the case of both plots the decrease in resonance frequency ceases after 25 and 30 hours indicating that hyphal propagation has entered the mass insensitive region along the cantilever's longitudinal axis (see more information in Chapter 5).

Through examination of Figure 6.2, it can be seen that there is greater hyphal coverage of the sensor onto which live spores were deposited when compared to the sensor where the

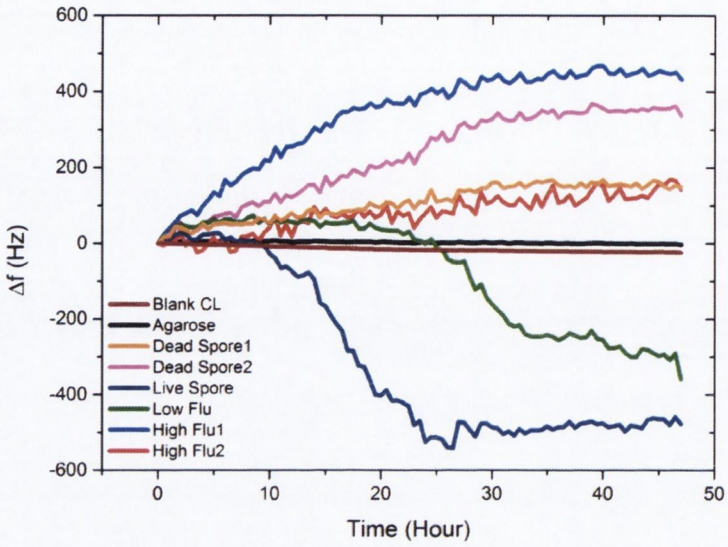


Figure 6.1: Fundamental mode frequency response versus time for cantilevers in an array during testing of *A. niger* susceptibility to antifungal fluconazole.

low concentration of fluconazole was deposited. Thus as expected, a larger magnitude of frequency shift is observed for the sensor with only live spores. Spores subjected to 128 µg/mL of fluconazole (High Flu, light blue and red) show no decrease in resonance frequency indicating that at this concentration fluconazole fully inhibits spore growth. These curves exhibit a gradual increase in resonance frequency as do those for cantilevers onto which dead spores have been deposited. These positive frequency shifts are a result of evaporation of the spotting solution resulting in a loss of mass on the sensor's surface. The different magnitudes of the frequency shifts observed can be attributed to (i) different amounts deposited, (ii) different solutions, and (iii) different deposition positions ($x$) along the cantilever's longitudinal axis.

In Figure 6.1 it can be seen that the curves 'High Flu1' (light blue) and 'Dead Spore 2' (pink) show a higher magnitude of increase when compared to 'Dead Spore 1' (orange) and 'High Flu 2' (red). Through examination of the images in Figure 6.2 it can be seen that the deposition is towards the centre of the cantilever, (where it has been shown in Chapter 5 there is a decrease in mass sensitivity) for 'High Flu2' and 'Dead Spore1'. Images for these cantilevers also show a greater retention of liquid around the deposited spores indicating that less evaporation took place. The reason for differences in liquid retention is unknown.

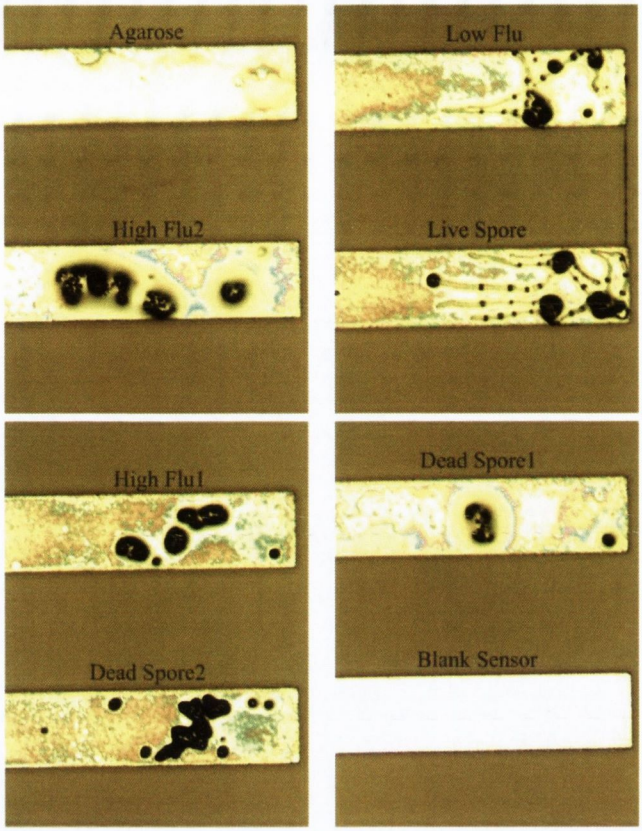


Figure 6.2 : Optical microscope image of cantilevers after fluconazole susceptibility tests. Labels on cantilevers correspond to curves in Figure 6.1 and 6.3. The hyphae grown on the sensors 'Live spores' and 'Low Fluconazole' are clearly visible. Width of cantilever sensor is 100 μm

Curves for cantilevers where no spore deposition was performed (Agarose and Blank CL) show no increase in resonance frequency, thus confirming that evaporation is the cause. Evaporation occurs over a longer period of time due to the high relative humidity levels around the cantilevers.

Figure 6.3 displays the second mode frequency shift for all cantilevers in the array. Here interpretation is difficult due to rises in resonance frequency caused by evaporation of spotted medium. Despite this it is possible to determine the effects of fluconazole on *A. niger* growth. Examination of the plot 'Live Spore' (dark blue) reveals an initial rise in resonance frequency similar to that observed in the plots for cantilevers with deposited dead spores ('Dead spore1' orange, 'Dead Spore2' pink). After ~12.5 hours there is a sharp rise in frequency followed by a plateau and then a decrease in resonance frequency at ~32.5 hours. This is similar to what was observed in Chapter 5. The sharp rise in resonance frequency at 12.5 hours is indicative of hyphal growth entering the region of the cantilever

around the node of vibration. In this region the stiffness of the growing hypha causes a positive frequency shift. The plateau in resonance frequency indicates that hyphal filaments are growing in a region of the sensor where mass and stiffness effects are cancelling each other. The decrease in resonance frequency indicates that hyphal growth has passed the point where curvature is maximal near the antinode of vibration. Thus through comparison with plots where no growth is occurring it is possible to determine that growth has been detected ~12.5 hours after the start of frequency measurements.

Similar features can be observed in the frequency response of the cantilever where spores have been inoculated with 0.03 µg/ml of fluconazole. There is a sharp rise in resonance frequency when compared to reference sensors after ~25 hours. This is the same time point where growth was detected in the fundamental resonance mode. Thus, it is again possible to determine that this concentration of fluconazole partially inhibits growth. By tracking two modes it is possible to determine if growth is still occurring. For example, if only the fundamental resonance mode was monitored it would indicate that growth has ceased after 32.5 hours in the case of the 'Low Flu' cantilever. However, the second mode plot reveals that growth is still continuing after this time point. The remaining curves in Figure 6.3 can be given the same treatment as they received in the case of the fundamental resonance mode.

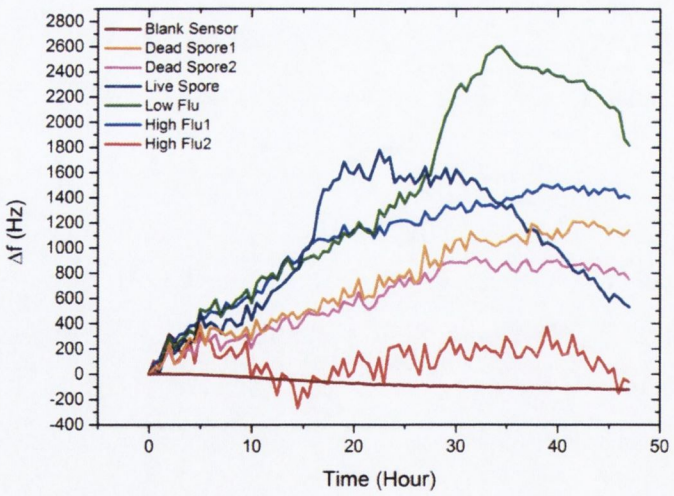


Figure 6.3: Second mode frequency response versus time for cantilevers in an array during testing of *A. niger* susceptibility to fluconazole.

The susceptibility of *A. niger* to different concentrations of the antifungal drug fluconazole has been demonstrated using multiple resonance modes. Due to differing magnitudes of frequency drift (due to solution evaporation from different positions on cantilevers) observed in this experiment it is evident that for the purposes of quantitative analysis cantilever arrays require better stability. Spores should be deposited using the glass needle method instead as described in chapter 5 and not via ink-jet printing as was the case here. They do however provide accurate qualitative results, as do conventional methods currently used. The advantage of using cantilevers for antibiotic susceptibility test is the fast analysis time provided.

### 6.3.2 Susceptibility of *A. fumigatus* to Amphotericin B

In this experiment relative humidity conditions were raised to 100 % in order to combat rises due to evaporation of spotted solutions. Figure 6.4 shows the fundamental mode frequency response for all cantilevers in the array. From these plots it is clear that three cantilevers show resonance frequency shifts relative to a group of sensors which remain relatively stable. Both of these curves, where live spores were deposited ('Live Spore1', 'Live Spore2') show large positive shifts in resonance frequency. These instantaneous increases in resonance frequency indicate an increase in the stiffness of the hypha on the cantilevers however the cause is unknown. Reference sensors showed no increase in frequency at these time points ruling out instabilities in the environmental conditions surrounding the sensors. The fact that these increases are observed on sensors where only live spores are deposited leads to the assumption that these features are indicative of certain events in the fungal life cycle however, this was not further investigated at this time point. It should be noted that these measurements were performed before implementation of the USB camera so real time imaging of the sensors was not possible.

Figure 6.5 shows the frequency response of 2 sensors which were spotted with live spores and 3 sensors which were spotted with live spores and amphotericin B. In these plots the large positive frequency shifts observed in 'Live Spore1' and 'Live Spore2' have been removed. In the case of sensors spotted with dead spores no frequency changes were observed and are not discussed further. Curves 'Live Spore1' and 'Live Spore2' show distinct resonance frequency shifts indicating that spore growth has been detected.

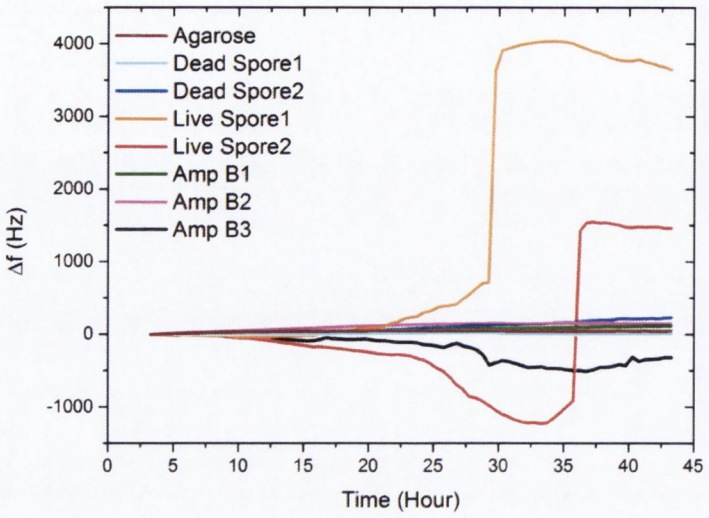


Figure 6.4: Fundamental mode frequency response for cantilevers in an array during testing of *A. fumigatus* susceptibility to amphotericin B.

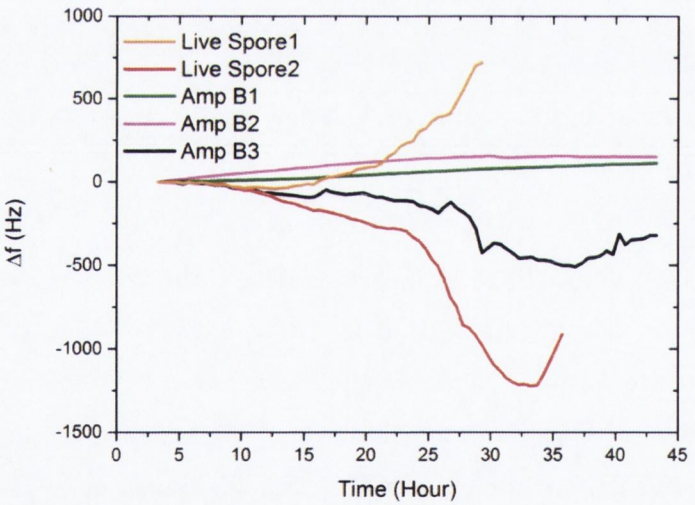


Figure 6.5: Fundamental mode frequency response for cantilevers in an array during testing of *A. fumigatus* susceptibility to amphotericin B. Jumps in resonance frequency have been removed for easier visualisation of frequency shifts.

Growth of hyphal filaments can be seen on the top and backside of both sensors in Figure 6.6. The differences in the sign of the resonance frequency shifts can be attributed to the initial location of the spotted spores. In the case of 'Live Spore2' it can be seen from Figure 6.6 that hyphal growth originates from spores located towards the cantilevers free

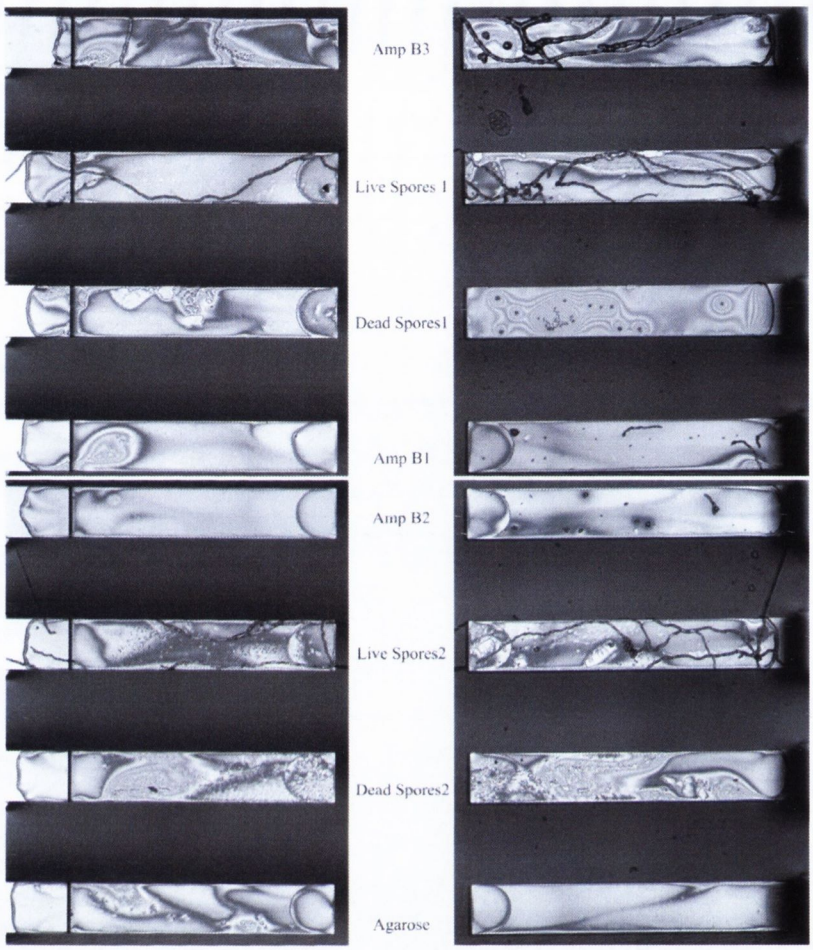


Figure 6.6: Optical microscope images of cantilevers after fluconazole susceptibility tests. Labels on cantilevers correspond to curves in Figure 6.4, 6.5, 6.7, and 6.8.

end, hence a negative frequency shift is observed. At 34 hours a positive frequency shift is observed indicating that growth has propagated towards the cantilever's clamped end where stiffness effects dominate. In the case of 'Live Spore1'(Figure 6.6) it can be seen that growth is originating from spores located near the cantilever's clamped end where the stiffness effect dominates; hence a positive frequency shift is observed. It is clear from both curves that growth of *A. fumigatus* has been detected within 15 hours.

Curves 'Amp B1' and 'Amp B2' (Figure 6.5), where spores were incubated with amphotericin B, shown no frequency changes. Thus, it can be concluded that at a concentration of 0.03 µg/mL *A. fumigatus* is susceptible to amphotericin B. From the corresponding images in Figure 6.6 very limited growth is observed. 'Amp B3' however does show a decrease in resonance frequency indicating the detection of fungal growth.

Examination of the corresponding image in Figure 6.6 shows hyphal growth. However, when compared to images for 'Live Spore1' and 'Live Spore2' the abnormal hypha morphology indicates that conditions are suboptimal for growth. The reduced magnitude of the frequency shift is believed to be a result of unsuitable growth conditions resulting in changes in the hyphal structure. No jump in resonance frequency is observed as was the case for sensors inoculated with live spores. This indicates that amphotericin B is reducing cellular functions. The fact that growth occurs on this sensor can possibly be linked to the fact that during ink-jet deposition of spore suspensions, the same filled spotting nozzle was used after spotting on 'AmpB 2' as indicated in Table 6.4. When performing ink-jet printing sedimentation of spores is seen at the front of the nozzle after some time. When this occurs there may no longer be an even distribution of concentrations in the spore suspension, thus when spotted on this sensor the concentration of amphotericin B may be less than what was spotted on the other sensors. For future experiments needle deposition is recommended.

Similar observations can be made through examination of the second mode frequency response shown in Figure 6.7. It can be seen that the same three sensors show frequency shifts as was the case for the fundamental resonance mode. A closer look at these plots is given in Figure 6.8. Figure 6.6 shows that in the case of 'Live spore 1' and 'Amp B3' hyphal growth is originating from the same position on the cantilever's longitudinal axis.

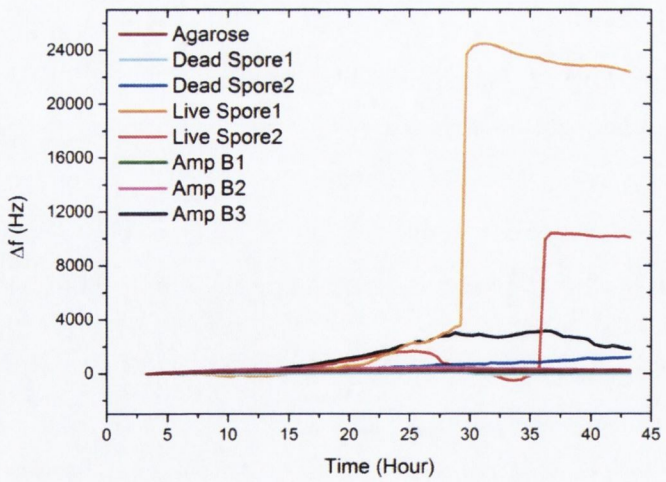


Figure 6.7: Second mode frequency response for cantilevers in an array during testing of *A. fumigatus* susceptibility to amphotericin B.

Both curves show an initial positive resonance frequency shift followed by a stationary resonance frequency and then a negative frequency shift. Examination of these features reveals that hyphal growth is occurring at a slower rate in the presence of amphotericin B. For example, the decrease in resonance frequency typically observed when hyphal growth reaches the antinode of vibration occurs at ~25 hours in 'Live Spore2' and ~ 37.5 hours in the case of 'Amp B3'. A more exact determination in the reduction of growth rate is not possible as propagation of hyphal filaments is occurring in multiple directions.

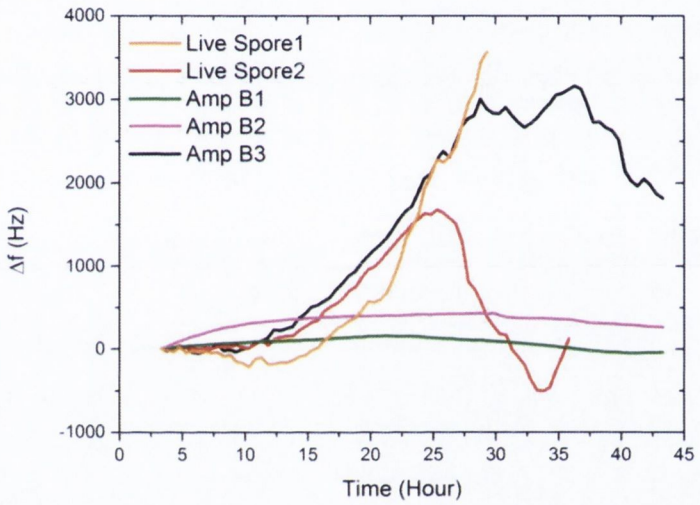


Figure 6.8: Second mode frequency response for cantilevers in an array during testing of *A. fumigatus* susceptibility to amphotericin B. Jumps in resonance frequency have been removed for easier visualisation of frequency shifts.

## 6.4 Conclusion

In this chapter the use of cantilever arrays for monitoring the susceptibility of *Aspergilli* to antifungal drugs has been demonstrated using cantilevers for the first time. In the case of *A. niger* it has been shown that at a concentration of 0.03 μg/mL fluconazole delays germination time. This low concentration inhibits spore growth however it does not result in spore death. It is believed that at a higher spore concentration this low antifungal concentration would be ineffective. Hence, the concentration of fluconazole required would need to be increased accordingly. At a concentration of 128 μg/mL fluconazole spore germination is inhibited. Thus it can be concluded that *A. niger* is susceptible to

fluconazole at a concentration of 128 µg/mL.

*A. fumigatus* was seen to be susceptible to amphotericin B at 0.03 µg/mL. Gehrt and co-workers have investigated the inoculum size effect on MICs using micro-dilution broth methods [11]. This micro-well effect may be related to the different mechanisms of action present in different antifungal drugs and it is also observed in bacteria and yeasts [12]. The explanation for this is that the number of microbial targets present in a suspension may exceed the capability of a drug at a given concentration. This results in a failure to inhibit the growth of the organism in an *in vitro* test system. Inoculum concentration may particularly affect antifungal drugs whose antimicrobial activity is based on an enzymatic mechanism (*e.g.* fluconazole) [11]. In contrast, amphotericin B exhibits little inoculum size effects against most fungal species which is a result of its mechanism of action. Amphotericin B acts through a direct interaction with ergosterol in the fungal cell membrane rather than through an enzymatic target. This mechanism reduces the likelihood of alteration of the fungal target despite increasing numbers of fungal cells [11]. In cantilever-based antifungal testing the inoculum size effect has to be taken into account due to lower number of tested spores. According to EUCAST-AST published documents [13], tested *A. niger* isolates had a MIC between 0.03-2 µg/mL which agrees with the inhibition observed in our experiments. There is no similar data available regarding fluconazole's MIC. In the case of both experiments quantitative results were obtained within 25 hours in an automated fashion. It is known that the length of incubation also has an effect on MICs in antifungal testing [11]. This is explained by the fact that extended incubation times allow resistant organisms to overgrow the initially susceptible subpopulation. On the other hand, during prolonged incubation a degradation of antifungal compounds may also occur [14]. Automatised continuous measurement provided by the use of cantilevers for AST allows for such incubation time effects to be monitored as shown in the case of fluconazole incubation at 0.03 µg/mL.

## 6.5 References


1. Cornaglia, G., et al., *European Manual of Clinical Microbiology*. 2012: European Society for Clinical Microbiology and Infections Diseases.
2. Rodloff, A., et al., *Susceptible, Intermediate, and Resistant - The Intensity of Antibiotic Action.* Deutsches Arzteblatt International, 2008. **105**(39): p. 657-662.
3. Jorgensen, J.H. and M.J. Ferraro, *Antimicrobial Susceptibility Testing: A Review of General Principles and Contemporary Practices.* Clinical Infectious Diseases, 2009. **49**(11): p. 1749-1755.
4. EUCAST. *Method for the determination of broth dilution minimum inhibitory concentrations of antifungal agents for conidia forming moulds (http://www.eucast.org/antifungal_susceptibility_testing_afst/methods_of_antifungal_susceptibility_testing/susceptibility_testing_of_moulds/ )*. 2008 Accessed on 20th April 2013].
5. Subcommittee on Antifungal Susceptibility Testing of the, E.E.C.f.A.S.T., *EUCAST Technical Note on the method for the determination of broth dilution minimum inhibitory concentrations of antifungal agents for conidia–forming moulds.* Clinical Microbiology and Infection, 2008. **14**(10): p. 982-984.
6. Alcazar-Fuoli, L. and E. Mellado, *Ergosterol biosynthesis in Aspergillus fumigatus: its relevance as an antifungal target and role in antifungal drug resistance.* Frontiers in microbiology, 2012. **3**: p. 439.
7. Vandeputte, P., S. Ferrari, and A.T. Coste, *Antifungal resistance and new strategies to control fungal infections.* International journal of microbiology, 2012. **2012**: p. 713687.
8. Lemke, A., A.F. Kiderlen, and O. Kayser, *Amphotericin B.* Applied Microbiology and Biotechnology, 2005. **68**(2): p. 151-162.
9. Ellis, D., *Amphotericin B: spectrum and resistance.* Journal of Antimicrobial Chemotherapy, 2002. **49**: p. 7-10.
10. Maloney, N., et al., *Fibre Optic Readout of Microcantilever Arrays for Fast Microorganism Growth Detection.* Journal of Sensors, 2012. 6 pages. doi:10.1155/2012/405281.
11. Gehrt, A., et al., *Effect of increasing inoculum sizes of pathogenic filamentous fungi on MICs of antifungal agents by broth microdilution method.* Journal of Clinical Microbiology, 1995. **33**(5): p. 1302-7.
12. Brook, I., *Inoculum effect.* Rev Infect Dis, 1989. **11**(3): p. 361-8.
13. Testing, E.C.o.A.S. *Amphotericin B and Aspergillus spp.: Rationale for the clinical breakpoints*. 2012. **1**.
14. Müller, F.-M.C., M. Seidler, and A. Beauvais, *Aspergillus fumigatus biofilms in the clinical setting.* Medical Mycology, 2011. **49**(S1): p. S96-S100.

# Chapter 7

# *A. niger* Growth Detection using Piezoresistive Microcantilevers

In this chapter the use of cantilevers with integrated Au piezoresistors located in the cantileve's clamped end is described. First a description of the cantilever arrays is provided, followed by the methods used for the dynamic operation of these sensors. The steps required for the successful functionalisation of the sensors for microbial growth measurements are outlined prior to a description of the growth measurements performed.

## 7.1 Introduction

A mechanical stress applied to a conducting material results in a change in resistivity. This effect was first reported in the 1870s where the change of resistance in wires due to elongation was observed [1]. This effect has since been termed piezoresistivity. In the 1950s it was discovered that semiconducting materials, such as silicon and germanium, demonstrate piezoresistive coefficients that are up to one hundred times greater than those observed in metallic conductors [2]. This has led to the application of piezoresistive sensors to AFM [3] in the early 1990s.

Piezoresistive cantilevers have an integrated resistor typically located at the cantilever's clamped end where stress due to displacement is maximal. The resistance ($R$) of a material is dependent on its dimensions as shown in the following equation

$$R = \frac{\rho l}{A} \qquad 7.1$$

where $\rho$, $l$, and $A$ correspond to the materials resistivity, length, and average cross sectional area respectively. Thus an applied stain results in a resistance change ($\Delta R$) due to changes in the material's dimensions. Typically the property of value for a piezoresistive material is its gauge factor ($GF$), which is a measure of the fractional change of resistance with strain ($\varepsilon$) given by [4],

$$GF = \frac{\Delta R}{R}\frac{1}{\varepsilon} = (1 + \upsilon) + \frac{\Delta \rho}{\rho}\frac{1}{\varepsilon}. \qquad 7.2$$

Here $\upsilon$ corresponds to the material's Poisson's ratio.

Integrated piezo resistive cantilevers were initially developed in the early nineties for AFM imaging by the Quate group in Stanford [5]. Boisen and co-workers reported the use of piezoresistive cantilevers for environmental sensing purposes [6]. Here, a dual cantilever setup is used. Four resistors (two in two individual cantilevers, two on the substrate) in a Wheatstone bridge configuration are used to measure environmental changes. The dual cantilever setup allows differential measurements to be performed where the signals from the two cantilevers are subtracted from each other. The same set-up has also been employed as an alcohol vapour sensor [7]. More recently, piezoresistive sensors have been used as organic vapour detectors [8] and for the detection of glucose and ethanol for the monitoring of processes involving microorganisms [9, 10]. Typically semiconducting materials have been utilised as piezoresistive elements in cantilevers due to their high gauge factors. The use of Au piezoresistors as the sensing element in SU-8 polymer cantilevers has been reported in [11-13]. Polymer sensors are used due to their low Young's modulus rendering them highly sensitive static sensors. While the *GF* value of gold is small compared to that found in semiconductors, this is compensated by the low electrical noise observed in the gold films [14]. An alternative to integrated Au piezoresistors is to use a conductive composite of SU-8 and carbon back particles. The increase in *GF* compared to that of Au results in a more sensitive strain sensor [15]. The above demonstrates the use of piezoresistive cantilevers as static deflection sensors however, they have also been employed as dynamic mode mass sensors. In [4], a nano electro mechanical cantilever sensor (NEMS) with an Au piezoresistors has achieved a mass resolution of 1 ag in ambient conditions. More recently dynamic operation of cantilevers with a GaN piezoresistor have also been demonstrated [16] where a Q factor of 200 is measured in air.

In plane oscillations of piezoresistive sensors have been employed for detection of *E. coli* in phosphate buffered saline (PBS) solution using specific antibody immobilisation [17]. The detection of microorganism growth using piezoresistive cantilever sensors has not been performed to date (to the best our knowledge). Here it is proposed to use SiN on Si cantilevers with integrated Au piezoresistors for the real time monitoring of *A. niger*

growth. The use of sensors with an integrated readout removes the need for bulky optical equipment where sophisticated alignment is required and allows a portable handheld device to be developed in the future.

## 7.2 Piezoresistive Cantilever Arrays

The piezoresistive cantilevers were fabricated in the group of Prof. Michael Roukes (California Institute of Technology). Each array consists of eight cantilevers separated by a pitch of 250 μm. The arrays were fabricated to resemble those currently used in our group to allow for easy integration into our currently developed functionalisation techniques. The arrays are fabricated from a silicon on insulator substrate (SOI) with a 5 μm Si device layer and a 400 μm handle. A 200 nm low stress silicon nitride (SiN) layer is deposited on the top side of the wafer using low pressure chemical vapour deposition (LPCVD). 800 Å of Au on 30 Å of Cr act as the piezoresistive element for these devices. Encapsulation of the piezoresistive elements was deemed unnecessary for the first generation of these devices by the fabricator. Hence, to ease fabrication the piezoresistive elements have not been isolated from the environment. Several fabrication steps are performed with the end result being the array shown in Figure 7.1.

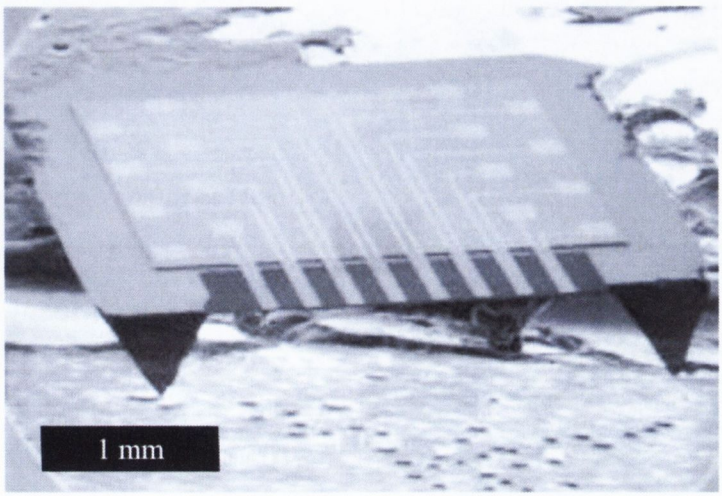


Figure 7.1: SEM image of a piezoresistive cantilever array. Each array consists of eight cantilevers separated by a pitch of 250 μm. Each cantilever has a length, width, and thickness of 466, 98.5, and 5.2 μm respectively. Image courtesy of Warren Fon (Caltech).

## 7.3 Resonance Frequency Measurement

A piezoelectric actuator (36a, TRS Ceramics) is used to actuate cantilevers for resonance frequency measurements. The actuator is fixed to an 84 lead pin grid array (PGA 08447002) using silver conductive paint (186-3600, Radionics). Curing time for this step is 10 hours at 50 °C. The array is glued (Super glue, Bostik) to the piezoelectric actuator and allowed to cure overnight. Electrical connections are via gold wire (S-W-AU-0012/4/01, 99.99 % Au wire, diameter 30 μm; SPM, NJ, USA) wedge bonding (4700 Convertible Ball and Wedge Bonder; Kulicke and Soffa). Wire bonds are made to the gold pads on the cantilever array and PGA mount. For each cantilever two wire bonds are required. Both sides of the piezoelectric actuator are also connected via gold wire to PGA bond pads. This set up is shown in Figure 7.2 (A). A schematic of the cantilever is also shown indicating positions of gold pads and piezoresistors. Pins on the back side of the PGA correspond to individual bonding pads and allow for electrical connections to be made to measurement instruments. Two pins from an IC socket are soldered to the inner conductor and outer conducting shield of a coaxial cable. This modified coaxial cable is used to make connections to the pins on the backside of the PGA. To ensure that wire bonding has been successfully performed the resistance of the gold piezoresistor can be checked. Typically resistance values vary between 50 – 250 Ω dependent on the cantilever being measured. This variation is due to the longer gold lines for cantilevers in the centre of the array resulting in a higher resistance value.

A schematic of the set up used for the measured of resonance frequencies is shown in Figure 7.3 A bias tee (ZFBT-4R2G+; Mini Circuits) acts as the central hub of the setup where connections between piezoresistors and electrical instruments are made. The bias tee has three connection ports for radio frequency (RF), direct current (DC), and RF + DC. The piezoresistor is connected to the RF + DC port. A DC power supply (E3614A; Agilent Technologies), operated in constant voltage mode, supplies the required DC bias voltage. A voltage of 0.2 – 1 V is typically used for biasing in non-biological measurements. Connection of the power supply to a piezoresistor is via the DC port on the bias tee. A network analyser (3577A; Hewlett Packard) is used for measurement of resistance changes caused by cantilever oscillation. The signal output of the RF port on the bias tee is pre-amplified (SR560, Stanford Research Systems) before acquisition by the network analyser.

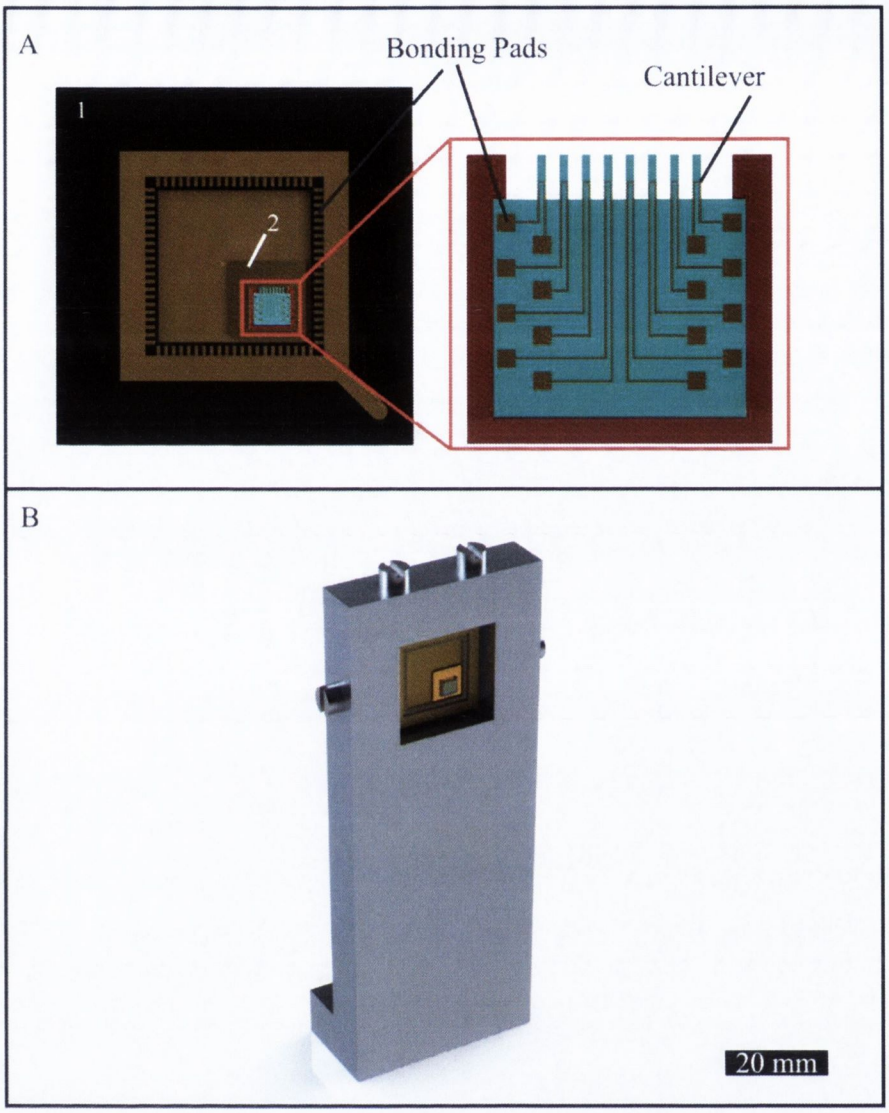


Figure 7.2: Piezoresistive cantilever measurement. (A) A PGA is used for acquisition of electrical signals (1). A piezoelectric actuator is fixed to the PGA using silver paint and the cantilever array is glued on top (2). Wire bonds made between the gold pads on the arrays chip body and bond pads on the PGA facilitate acquisition of electrical signals. (B) The PGA is mounted in the environmental chamber using the mount shown. This allows visualisation of the sensors using a USB digital camera.

The output of the network analyser is connected to the piezoelectric actuator. The network analyser has three inputs allowing for the acquisition of signals from up to three cantilevers in an array. Each cantilever requires an individual bias tee and DC power supply.

When performing growth measurements the cantilever is housed in the environmental chamber described in Chapter 3, which is mounted on a floating optical bench. The

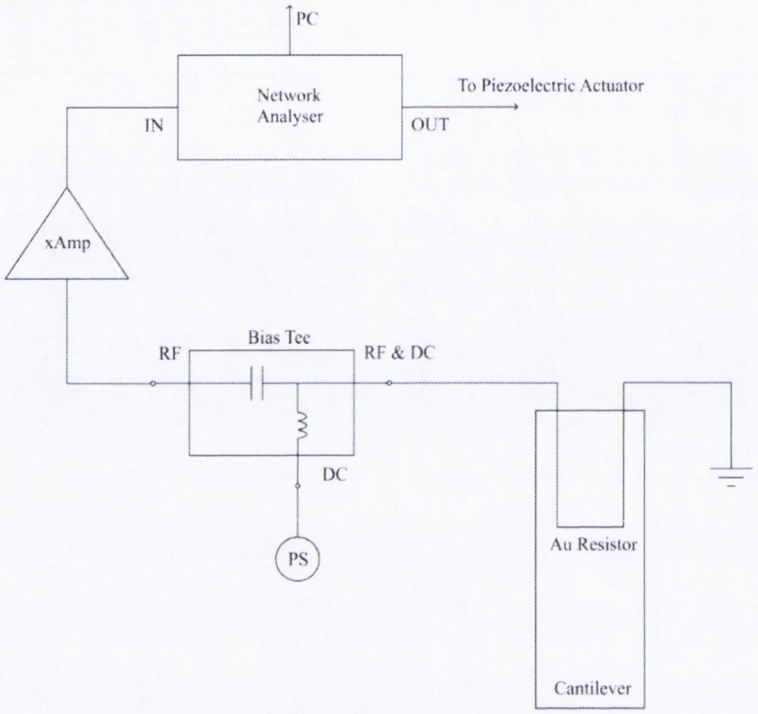


Figure 7.3: Schematic of experimental set up. A bias tee acts as the central hub of the setup where connections between piezoresistors and electrical instruments are made. The piezoresistor is connected to the RF + DC port. A DC power supply operated in constant voltage mode, supplies the required DC bias voltage. A network analyser is used for measurement of resistance changes caused by cantilever oscillation. The output of the RF port on the bias tee is pre amplified before acquisition by the network analyser. The output of the network analyser is connected to the piezoelectric actuator.

environmental conditions used for previous growth measurement (94% RH and 30 °C) are used. Access for cables used for electrical connections is through the iris ports on the front of the chamber. The USB digital camera described in Chapter 5 is also used here to image conditions on the cantilevers surface. The PGA is held in a custom designed mount as shown in Figure 7.2 (B), which is attached to an optical bread board.

The front panel of the LabVIEW VI used for recording of frequency and phase spectra is shown in Figure 7.4. Communication with the network analyser is via a GPIB-USB interface (NI GPIB-USB-HS; National Instruments). Using this VI it is possible to record up to 3 frequency spectra for each network analyser input. It is also possible to control the bias voltage used for measurement. Measurement parameters are predetermined using the network analyser hard controls prior to being entered in the VI front panel.

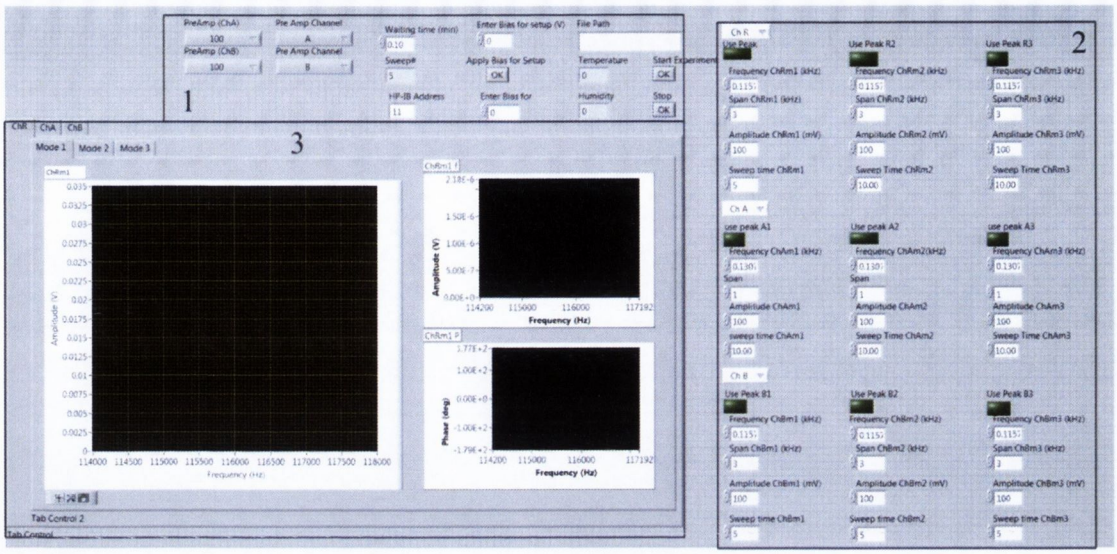


Figure 7.4: Front panel of the LabVIEW VI. Communication with the network analyser is via a GPIB-USB interface (NI GPIB-USB-HS; National Instruments).

## 7.4 Measurement

Arrays are cleaned using oxygen plasma, silanised, and agarose functionalised as described in Chapter 2. Care is taken to ensure no damage to the gold lines on the arrays occurs during handling.

### 7.4.1 Response to Humidity

An Agarose functionalised array was glued to a piezoelectric actuator on a PGA and wire bonding was performed as outlined in Section 7.3. The PGA was placed into the mount shown in Figure 7.2 (B) and the necessary wire connections were made. The cantilever array was placed into the optical path of the Dual Translation Stage Device described in Chapter 4, (the mount (4) shown in Figure 4.6 was removed) to allow for a comparison between piezoresistive and optical measurement of resonance frequencies to be made. The differential output of the PSD was connected directly to an input of the network analyser. The fundamental resonance frequency of one cantilever in the array was tracked as relative humidity levels were ramped from 80 – 94 % at 30 °C. The total resistance of the gold line for this specific cantilever was 203 Ω.

For the piezoresistive measurement 400 data points were recorded in a 2 kHz range with a resolution bandwidth of 1 Hz. 1 V was used to actuate the piezoelectric actuator and a pre-amplification of x500 was applied to acquired signals. A DC bias of 1 V was applied to the piezoresistor.

For the optical measurement the same parameters were used. No pre-amplification of the acquired signal was required. 40s was required for the measurement of each spectrum. Frequency spectra were recorded at intervals of 100 s.

### 7.4.2 Growth Measurements

An agarose functionalised array was dipped into Roswell Park Memorial Institute medium broth (RPMI – 1640, Sigma Aldrich) (supplemented with 0.165 M MOPS and 0.2% glucose) for 10 minutes in order to load the agarose layer with nutrition. The base of the array was cleaned with ethanol in order to remove nutrition/medium residues from electrical contacts. The array was then glued to the piezoelectric actuator. Deposition of spores using the glass needle technique onto dry sensors was not possible, therefore 1 drop of RPMI was spotted on three cantilevers in the array using the inkjet printing technique described in Chapter 2 prior to spore deposition. Eight *A .niger* spores were deposited into the drops of medium on two of the cantilevers (test cantilever) using the glass needle technique described in Chapter 2. The other cantilever is used as a reference. The array was placed into the environmental chamber at experimental conditions (94% RH, 30 °C).

Amplitude spectra were recorded for one test cantilever and the reference cantilever at 30 minute intervals. 400 data points were recorded in a 4 kHz frequency range using a resolution bandwidth of 1 Hz. A DC bias of 0.5 V was applied to the piezoresistive elements. A scan time of 40s was used for each cantilever. In between frequency measurements the bias voltage to the piezoresistors was reduced to 0 V. A x200 pre-amplification factor was applied to the acquired signals. 1 V was applied to the piezoelectric actuator. The second test cantilever was used as a growth control; no DC bias voltage was applied. Images of the cantilevers were recorded at 30 minute intervals.

## 7.5 Results

### 7.5.1 Piezoresistive and Optical Peaks

Figure 7.5 and Figure 7.6 show amplitude spectra for the fundamental resonance mode of an agarose functionalised cantilever, which has been measured using the piezoresistive method and optical method respectively. These peaks were measured at experimental environmental conditions (94% RH and 30 °C). This indicates that the operation of these sensors, where the piezoresistive element has not been passivated against the environment, can be performed at these elevated conditions without issue. It can be observed that the piezoresistive peak is inverted compared to the optical peak and has an increasing base line. In both cases the resonance frequency of the cantilever is 32577 Hz. From 130 measurements the signal to noise ratio is found to be 157:1 for the piezoresistive method and 140:1 for optical method. It should be noted that the optical signal was recorded using no pre-amplification while a pre-amplification of x500 was used for measurement of the piezoresistive peak. The quality factor ($Q$) of both peaks is ~ 260.

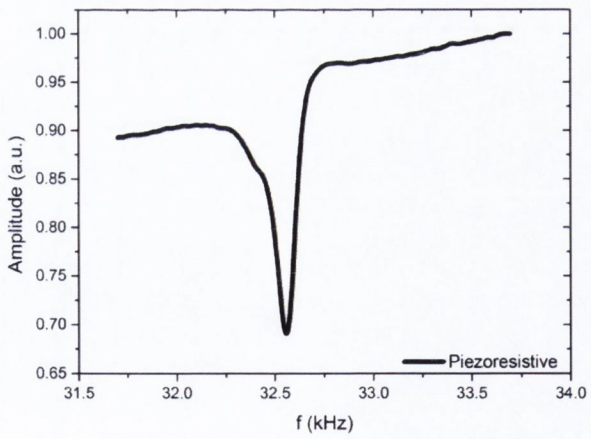


Figure 7.5: Fundamental mode resonance peak measured using piezoresistive readout. The peak has a signal to noise ratio of 157:1 at experimental conditions (94% RH, 30 °C).

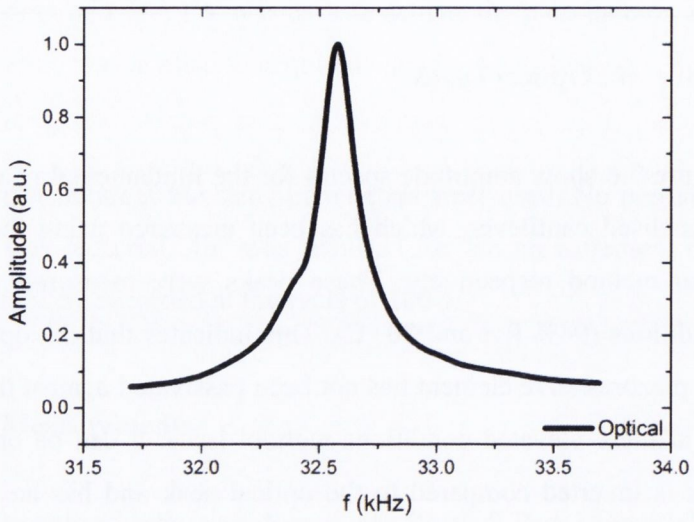


Figure 7.6: Fundamental mode resonance peak measured using laser beam deflection. The peak has a signal to noise ratio of 140:1 at experimental conditions (94% RH, 30 °C).

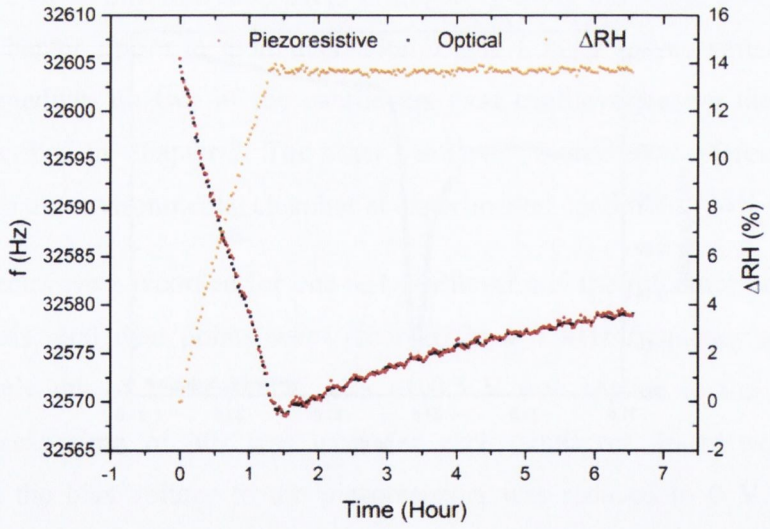


Figure 7.7: Fundamental mode frequency response of an agarose functionalised cantilever due to changes in relative humidity (RH). The zero point in the right had axis corresponds to 80 % RH. The measured frequency shift is the same for the piezoresistive and optical measurement.

### 7.5.2 Response of Agarose Functionalised Sensor

Figure 7.7 shows the change in resonance frequency for an agarose functionalised cantilever due to changes in humidity. It can be seen that there is a decrease in resonance frequency as humidity levels increase. The decrease is due to the absorption of water by the agarose layer. Both the optical and piezoresistive readout methods show the same magnitude of frequency shift indicating that there is no loss of sensitivity. Where relative humidity levels are stable there is a positive drift in resonance frequency at a rate of ~ 2 Hz/hour. There is an observable fluctuation in the frequency during stable humidity operation. This is due to humidity fluctuations in the environmental regulation. The mass responsivity of this sensor is found to be ~ 32 pg/Hz using both methods. Operation at elevated relative humidity conditions was seen to have no observable effect on the quality of the recorded resonance spectra.

### 7.5.3 Growth Measurement

Several attempts have been made to measure the growth of *A. niger* spores using piezoresistive cantilevers. In each case the varying parameter was the DC bias voltage used. Values for the DC bias used ranged from 0.2 V – 1V. These values were recommended for use by the fabricator of these arrays. An increase of temperature due to Joule heating was previously assumed to be insufficient to result in a reduction in spore viability.

In all cases no growth occurred when a DC bias was applied. Hyphal growth was observed on growth control cantilevers where no bias has been applied. This led to the conclusion that Joule heating of the piezoresistive elements on the cantilevers is resulting in unsuitable conditions for biological growth to occur. In order to overcome this issue, the bias voltage applied to the piezoresistive elements was reduced to 0 V when frequency data was not being recorded. Hence, Joule heating was occurring for 80 seconds per half hour. This reduction in the duration of time at which the fungal spores were subjected to elevated temperatures still did not create conditions suitable for growth to occur. Multiple attempts were made to measure growth all to no avail. This would indicate that the temperature on the cantilevers is not suitable for viable microorganism growth. The experiment described

in Section 7.4.2 is typical of those performed. After 24 hours no growth was observed on the test sensor however hyphal filaments were clearly visible on the growth control sensor. At this point resonance frequency measurements were ceased.

Figure 7.8 shows images, taken using the USB digital camera, of the test cantilever when different DC bias voltages are applied to the piezoresistive element on the cantilever.

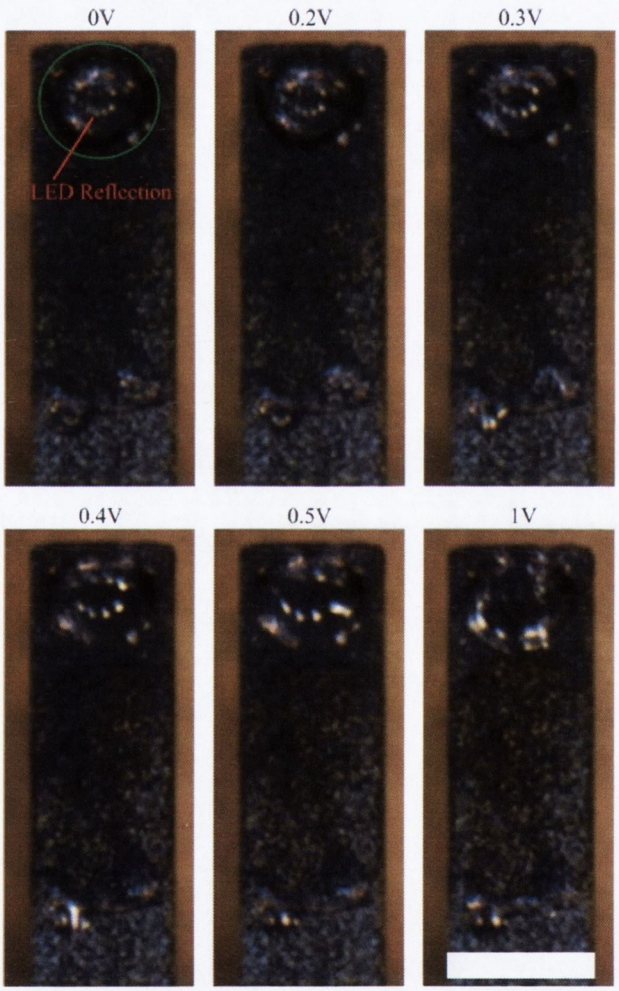


Figure 7.8: Effect of applied bias voltage. Joule heating of the Au piezoresistor prevents growth of *A. niger* spores. The rise in temperature is sufficient to cause changes in the droplet of nutritional medium into which spores are deposited. At lower voltages changes in droplet shape can be observed by tracking the motion of the reflection of the LEDs from the USB digital camera. The white scale bar corresponds to the width of a cantilever (~ 98.5 μm).

From this figure it is clear that the bias voltage has an effect on the conditions on the cantilevers surface. Joule heating of the piezoresistive element is causing a loss/reduction in surface tension of the liquid on the cantilever's surface. By tracking the LED reflections from the USB camera in the liquid drops it can be seen that at voltages as low as 0.2 V Joule heating is having an effect on conditions on the cantilever's surface. Similar observations have been made on blank sensors, where only a droplet of RPMI has been deposited, indicating that agarose functionalisation and immersion of the entire array in RPMI is not having any adverse effects.

Figure 7.9 shows hyphal filaments growing off the piezoresistive integrated sensors surface. Through growth measurements performed using Si cantilevers (as described throughout this thesis) it has been observed that typically hyphal growth remains on the cantilevers surface rather than propagating in an aerial fashion. The fact that hyphae immediately propagate off the sensors surface indicates that surface conditions are suboptimal for growth. A bias voltage was not supplied to the Au resistor on the control sensor. This indicates that heating from the adjacent test sensor is sufficient to change conditions on the growth reference cantilever's surface. This effect is observable in videos where voltages as low as 0.7 V are applied. For the purposes of demonstration images of the observed effect when 1.5 V is applied are shown in Figure 7.9. This result indicates that heating from the gold line on the cantilevers body and adjacent sensors must be considered.

Determination of the change in temperature due to the magnitude of the bias voltage used is not trivial due to various reasons; (i) the sensors are coated with agarose hydrogel, (ii) the cantilevers within one array have different gold paths resulting in variances in resistance. For these reasons determination of the change in temperature is deemed beyond the scope of this work. In the case of fungal growth a few degrees Celsius miscalculation could be significant. Typically the effects of Joule heating are ignored for measurements conducted using piezoresistive cantilevers. However, it is clear from what is presented here that Joule heating has an adverse effect when piezoresistive sensors are used for biological measurements. The effect of self-heating on the sensitivity of static readout of piezoresistive cantilevers is discussed in [18, 19]. It is concluded that self-heating has adverse effects on the sensitivity of the technique and that operation in air results in a temperature increase at the cantilever's tip that is 20 times larger than that observed in a

liquid environment. In [12], the use of Au piezoresistors embedded in SU-8 polymer cantilevers are seen to result in plastic deformation of the sensor when large bias voltages are used. The authors recommend the use of a bias voltage below 1.5 V and 3 V, in the case of a 600 Ω and 7.5 kΩ resistor respectively, to avoid damage to the polymer cantilevers which occurs at 180 °C. Simulations performed in the same work show that a bias of 0.5 V applied to a 600 Ω Au resistor results in a 6 K increase in temperature. Hence, the application of 0.5 V across the cantilever array used in this work would produce temperature changes of between 14 – 72 ° K, dependant on the cantilever used. This would indicate that in our experiments the use of bias voltages below 0.5 V on cantilevers located at the centre of the array, where total resistances are higher (due to the designed longer gold paths), may produce conditions suitable for growth. Growth measurements have been performed using central cantilevers however the use of voltages below 0.5 V was not possible due to reduced signal to noise levels. Further tests have to be performed to see at which voltages spores could grow with the current design of these piezoresistive sensors. At this stage of the project the optical readout provided clear experimental evidence that nanomechanical measurement are suitable for growth detection of fungi whereas the integrated method did not provide the benefits which were expected.

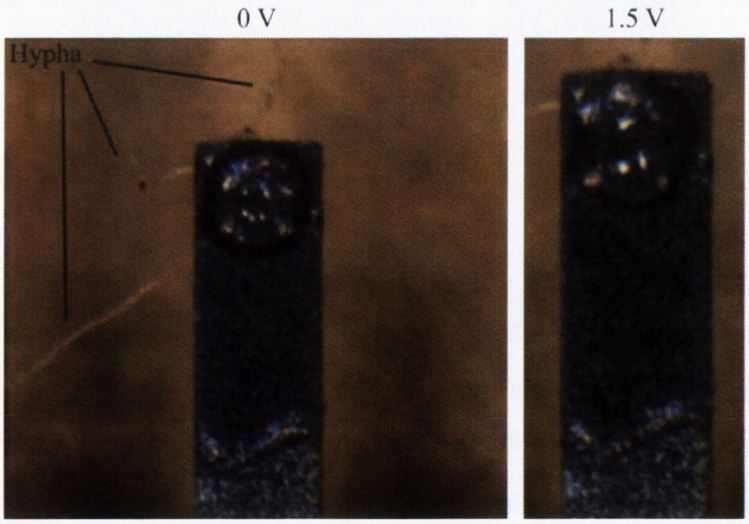


Figure 7.9: Hyphal filaments on cantilever where no bias voltage has been applied. Hyphal growth propagates off the sensors surface. Bias voltages as low as 0.7 V applied to the adjacent sensors causes an observable change on this sensors due to Joule heating (data not shown here).

In order to determine the affect of periodic heating on the viability of *A. niger* spores, tests were performed using a polymerase chain reaction (PCR) thermal cycler (Genetec, Witek, Germany). Here spore suspensions in an Eppendorf tube were subject to periodic heating. In order to replicate conditions in piezoresistive cantilever measurements two tests were performed where the temperature was increased from 30 °C to 45 °C or 55 °C for 80s every 30 minutes. Figure 7.10 shows images of the spores after 24 hours at 30 °C, and those which have been subjected to heat shocks of 45 °C and 55 °C. Spores incubated at 30 °C show normal hyphal growth. Spores subjected to shocks of 45 °C are able to germinate but show short irregular branching hyphae indicating that spores can survive but these conditions are suboptimal for growth.

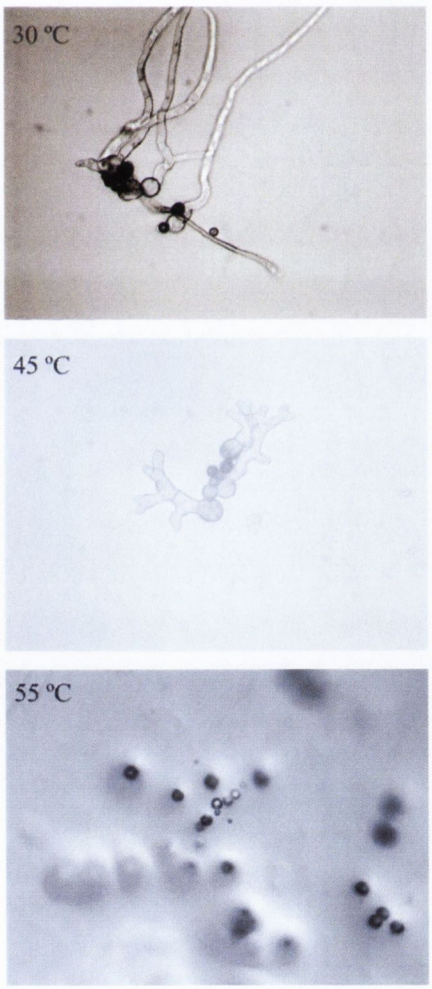


Figure 7.10: Images of *A. niger* spores after 24 hours at different temperatures. Spores at 30 °C are able to germinate and grow hyphal filaments. Spores subjected to 45 °C for 80 seconds every 30 minutes show short branching hypha indicating suboptimal growth conditions. Spores subjected to 55 °C for 80 seconds every 30 minutes show no visible growth.

Those spores subjected to ramps of 55 °C are unable to germinate indicating that these short exposure times to higher temperatures are resulting in spore death. These tests indicate that the temperatures on the cantilever are higher than 45 °C. It has been reported that *A. niger* can withstand temperatures within the range of 6 – 47 °C [20] however, irregular and slower growth can be expected at both extremes of this range.

## 7.6 Conclusion

The use of piezoresistive cantilevers at elevated environmental conditions (94% RH, 30 °C) has been demonstrated successfully without issue. Immersion of the arrays in nutritional medium prior to dynamic mode measurements was seen to have no adverse effects on the quality of recorded frequency spectra. This indicates that the passivation of piezoresistors against the external humid environment is not required. In comparison to the use of the laser beam deflection method there is no loss in sensitivity when using the piezoresistive readout technique. Both methods reveal a mass sensitivity of ~ 32 pg/Hz for an agarose functionalised cantilever. Peaks have been found to have a higher signal to noise ratio (157:1) when compared to the optical beam deflection method (140:1) however, pre-amplification of acquired signals is required.

Fast *A. niger* growth detection has not been possible using piezoresistive sensors. It has been clarified that Joule heating of the Au piezoresistors due to the required application of a DC bias voltage renders these type of sensors unsuitable for sustaining viable microorganisms. The time at which heating is occurring was reduced to 80 s per 30 minutes however, suitable conditions for growth were not achieved. It was not possible to accurately determine the temperature increase due to a lack of additional piezoresistive cantilever arrays. Determination of this value is planned in the near future. Comparison with published work using SU-8 polymer cantilever with embedded Au piezoresistors and tests performed using a PCR thermal cycler indicate that temperatures on the sensors surface most probably are exceeding 47 °C.

It is believed that the use of piezoresistors with higher resistances will result in suitable conditions for the support of spore growth. A possible solution is a redesign of the Au piezoresistors to resemble those used in [12], which have a zigzag pattern resulting in a longer conductive path and thus an increased resistance. An alternative route to integrated

readout would be provided by piezo electric readout. Here optimal frequencies for actuation and readout would be in a range above MHz. It would have to be tested whether the mass-uptake would be favourably measured at such high frequencies.

## 7.7 References


1. Tomlinson, H., *On the Increase in Resistance to the Passage of an Electric Current Produced on Wires by Stretching.* Proceedings of the Royal Society of London, 1876. **25**(171-178): p. 451-453.
2. Smith, C.S., *Piezoresistance Effect in Germanium and Silicon.* Physical Review, 1954. **94**(1): p. 42-49.
3. Tortonese, M., R.C. Barrett, and C.F. Quate, *Atomic resolution with an atomic force microscope using piezoresistive detection.* Applied Physics Letters, 1993. **62**(8): p. 834-836.
4. Li, M., H.X. Tang, and M.L. Roukes, *Ultra-sensitive NEMS-based cantilevers for sensing, scanned probe and very high-frequency applications.* Nature Nanotechnology, 2007. **2**(2): p. 114-120.
5. Minne, S.C., S.R. Manalis, and C.F. Quate, *Parallel atomic force microscopy using cantilevers with integrated piezoresistive sensors and integrated piezoelectric actuators.* Applied Physics Letters, 1995. **67**(26): p. 3918-3920.
6. Boisen, A., et al., *Environmental sensors based on micromachined cantilevers with integrated read-out.* Ultramicroscopy, 2000. **82**(1–4): p. 11-16.
7. Jensenius, H., et al., *A microcantilever-based alcohol vapor sensor-application and response model.* Applied Physics Letters, 2000. **76**(18): p. 2615-2617.
8. Yoshikawa, G., et al., *Sub-ppm detection of vapors using piezoresistive microcantilever array sensors.* Nanotechnology, 2009. **20**(1): p. 015501.
9. Baker, G.A., R. Desikan, and T. Thundat, *Label-Free Sugar Detection Using Phenylboronic Acid-Functionalized Piezoresistive Microcantilevers.* Analytical Chemistry, 2008. **80**(13): p. 4860-4865.
10. Kim, S., et al., *Piezoresistive cantilever array sensor for consolidated bioprocess monitoring.* Scanning, 2009. **31**(5): p. 204-10.
11. Thaysen, J., et al., *Polymer-based stress sensor with integrated readout.* Journal of Physics D: Applied Physics, 2002. **35**(21): p. 2698.
12. Johansson, A., et al., *Temperature effects in Au piezoresistors integrated in SU-8 cantilever chips.* Journal of Micromechanics and Microengineering, 2006. **16**(12): p. 2564-2569.
13. Johansson, A., et al., *SU-8 cantilever sensor system with integrated readout.* Sensors and Actuators A: Physical, 2005. **123–124**(0): p. 111-115.
14. Anja, B., et al., *Cantilever-like micromechanical sensors.* Reports on Progress in Physics, 2011. **74**(3): p. 036101.
15. Gammelgaard, L., et al., *Microfabricated photoplastic cantilever with integrated photoplastic/carbon based piezoresistive strain sensor.* Applied Physics Letters, 2006. **88**(11): p. 113508-3.
16. Talukdar, A., M. Qazi, and G. Koley, *High frequency dynamic bending response of piezoresistive GaN microcantilevers.* Applied Physics Letters, 2012. **101**(25): p. 252102-5.
17. Tao, Y., et al., *Resonant cantilever sensors operated in a high-Q in-plane mode for real-time bio/chemical detection in liquids.* Sensors and Actuators B: Chemical, 2011. **157**(2): p. 606-614.
18. Mohd Zahid, A. and C. Chongdu, *On self-heating in piezoresistive microcantilevers with short piezoresistor.* Journal of Physics D: Applied Physics, 2011. **44**(28): p. 285402.

19. Doll, J.C., et al., *Self-heating in piezoresistive cantilevers.* Appl Phys Lett, 2011. **98**(22): p. 223103.
20. Schuster, E., et al., *On the safety of Aspergillus niger - a review.* Applied Microbiology and Biotechnology, 2002. **59**(4-5): p. 426-435.

# Chapter 8
# Conclusions and Outlook

## 8.1 Conclusions and Outlook

Two devices based on the laser beam deflection method have been described which are capable of measuring the resonance frequencies of cantilevers in an array. These devices have been geared towards biological measurements and have thus been designed accordingly. A device utilising a fibre optic based readout technique was successfully employed for the detection of fungal growth an order of magnitude faster than conventional colony counting techniques. Despite this success the device had several issues in regards to practicality and ease of use and it has since been disassembled. The development of this device and experiments performed using it were carried out within the first 18 months of this study.

A second device based on the laser beam deflection method was developed. This device incorporates a position sensitive detector for the measurement of cantilever resonance frequencies. Measurement of higher resonance modes of cantilevers in an array was facilitated by the use of automated translation stages. These stages ensure that clean frequency spectra can be measured for all cantilevers. The stable operation of this device for > 48 hours at elevated temperatures and relative humidity conditions up to 100% has been demonstrated. Further development of this device has seen the implementation of a high-magnification camera capable of imaging growth conditions on micron-sized cantilevers during measurements. This visual information, when coupled with frequency data, has allowed for complicated frequency spectra to be demystified and has resulted in quantitative data being extracted from microorganism growth measurements. Using this instrument the growth of single *A. niger* spores has been detected, thus indicating that no further development of this instrument is required in regard to detection limits and sensitivity.

Preliminary antimicrobial susceptibility testing (AST) has been performed using this instrument. The results obtained are promising and indicate that the use of cantilevers for

performance of these tests is advantageous. From the data presented it is clear that deposition of antifungal drugs on the sensors in a liquid droplet produces significant drift due to evaporation. Whilst frequency shifts due to the growth of fungi are able to exceed this drift it is believed that detection times can be further reduced if local humidity around sensors is stabilised. It has been shown that this effect can be greatly reduced by operating the device at 100 % RH. However, device operation at these conditions results in significant condensation on sensors with consequent attenuation of the optical signal used for frequency detection. An alternative method to the currently employed functionalisation techniques would be the incorporation of the antifungal drugs and spores in the agarose solution prior to cantilever functionalisation. One obstacle to this is the high temperature (> 100 °C) required during agarose functionalisation which may well result in damage to the drugs tested. A solution to this would be the use of a low gelling point agarose which typically gel at 25 °C.

It is planned in the near future to perform ASTs in conjunction with imaging of the sensors *in situ*. This will allow for quantitative data to be obtained and provide further insights into the effects of low antibiotic concentrations on morphology and structure of fungal hyphae. Currently used micro-dilution techniques are performed in 96 well microtiter plates. Typically tests are carried out using 8 different antifungals at 12 different concentrations. In order to compete with this technology it is clear that the size of cantilever arrays will need to be scaled up to provide more sensors.

In order to develop user friendly instruments it is desirable to remove bulky optical equipment. This will greatly reduce the size of devices, while the removal of required optical alignment protocols will allow for ease of use. In order to realise this the use of piezoresistive cantilever arrays has been attempted. It was observed that Joule heating of piezoresistive sensing elements resulted in non-viable conditions for the species under investigation. In order to overcome these heating issues it is proposed, as future work, to use pulsed biasing of the piezoresistive elements which may reduce the observed Joule heating effects. A redesign of the sensors may also be required where the resistances of the piezoresistors in all sensors are equal to allow proper reference sensors to be implemented. An increase in the resistance of the piezoresistor should also be considered to reduce current flow and Joule heating. However, it is not known what effect an increased resistance will have on measurement sensitivities.

The issues experienced when trying to perform biological measurements using piezoresistive cantilevers indicates that it is vital to consider the effects of the measurement process on cell viability. For instance, in this work where optical beam deflection is used for the measurement of cantilever resonance frequencies a wavelength in the infra-red was chosen to limit any damage that may be caused to biological material. Resonance frequency measurements are also taken at intervals of 15 or 30 minutes as excessive shaking of microorganisms has been seen to have an effect on cell viability. It may be possible to increase the rate of resonance frequency measurement however further work is required to determine an optimum. These issues, as well as others, must be considered for further development of new microorganism growth monitoring techniques/instruments. As microorganisms vary greatly rigorous testing of new techniques must be performed to ensure their suitability for monitoring of all microbial species.

It is evident that there are many challenges involved in the transfer of the cantilever sensing technology to biological applications. This is reflected in the few successfully developed instruments which have made an impact at a commercial level. This issue has to be addressed for the survival of this technology as a biosensing platform. One also has to consider the shelf life of the bio functionalised cantilever sensors. In some areas such as nanomechanical cantilever diagnostics this time is very short. The biggest challenge is the number of biological assays which would require standardisation and automisation to facilitate cantilever biosensors as a plotform technology.

# Appendix

# A1: Piranha Cleaning of Cantilever Arrays

This protocol is used for the cleaning of the cantilever arrays prior to silanisation. Piranha cleaning removes organic contaminants from the surface of the cantilevers and leaves them hydrophilic. For best results silanisation should be performed immediately afterwards.

**Precautions:** Extreme care must be taken when working with piranha solution and full PPE including face shield, lab coat, and suitable gloves must be worn. The piranha solutions should be prepared in minimal amounts and all work should be performed in a fume hood due to gases produced by the solution. Due to its violent reaction upon contact with organic materials, and the high temperatures reached during reactions (>100 °C.), piranha solution should not be stored. It should always be prepared fresh before use and disposed of in an appropriate manner immediately after use to avoid risk of explosion.

**Materials**

- Sulphuric Acid ($H_2SO_4$), 99.99%
- Hydrogen Peroxide ($H_2O_2$), 30%
- RBS detergent solution, 2% in nanopure water
- Sodium Chloride (NaCl), 1 M
- Ethanol ($C_2H_6O$), HPLC Grade
- Isopropanol ($C_3H_8O$), HPLC Grade
- Nanopure water, 18 M Ω
- Teflon beakers and teflon coated tweezers
- Large beaker of water (e.g. 2 L) for quenching solution after use

**Method**

**1. Preclean:**

- Wash array in 2% RBS detergent solution for 2 minutes.

- Rinse in 1 M NaCl for 30 seconds.
- Rinse in nanopure water for 30 seconds.

**2. Bath 1:**

- Prepare 5-10 mL piranha solution ($H_2SO_4$:$H_2O_2$ = 1:1) by slowly adding the $H_2O_2$ to the $H_2SO_4$.
- Dip the cantilever array in the piranha solution for 30 seconds.
- Rinse in 1 M NaCl for 30 seconds.
- Rinse in nanopure water for 30 seconds.

**3. Bath 2:**

- Prepare 5-10 mL piranha solution.
- Bath in piranha solution for 20 minutes.
- Bath in 1 M NaCl for 5 minutes.
- Bath in ethanol/nanopure water ($C_2H_6O$:$H_2O$ = 1:1) for 5 minutes.
- Rinse in nanopure water for 30 seconds.

**4. Bath 3:**

- Prepare 5-10 mL piranha solution.
- Bath in piranha solution for 10 minutes.
- Bath in 1 M NaCl for 5 minutes.
- 2 × Bath in ethanol/nanopure water ($C_2H_6O$:$H_2O$ = 1:1) for 5 minutes.
- Bath in isopropanol for 2 minutes.

**5. Dry on filter paper and store in vacuum.**

# A2: Plasma Cleaning of Cantilevers or Glass Capillaries

This protocol is designed to clean the cantilever surface prior to silanisation. Plasma cleaning removes organic contaminants from the surface of the cantilever arrays. The plasma cleaning in performed in a Diener PICO Barrel Asher (Diener Electronic GmbH & Co. KG, Nagolder Str. 61, D-72224 Ebhausen, Germany). Silanisation should be performed immediately after cleaning for best results. This protocol can also be used for cleaning capillary tubes.

**Method**

- Place cantilevers or capillaries in customised holder and place in plasma chamber.
- Flush plasma chamber 3 times with $O_2$.
- 3 minutes exposure to $O_2$ plasma, $O_2$ at 0.3 mbar, 160 W, 40 kHz.
- If cleaning capillary tubes flush with HPLC grade ethanol.

# A3: Silanisation

This protocol outlines the steps for Silanisation of the cantilever with an epoxy terminated silane for covalent binding of an agarose matrix to the cantilever. This should be performed immediately after cleaning for best results.

**Materials**

- 3-glycidyloxypropyl-trimethoxysilane
- N-ethyldiisopropylamine
- Water free toluene
- Steel tweezers
- Glass beakers
- 5 mL Syringe
- 1 mL Syringe
- Nitrogen gas

**Methods**

- Prepare a silane solution (3-glycidyloxypropyl-trimethoxysilane: N-ethyldiisopropylamine : water free toluene; 1 : 1 : 100)
- Incubate cantilever in silane solution for 45 minutes. Place on shaker at 70 rpm.
- Wash twice in water free toluene for 15 minutes
- Dry under nitrogen.

**Note:** Plastic containers should not be used.

# A4: Agarose Functionalisation

This protocol outlines the steps required for the successful coating of cantilevers with an agarose matrix. For best results this should be performed directly after silanisation.

**Materials:**

- SeaKem Gold™Agarose, powder
- Nano pure water
- Cleaned, epoxy-silanised cantilever array
- Cleaned capillary tubes
- Radiation Lamp
- Functionalisation Device
- 2M NaOH

**1% Agarose Solution Preparation:**

- Dissolve 0.1g of SeaKem Gold™Agarose, powder in 10 mL nano pure water. Heat sealed falcon tube in water bath until white powder is dissolved.
- Make 500 µL aliquots in eppendorf tubes and seal with nescofilm.
- Store at 4 °C until required.

**Cantilever Functionalisation:**

- Arrange cleaned capillaries tubes and cantilever on functionaliser and align. Insert end of tubes into tip of eppendorf tube.
- Preheat capillaries using radiation lamp (Osram) (35 min).
- After heating the capillary tubes add 2 µL of 2M NaOH to the 500 µL agarose solution to adjust the pH to 11.9.
- Immediately pipette the agarose solution into the reservoir. When the agarose reaches the ends of the capillary tubes immerse the cantilevers in the solution for 2-3 sec.
- Store cantilever at room conditions.

# A5: Cell Dehydration for SEM

This protocol is used for the preparation of cantilevers coated with microbes for imaging using scanning electron microscopy (SEM). Due to the low pressure used in the imaging chamber cells must be dehydrated and fixed to remain intact.

**Precautions:** Most chemicals used are toxic and should be treated with extreme caution. Full PPE including lab coat and suitable gloves must be worn. All procedures should be carried out in a fume-cupboard. The fume-cupboard should be kept clean at all times.

**Stock Solutions:** (refrigerated)

- 1M Potassium dihydrogen phosphate ($KH_2PO_4$) (stored at -4°C)
- 1M Dipotassium hydrogen phosphate ($K_2HPO_4$) (stored at -4°C)
- 25% Glutaraldehyde in water (stored at -20°C)

**Other Solutions required:**

- 0.5M Phosphate Buffer (pH 6.8): Mix 51 mL of stock 0.5M $KH_2PO_4$ with 49 mL of 0.5M $K_2HPO_4$.
- 0.05M Phosphate Buffer (pH 6.8): Dilute 10 mL of 0.5M phosphate buffer with 90 mL of distilled water.
- Filter the solutions prior to autoclaving.

**Fixative solutions:**

- 5% Glutaraldehyde in 0.05M Potassium Phosphate buffer (pH 6.8) 50mL
- 35 mL filtered deionised water
- 5 mL 0.5M Phosphate buffer
- 10 mL 25% Glutaraldehyde

**Fixation Procedure:**

- Dry samples for at least 12 hours.
- Put CLAs in 5 mL glutaraldehyde fixative in glass beaker fix for 1 to 1.5 hours (4hrs) at room temperature while agitating the solutions on a rotator (100 rpm).

**Washing Procedure:**

Wash 6 times for 1 hour with 0.05M Phosphate buffer to remove any unreacted glutaraldehyde from the samples before drying steps. Leave the samples in the vial and change the wash solutions using a pipette.

**Dehydration Series:**

An acetone dehydration series is normally used for plant and fungi samples (*i.e. Aspergillus*). An alcohol dehydration series is normally used for animal tissue and bacteria (at room temperature).

- 10% acetone/ethanol in water, 10 min
- 30% acetone/ethanol in water, 10 min
- 50% acetone/ethanol in water, 10 min
- 70% acetone/ethanol in water, 10 min
- 95% acetone/ethanol in water, 10 min
- 100% acetone/ethanol, 15 min
- 100% acetone/ethanol, 15 min
- 100% acetone/ethanol, 30 min
- 50:50 ethanol:hexamethyldisilazane
- 10% acetone/ethanol in water, 10 min
- 30% acetone/ethanol in water, 10 min
- 100% hexamethyldisilazane

**Metal coating:**

- Deposit 10 nm Pd on dried samples.

# A.6 Dilution Series for Antibiotic Susceptibility Tests

The protocol described is based on the recommendations from EUCAST antifungal MIC methods for conidia forming molds. The follow steps are taken in preparation of cantilevers for antifungal susceptibility testing.

**Preparation of antimicrobial stock solutions:**

- **Amphotericin B** (A4888, Sigma) powder, stored at 2-8 °C. Stock solution is prepared at a concentration of 40x256 mg/L in dimethyl-sulfoxide (DMSO).
- **Fluconazole** (RTC-Pharma, PHR-1160, Sigma) powder stored at room temperature. Stock solution is prepared at a concentration of 40x256 mg/L in deionized water
- Prepared stock solutions can be stored at -70 °C or at -20 °C for up to 6 and 1 months, respectively.
- Stock solutions are diluted in deionized water in two dilution steps to 4x128 mg/L before use then dilutions are prepared as outlined in Table 1.

Table 1: Spore suspensions used in antifungal susceptibility testing

| **Antifungal concentration (µg/mL)** | **4 x 128** | **...two fold dilution series...** | **4 x 0.03** | **0** |
|---|---|---|---|---|
| **Volume of antifungal solution in DI water (µL)** | 200 | | 200 | 200 |
| **Volume of spore suspension, DI water + tween 0.01% (µL)** | 200 | | 200 | 200 |
| **Volume of double strength RPMI-1640, 0.165 M MOPS, 2% glucose (µL)** | 400 | | 400 | 400 |
| Total volume (800 µL), 1-5x$10^6$ (spores/mL) | | | | |

**Preparation of inoculum:**

- Culture isolates on potato dextrose agar slants (PDA) for 5 days at 35 °C.
- Wash spores from slants with 7-8 mL sterile water supplemented with 0.1% Tween 80 (Tween acts as a surfactant).
- Vortex slants to release conidia. Transfer spore suspension to eppendorf tubes and harvest via centrifugation (10000 rpm, Genofuge 16 M, Techne) for 5 minutes.
- Conidia concentration can be adjusted to desired cfu/mL by counting the conidia in a haemocytometer.
- Resuspend spores in 1 mL 0.1% Tween, and divide into 200 µL portions to ensure that initial spore suspensions are at the same concentration and have same viability conditions.
- Prepare dead spores by heating of 200 µL of the spore suspension at 104 °C for 10 minutes. Harvest cells via centrifugation (10000 rpm, Genofuge 16 M, Techne) for 5 minutes. Discard supernatant and resuspended spores in an equal volume of 0.1% Tween 80.
- Mix with stock solutions as outlined in Table 1.
- Determine suspension concentration using haemocytometer (typically between 1-5 x $10^6$ cfu/mL). When counting also check the quality of the suspension. Pay special attention to spore clamping or suspensions contaminated with broken hyphal filaments which will interfere with ink-jet printing.
- Load suspensions to be deposited on cantilevers into a 96 well micro-titer plate.
- Deposit 1 droplet per cantilever using ink-jet printing.

# A.7 Dual Translation Stage LabVIEW Operating Procedure

Due to its size the block diagram is not displayed but its key features are described and displayed in the subsequent sections. The block diagram consists of one main while-loop (code is executed repeatedly) which contains the two main parts of the VI. The first part is a stacked sequence (frames are executed in numerical order) containing two frames; the first frame contains a case structure (contains one or more sub diagrams which are executed dependant on the value wired to the selector terminal). When alignment is to be performed a sub diagram (of the aforementioned case structure) containing a while-loop is executed which contains the alignment flat-sequence. The second frame of the stacked sequence contains the controls where the waveform parameters determined using the alignment tab can be input by the user. A case structure where the measurement of dynamic and static data is carried out and recorded is the second part of the main while loop. After the determination of waveform parameters the sub diagram containing the measurement sub VIs is executed. The sub diagram contains a flat-sequence (two frames) inside a while-loop. The first frame contains four for-loops (executes sub diagram N times) one for each "peak" to be recorded. These are executed in numerical order. For-loops for each "peak" contain a case structure where the control at the selector terminal determines if dynamic and/or static data is to be recorded for a specified cantilever. If the data is to be recorded a sub diagram containing several VIs in a flat-sequence is executed.

**VI Initialisation:** When the main VI is started a while loop separate to the main while loop is executed. Here several pieces of data such as cantilever number, position of laser spot along cantilever, and environmental conditions are written to global variables (allows passing of data among several VIs) and passed throughout the main VI. This is shown in Figure A7.1 (A). Also in this loop it is possible to execute a sub VI which displays the sum ($I_1+I_2$) and differential ($I_1-I_2$) voltage signal of the PSD on the computer screen for laser alignment purposes. The sub VI contains several DAQmx VIs (VI supplied by NI) which allow interfacing with the PSD through a NI PCI board (NI PCI-6010 16-Bit, 200 kS/s, 16 Analog Input Multifunction DAQ; National Instruments, TX, USA). The DAQ board reads

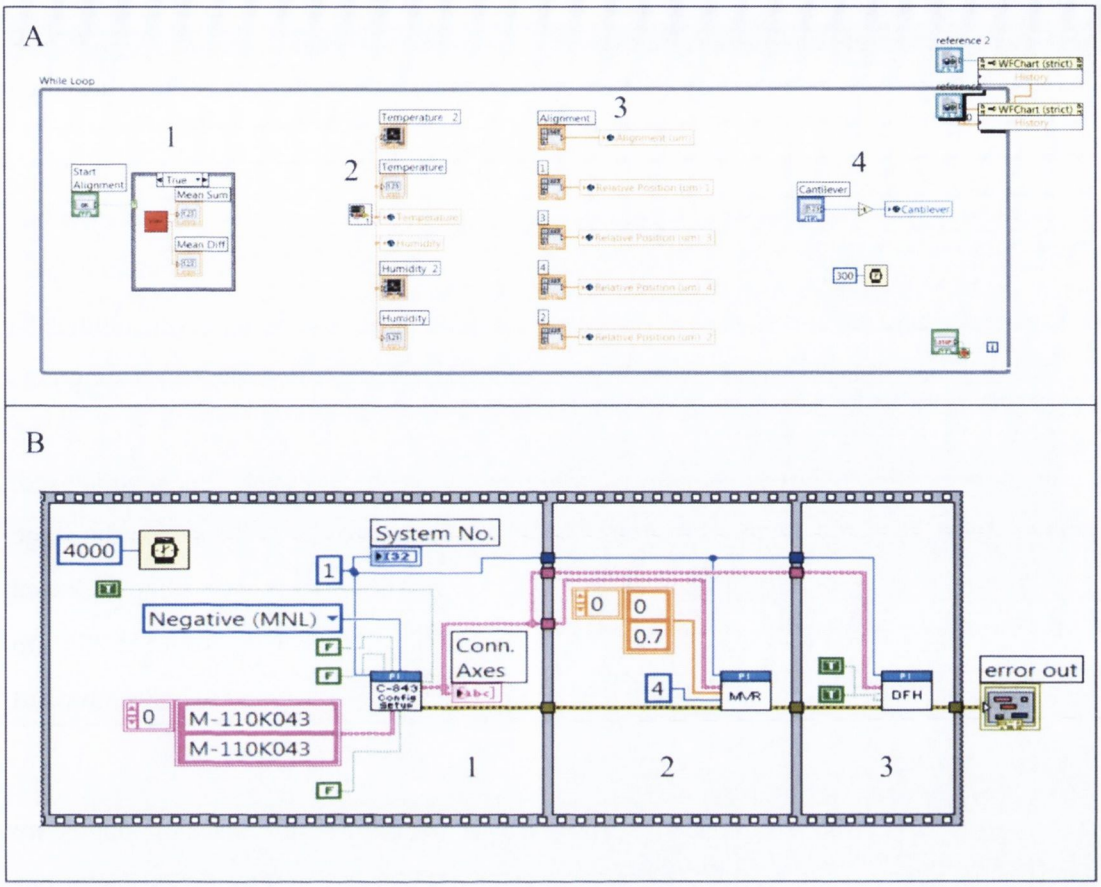


Figure A7.1: (A) While loop containing global variables and a VI to display sum and differential voltages from the PSD. (1) Case structure containing sub VI for sum and differential voltage display. (2) Sub VI which writes environmental conditions to indicators and global variables. (3) Control for position of laser spot along cantilever. Values are written to global variables. (4) Control for selection of cantilever number which is written to a global variable. (B) Block Diagram of sub VI for configuration of translation stages. The flat-sequence is executed in numerical order. (1) Stages are moved to the negative limit of their movement range and returned to the centre position. (2) Stages are moved set distances relative to the centre position. (3) This new position is set as the new 'home' position.

a differential voltage from two channels corresponding to the difference and sum voltages from the PSD. The mean values displayed are comprised of 100 samples taken at a rate of 1000 samples/s. Configuration of the PI stages is also performed on VI start. Here the sub VI shown in Figure A7.1 (B) is executed once. The sub VIs shown are supplied by PI for interfacing with the translation stages through a PCI board (C-843 PCI Servo Motion Controller Card, PI). To communicate with the stages information such as stage name and system number (enables communication with PCI board) must be supplied. When the VI

executes the stages are moved to their negative displacement limit and then moved to positions relative to the midpoint of their movement range. These positions are then defined as new "home" positions. The stages are now configured.

**Translation Stage Movement:** Once initial configuration of the translation stages has been performed they are ready for use. With the stages in their home positions the laser spot is initially aligned to the lowest cantilever vertically (typically cantilever number 8) using the XYZ micro translation stage. Figure A7.2 (A) and (B) show the block diagrams of the VIs responsible for movement to a desired cantilever and movement along cantilevers respectively. For movement to cantilevers the vertical translation stage is used. Movement is controlled using a case structure. If cantilever number 8 is selected the stage is sent to the home position using a "GOH" PI VI. If cantilever number 8 is not selected then the instruction to the stage will be to move $(8\text{-Cantilever Number}) \times 250\ \mu m$ relative to the "home" position. While the stage is moving a "general wait" command ensures that no further routines are executed while the stage is moving.

For movement along the cantilever the same "MOV" and "general wait" commands are used. The distance to be moved is defined entirely by the user. A multiplication factor has been included to account for the 45° angle of the cantilever relative to the axis of motion of the stage.

**Laser Alignment:** After configuration of the automated translation stages, alignment of the laser spot onto a cantilever is performed using the XYZ micro translation stage. As the laser emits in the infra-red (*i.e.* 830 nm) alignment is aided by the use of infra-red viewing cards and an IR viewing camera (IVR2-1300, Newport Corporation). The display of the sum and differential signal can be used to aid in alignment of the PSD. They are also used for the correct selection of neutral density filters so that the intensity of the light deflected by the array is in a desirable range and is not saturating the capacity of the PSD. Fine alignment of the laser spot can now be performed for the different resonance modes ("peaks") to be recorded for each cantilever. In order to measure flexural resonance peaks of higher modes with good signal to noise ratios, positioning of the laser spot at vibrational nodes is required. Figure A7.3 shows the part of the block diagram responsible for alignment. The while loop inside the case structure contains a flat-sequence which controls

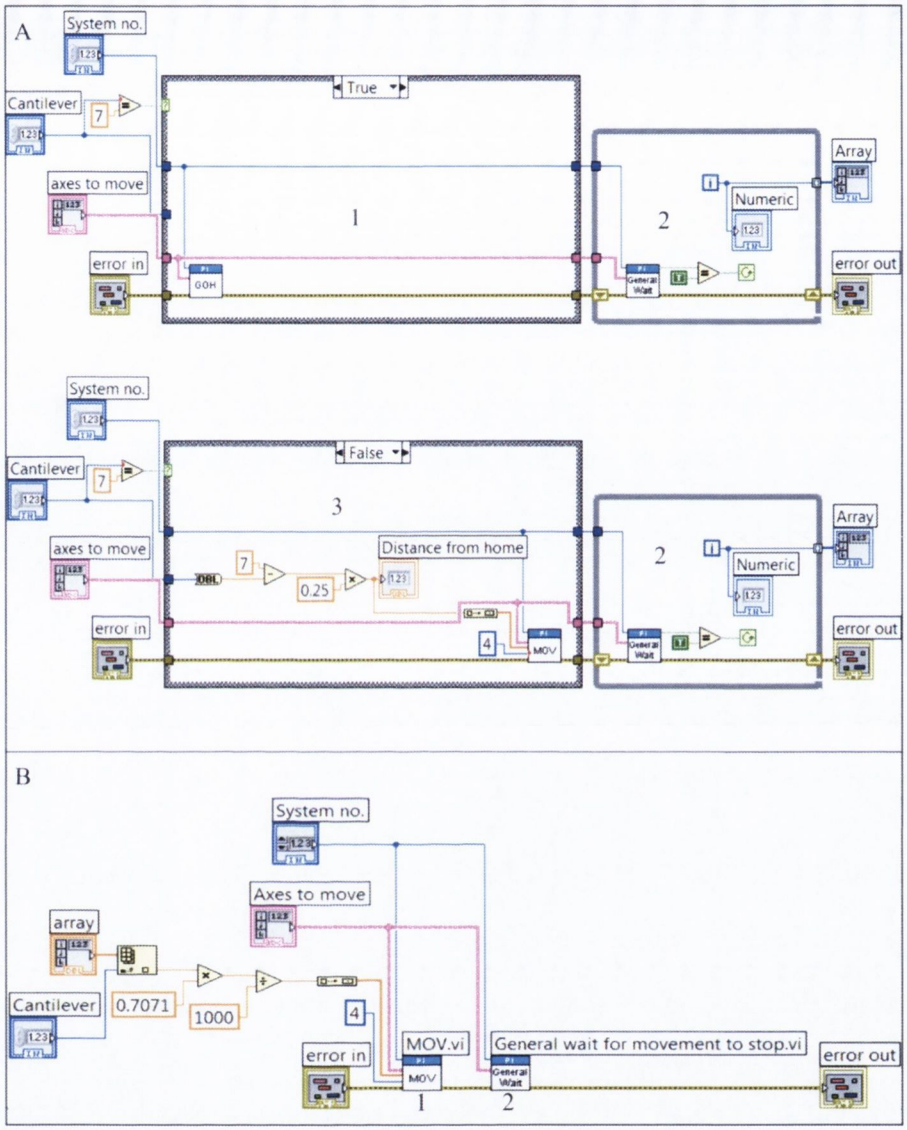


Figure A7.2: (A) Block diagram controlling the motion of the vertical translation stage. The laser spot can be moved to different cantilevers in the array. If cantilever number 8 is selected the stage is sent to the home position using a "GOH" PI VI. If cantilever number 8 is not selected then the instruction to the stage will be to move $(8\text{-Cantilever Number}) \times 250\ \mu m$ relative to the "home" position. While the stage is moving a "general wait" command ensures that no further routines are executed while the stage is moving. (1) Go to home. (2) Wait till motion has stopped. (3) Move to cantilever other than one at home position. (B) Block diagram controlling motion of horizontal translation stage to move the laser spot along one cantilever. The same "MOV" and "general wait" commands are used. The distance to be moved is defined entirely by the user. A multiplication factor has been included to account for the 45°angle of the cantilever relative to the axis of motion of the stage.

the movement of the laser spot to and along the desired cantilever. These VIs are discussed further below in the section concerning stage movement. A "dynamic" VI which actuates the piezoelectric actuator and records the modulation in the differential voltage of the PSD is then executed. The block diagram (not shown due to its size) of the "dynamic" VI contains several VIs which are used to interface with two PCI boards. A waveform generator (NI PCI-5412, 100 MS/s, 14-Bit Arbitrary Waveform Generator; National Instruments, TX, USA) applies a sinusoidal chirp dependant on the selected waveform parameters set by the user. A digitiser (NI PCI-5112 High speed digitiser; National Instruments, TX, USA) records the modulation of the differential voltage from the PSD to produce amplitude spectra. The waveform generated by the waveform generator is also recorded to produce phase spectra which aid in the identification of resonance peaks. While this loop is being executed it is possible to change the position of the laser spot along the cantilever using the global controls on the front panel. This allows optimisation of signal to noise ratios in frequency spectra. During alignment it is also possible to adjust the amplification factor applied by the preamplifier (SR560, Stanford Research Systems, CA, USA) using the VI front panel. Using this procedure it is possible to select different waveform parameters, laser spot positions, and amplification factors for each spectrum to be recorded.

**Dynamic and Static:** Once optimisation of the parameters has been carried out the recording of resonance frequencies can be performed. Figure A7.4 shows the key parts of the block diagram for the recording of frequency spectra and also the measurement of cantilever deflection. Display of the full block diagram code is not possible due to its size. For each "peak" a for-loop is executed eight times (once for each cantilever in the array). The for-loop contains a case structure; if a peak is to be used the sub diagram containing a flat-sequence with several sub VIs is executed. When the flat-sequence is executed the laser spot is moved to the desired cantilever and position along the cantilever using the VIs described in the **translation stage movement** section. The amplification factor applied by the preamplifier is adjusted before the dynamic VI is executed as described in the **Alignment** section. The laser spot is then returned to the tip of the cantilever using the move along cantilever VI. After a 500 ms wait the static deflection of the cantilever is then recorded. The 500 ms wait is to ensure that induced oscillations of the cantilever have

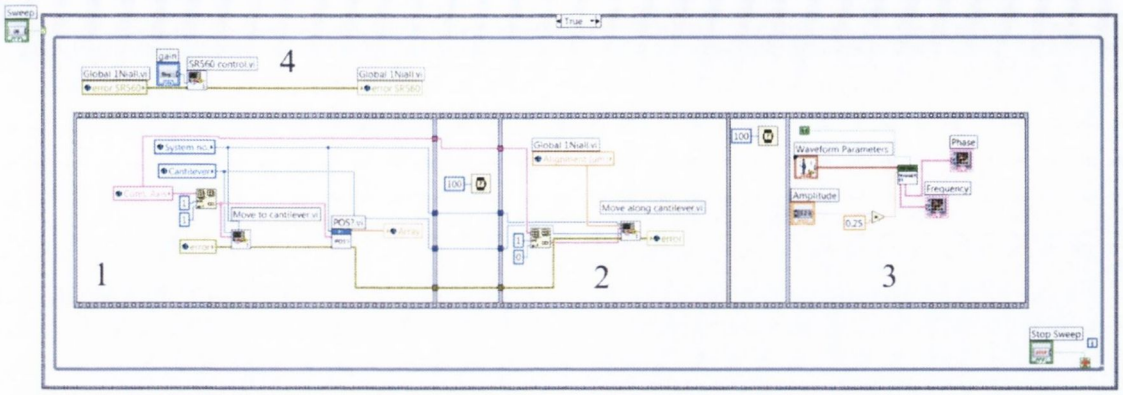


Figure A7.3: Block diagram for alignment and waveform parameter selection. This routine allows the waveform parameters, position of laser spot along the cantilever, and amplification factor applied to be optimised for each spectrum to be recorded. (1) Moves the laser spot to the desired cantilever in the array. (2) Moves the laser spot along a cantilever. (3) Sends a sinusoidal chirp voltage via a PCI waveform generator to the piezoactuator. A digitiser records the signal emitted by the waveform generator and also the modulation of the PSD differential voltage to produce amplitude and phase spectra. (4) Sub VI containing VIs which allows the amplification factor applied by the preamplifier to be changed.

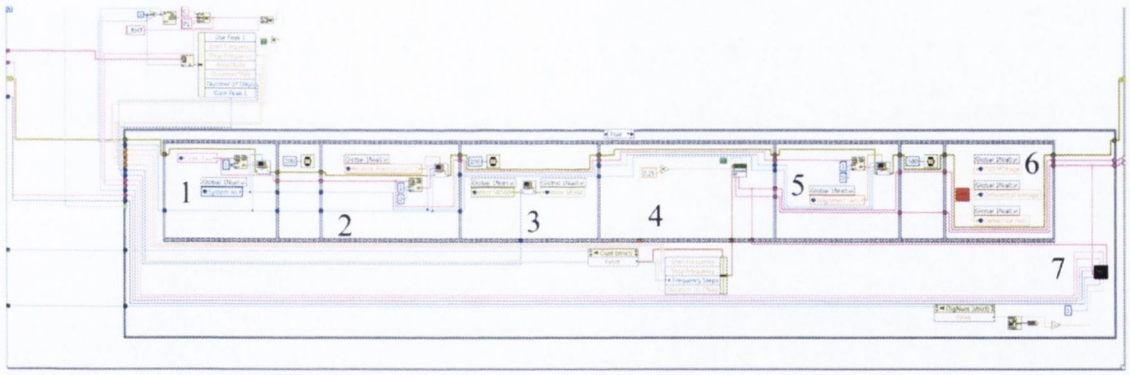


Figure A7.4: Block diagram for measurement of dynamic and static signal. A for-loop is executed 8 times. If a "peak" is to be recorded a flat-sequence in a case structure is executed which contains several sub VIs which move the laser spot and record dynamic and static data. (1) Moves laser spot to desired cantilever. (2) Move laser spot to desired position along cantilever. (3) Sets amplification factor applied by preamplifier. (4) Performs dynamic measurement. (5) Moves laser spot to tip of cantilever. (6) Measures static defection of cantilever. (7) Saves all data including humidity and temperature values at time of measurement.

ceased after the dynamic measurement. The nominal deflection of the cantilever is then calculated using Equation 4.1. The dynamic and static values recorded are then passed to the "save" sub VI. Here humidity, temperature and cantilever deflection are saved to a text file. Each dynamic spectrum is saved in a separate text file with the time in seconds contained in the file name. This allows for efficient data analysis. As with the fibre optic device the laser is turned off when data is not being recorded to ensure that no laser irradiation is influencing the growth of microorganisms.

# A.8 List of Publications and Presentations

**Publications:**

- N. Maloney, G. Lukacs, N. Nugaeva, W. Grange, J. P. Ramseyer, J. Jensen, and M. Hegner. Fibre Optic Readout of Microcantilever Arrays for Fast Microorganism Growth Detection. *Journal of Sensors* 2012: 405281, 2012. DOI:10.1155/2012/405281.
- G. Lukacs, N. Maloney, and M. Hegner. Ink-Jet Printing: Perfect Tool for Cantilever Array Sensor Preparation for Microbial Growth Detection. *Journal of Sensors* 2012: 561256, 2012. DOI:10.1155/2012/561256.
- J. Jensen, N. Maloney and M. Hegner. A Multi-Mode Platform for Cantilever Arrays Operated in Liquid. *Sensors and Actuators B:* Chemical. In press 2013.
- N. Maloney. Hydrogel Functionalised Cantilevers or Microorganism Growth Detection. *SurFACTS in Biomaterials*. Vol 18, Issue 1. Winter 2013.

**Oral Presentations:**

- 8th International Workshop on Nanomechanical Cantilever Sensors. Dublin, Ireland; May 2011.
- Advances in Biodetection and Biosensors, Barcelona, Spain; March 2013.

**Poster Presentations:**

- BioNano Inspire 2009, Dublin, Ireland. *Nanomechanical Sensors For Fast Microorganism Growth Detection* Gyöngyi Lukács, **Niall Maloney**, Martin Hegner.
- Biointerface 2012, Dublin, Ireland. *Hydrogel Functionalised Cantilevers for Microorganism Growth Detection.* **Niall Maloney**, Gyöngyi Lukács, Martin Hegner – Best student poster award.